

DISRUPTION OF CELLULAR CALCIUM HOMEOSTASIS AND MITOCHONDRIAL
FUNCTION FOLLOWING CHRONIC METHYLMERCURY TREATMENT

By

Sara Michelle Ciotti

A DISSERTATION

Submitted to
Michigan State University
in partial fulfillment of the requirements
for the degree of

Pharmacology and Toxicology – Environmental Toxicology - Doctor of Philosophy

2013

ABSTRACT

DISRUPTION OF CELLULAR CALCIUM HOMEOSTASIS AND MITOCHONDRIAL FUNCTION FOLLOWING CHRONIC METHYLMERCURY TREATMENT

By

Sara Michelle Ciotti

Methylmercury (MeHg) is a potent environmental neurotoxicant that impairs several neurological functions upon short and long-term exposure. MeHg causes cell-type specific damage in the cerebellum and this effect seems to be due to a disruption of intracellular calcium ($[Ca^{2+}]_i$) homeostasis and voltage-gated Ca^{2+} channel (VGCC) function. The striatum may be a sensitive target due to its high expression of $Ca_v1.3$, an L-type VGCC. Exposure to low levels of MeHg throughout ones lifetime is of contemporary concern. *In vitro* and *in vivo* studies were designed to mimic a lifetime exposure to low-levels of MeHg. Following prolonged exposure to low-nanomolar MeHg *in vitro* we found that MeHg causes a time- and subtype-dependent block of VGCCs, as well as increased resting $[Ca^{2+}]_i$. Chronic MeHg exposure *in vivo* suggests that MeHg interacts with AMPA receptors altering the post-synaptic response to glutamate at striatal medium spiny neurons. Chronic MeHg treatment also altered striatal synaptosomal mitochondrial function. This work contributes to our understanding of the consequences of long-term exposure to MeHg on neuronal function.

ACKNOWLEDGEMENTS

First and foremost I would like to thank my mentor Dr. William D. Atchison for his invaluable guidance throughout my graduate career. I also want to thank my thesis committee members- Dr. Susan Barman, Dr. John Goudreau, and Dr. Steven Heidemann- for their suggestions and careful consideration of my experiments. I would also like to thank the Department of Pharmacology and Toxicology as well as the Center for Integrative Toxicology. They have provided me with the opportunity to come to MSU and train in the company of excellent scientists.

I would also like to acknowledge Dr. Ravindra Hajela for his continued support and guidance throughout my time in the lab. To my current and former lab mates- Dawn Autio, Dr. April Neal, Dr. Wen-hsin Ku, Dr. Erin Wakeling, Dr. Elizabeth Molina-Campos, Dr. Brenda Marrero-Rosado, Dr. Aaron Bradford, Alexandra Colón-Rodríguez, Duanghathai Wiwatrana, Kaitlyn Sherer, Heidi Hannon, Rosa Jaiman, and Mónica Ríos-Cabanillas- for making the lab an enjoyable place to work. To Ivelisse Cruz-Torres and Kaye Long-Roldan helping me run the *in vitro* experiments. I would not have been able to finish all of my experiments without their assistance.

Finally, I am forever grateful for my my family. They have always believed in me and have been a constant source of love and support. I would not have been able to finish graduate school without them. To my husband James, thank you for your patience, love, and support. He stayed by my side through this journey and I couldn't have done this without him.

TABLE OF CONTENTS

LIST OF TABLES	vii
LIST OF FIGURES	viii
KEY TO ABBREVIATIONS	xiv
CHAPTER ONE: INTRODUCTION	1
A) Background	2
a. Methylmercury	2
i. Methylmercury in the environment	2
ii. Methylmercury and human health	3
b. Neuronal calcium regulation	8
i. Calcium regulation	8
ii. Calcium and aging	13
iii. Methylmercury and calcium regulation	14
c. Striatal and nigrostriatal dopamine system	17
i. Neuronal organization	17
ii. Methylmercury and the striatum and the NSDA system	21
B) Objectives and Rationale	22
a. Hypothesis and aims	22
b. Model systems	23
i. SH-SY5Y cell model	23
ii. Synaptosomes	25
iii. Striatal slice	26
c. Techniques	27
i. Calcium imaging	27
ii. Mitochondrial function	29
CHAPTER TWO: PERTURBATION OF CALCIUM REGULATION FOLLOWING ACUTE AND CHRONIC METHYLMERCURY TREATMENT IN DIFFERENTIATED SH-SY5Y CELLS	31
A) Abstract	32
B) Introduction	34
C) Materials and methods	37
Chemicals and solutions	37
Cell culture	39
Single-cell microfluorimetry	39
MeHg treatments	41
Determination of $[Ca^{2+}]_i$	42
Statistics	44
D) Results	45

a.	Acute methylmercury treatment	45
b.	Chronic methylmercury treatment	48
E)	Discussion	54

CHAPTER 3: STRIATAL SLICES FROM AGED ANIMALS ARE MORE SUSCEPTIBLE TO METHYLMERCURY-INDUCED CALCIUM INCREASE THAN YOUNG ANIMALS **57**

A)	Abstract	58
B)	Introduction	59
C)	Materials and methods	62
	Chemicals and solutions	62
	Slice preparation	62
	Methylmercury treatment	62
	Confocal imaging	63
	Statistics	64
D)	Results	66
	a. Confocal imaging	66
	b. Comparative susceptibility of striatal and cerebellar slices	66
E)	Discussion	70

CHAPTER 4: CHRONIC METHYLMERCURY TREATMENT ALTERS STRIATAL CALCIUM REGULATION AND SYNAPTOSOME MITOCHONDRIAL FUNCTION **73**

A)	Abstract	74
B)	Introduction	75
C)	Materials and methods	78
	Chemicals and solutions	78
	Animal care and treatments	78
	Tissue collection	79
	Striatal synaptosome isolation	79
	Mitochondrial function analysis	80
	Striatal slice preparation	81
	High speed calcium imaging	82
	Statistics	83
D)	Results	89
	a. Animal health and behavior	89
	b. Trunk blood Hg concentration	89
	c. Mitochondrial function	91
	d. High speed $[Ca^{2+}]_i$ imaging	98
E)	Discussion	106

CHAPTER 5: SUMMARY AND CONCLUSIONS **111**

	Summary and conclusions	112
--	-------------------------	-----

LIST OF TABLES

Table 1.1	Characteristics of HVA and LVA Ca²⁺ channels. Summary of the properties of HVA and LVA Ca ²⁺ channels. Table from: Marrero et al., (2013).9
Table 3.1.	No difference in time-to-peak fluorescence between cerebellar granule cells and striatal medium spiny neurons. The time-to-peak fluoresce was determined for cerebellar granule cells and striatal medium spiny neurons in response to 20µM and 100µM MeHg. No differences were detected between the time-to-peak fluorescence (min) in the cerebellum and striatum at any age. Data are expressed at means ± SEM. (n ≥4).....69

LIST OF FIGURES

- Figure 1.1** **Acute MeHg exposure causes a biphasic increase in $[Ca^{2+}]_i$.** Diagram representing the MeHg-induced biphasic increase in $[Ca^{2+}]_i$. Acute MeHg exposure causes the release of Ca^{2+} from the SER and mitochondria followed by extracellular Ca^{2+} entry. For interpretation of the references to color in this and all other figures the reader is referred to the electronic version of this dissertation. 15
- Figure 1.2.** **Organization of the basal ganglia.** The basal ganglia is a highly organized circuit composed of multiple nuclei. GABAergic (inhibitory) projections are represented in red and glutamatergic (excitatory) projections are represented in green. This figure was modified from Obeso et al. (2008).18
- Figure 1.3** **A graphic representation of the location of SNc neurons in the human brain.** SNc cell bodies are located in the midbrain and their axons project to the striatum where they release DA.....19
- Figure 1.4** **A depiction of an XF Analyzer experiment measuring mitochondrial OCR.** Perturbation of mitochondrial oxidative phosphorylation allows for the determination of mitochondrial basal respiration, ATP production, maximal respiration, spare capacity, non-mitochondrial respiration, and proton leak.....30
- Figure 2.1** **Acute MeHg treatment in differentiated SH-SY5Y cells caused a biphasic increase in $[Ca^{2+}]_i$.** (A-B) Representative 340nm, 380nm, and ratio of (F_{340nm}/F_{380nm}) fura-2 tracings from a single differentiated SH-SY5Y cell treated acutely with 5 μ M MeHg. (A) Representative 340nm tracing is shown in black. 340nm fluorescence corresponds to changes in Ca^{2+} -bound fura-2. The onset of phase 1 was the time at which the 340nm tracing increases from baseline. Representative 380nm tracing is shown in grey. 380nm fluorescence corresponds to changes in unbound fura-2. The onset of phase 2 was the time at which the 380nm tracing had a sustained decrease from baseline. (B) Representative ratio of (F_{340nm}/F_{380nm}). An increase in fluorescence of the ratio corresponds to an increase in $[Ca^{2+}]_i$. Acute 5 μ M MeHg treatment caused a biphasic increase in $[Ca^{2+}]_i$38
- Figure 2.2** **Measurement of VGCC function.** (A) Schematic diagram of how VGCC function was measured. VGCCs were activated by depolarizing the cell membrane with 40mM KCl which activated VGCCs and allowed Ca^{2+} influx through L- and N-type channels. (B) Representative fura-2 tracing from a single

differentiated SH-SY5Y cell treated with 0nM MeHg for 48h. Application of 40mM KCl is indicated by the arrows. The amplitude of KCl-induced Ca^{2+} influx was measured for each depolarization and averaged to determine a mean amplitude for each experiment (n=1).....40

- Figure 2.3 Determination of VGCC subtype sensitivity to chronic MeHg treatment. (A)** Schematic diagram of how VGCC function was measured. SH-SY5Y cells were pretreated with either 1 μ M GVIA or 5 μ M nifedipine (as shown in diagram) and then depolarized with 40mM KCl. Subsequent Ca^{2+} influx was due solely to flow through the unblocked channel resulting in decreased Ca^{2+} influx. **(B)** Representative fura-2 tracing from a single differentiated SH-SY5Y cell treated with 0nM MeHg for 48h. Application of 40mM KCl is indicated by the arrows. The first depolarization was considered the control and occurred with no antagonist present. The following 3 depolarizations occurred in the presence of antagonist. The amplitude of KCl-induced Ca^{2+} influx was quantified for each depolarization. The mean amplitude of the depolarizations in the presence of antagonist was divided by the amplitude of the control depolarization to determine the percent of control.....43
- Figure 2.4 Acute MeHg caused a concentration-dependent decrease in the time-to-onset of Phase 1 and Phase 2 in differentiated SH-SY5Y cells.** Differentiated SH-SY5Y cells were superfused with 1, 2, 5, or 10 μ M MeHg and changes in $[\text{Ca}^{2+}]_i$ were continuously monitored. MeHg caused a concentration dependent decrease in the time-to-onset of phase 1 and phase 2. Acute treatment with 5 and 10 μ M MeHg resulted in a significant decrease in the onset of phase 1 and 2 compared to 1 μ M MeHg. Data are expressed as mean \pm SEM. * = significant difference compared to 1 μ M MeHg (One-Way ANOVA, $p < 0.05$, $n \geq 4$).....46
- Figure 2.5 N- or L-type VGCC antagonists delay the onset of phase 2.** Differentiated SH-SY5Y cells were superfused with 2 μ M MeHg alone, 2 μ M MeHg + 1 μ M GVIA, or 2 μ M MeHg + 5 μ M Nif and changes in $[\text{Ca}^{2+}]_i$ were continuously monitored. VGCC antagonists did not delay the onset of phase 1. Co-treatment with GVIA or Nif significantly delayed the onset of phase 2. Data are expressed as mean \pm SEM. * = significant difference compared to 2 μ M MeHg alone (One-Way ANOVA, $p < 0.05$, $n \geq 3$).47
- Figure 2.6 Chronic MeHg caused decreased KCl-induced Ca^{2+} influx.** Differentiated SH-SY5Y cells were treated with 0 or 20nM MeHg for 48 or 72h. Following MeHg treatment cells were loaded with fura-2AM and KCl-induced Ca^{2+} influx was measured. **(A)** Forty-eight hour 20nM MeHg treatment caused a slight reduction in the maximum amplitude of KCl-induced Ca^{2+} influx. **(B)** Seventy-two hour 20nM MeHg caused a significant decrease in the maximum amplitude of KCl-induced Ca^{2+} influx (Unpaired t-test, $p = 0.018$, $n \geq 4$).....49

Figure 2.7	Chronic MeHg treatment caused a time- and subtype specific block of VGCCs. The maximum amplitude of KCl-induced Ca^{2+} influx was measured in cells treated with 0 or 20nM MeHg for 48 or 72h. Cells were depolarized 4 times using 40mM KCl. The first depolarization was performed with KCl alone (control depolarization) the following 3 were performed in the presence of a VGCC antagonist. The amplitude of KCl-induced Ca^{2+} influx was quantified for each depolarization. The mean amplitude of depolarizations in the presence of antagonist was divided by the amplitude of control depolarization to determine percent (%) of control. Data are represented as percent (%) of control depolarization. (A) Forty-eight hour 20nM MeHg treatment, caused a significant decrease in Ca^{2+} influx through L-type VGCCs and no change in KCl-induced Ca^{2+} influx through N-type channels (Unpaired t-test, $p = 0.0122$, $n=3$). (B) Seventy-two hour 20nM MeHg treatment caused a significant decrease in KCl-induced Ca^{2+} influx through N - and L-type VGCCs (Unpaired t-test, $p<0.05$, $n\geq 3$). * = significantly different than the 0nM MeHg group. Data are expressed as mean \pm SEM.....51
Figure 2.8	Chronic MeHg treatment caused a significant increase in resting $[Ca^{2+}]_i$. Differentiated SH-SY5Y cells were treated with 0 or 20nM MeHg for 72h and the resting $[Ca^{2+}]_i$ was calculated. Cells treated with 20nM MeHg had a significant increase in mean resting $[Ca^{2+}]_i$ compared to 0nM MeHg treated cells.* = significant difference compared to 0nM MeHg group (Unpaired t-test, $p<0.05$, $n = 3$).....53
Figure 3.1	Striatal slices from aged animals are more susceptible to 20μM MeHg than slices from 1mo animals. Striatal slices from 1mo, 9mo, and 21mo mice were loaded with Fluo4 and superfused with 20 μ M MeHg for 45min. (A) Relative Fluo4 fluorescence (F/F_0) of striatal slices from 1mo, 9mo, and 21mo mice to 20 μ M MeHg treatment. (B) The time-to-peak fluorescence was quantified for each group. Striatal slices from 9 and 21mo mice had a significantly decreased time-to-peak compared to slices from 1mo animals. Data are means \pm SEM ($n\geq 4$) * = significantly different than 1mo animals.($p<0.05$, One-Way ANOVA, Tukey's post-test).....65
Figure 3.2	Age had no effect on the response of striatal slices to 100μM MeHg treatment. Striatal slices from 1 and 9mo animals were loaded with Fluo4 and superfused with 100 μ M MeHg for 21min. (A) Relative Fluo4 fluorescence (F/F_0) response of striatal slices from 1 and 9mo mice to 100 μ M MeHg treatment. (B) There was no difference in the time-to-peak effect between 1 and 9mo striatal slices to 100 μ M MeHg treatment. Data are means \pm SEM ($n\geq 4$).....67

- Figure 4.1** **Six or twelve month MeHg or Isr/MeHg treatments did not alter mouse weight.** Male balb/c mice were treated with 0ppm Isr/0ppm MeHg (Con/Con), 0ppm Isr/6.25ppm MeHg (Con/MeHg), 2ppm Isr/0ppm MeHg (Isr/Con), 2ppm Isr/6.25ppm MeHg (Isr/MeHg) for 6 or 12mo. Throughout the treatment period mice were weighed three times a week and their mean weight per week was determined. **(A)** Six or **(B)** twelve month treatments did not alter mouse weight. Treatment and time had a significant effect on mouse weight following 6 and 12mo treatments (Two-Way ANOVA, Bonferroni post-test, $p < 0.05$) ($n \geq 12$). Data are expressed as mean \pm SEM.....84
- Figure 4.2** **Six or twelve month MeHg or Isr/MeHg treatments did not alter mouse performance on the rotarod.** Male balb/c mice were treated with 0ppm Isr/0ppm MeHg (Con/Con), 0ppm Isr/6.25ppm MeHg (Con/MeHg), 2ppm Isr/0ppm MeHg (Isr/Con), 2ppm Isr/6.25ppm MeHg (Isr/MeHg) for 6 or 12mo. During the first 6mo of treatment mouse ability to remain on an accelerating rotarod was tested every 4wks and then every 2wks for the duration of the treatment. **(A)** Six or **(B)** twelve month treatments did not alter mouse ability to remain on an accelerating rotarod. Treatment and time had a significant effect on mouse ability to remain on the accelerating rotorod following 6 and 12mo treatments (Two-Way ANOVA, Bonferroni post-test, $p < 0.05$) ($n \geq 12$). Data are expressed as mean \pm SEM.....85
- Figure 4.3** **Six or twelve month MeHg or Isr/MeHg treatments did cause a consistent pattern of altered mouse limb cross.** Male balb/c mice were treated with 0ppm Isr/0ppm MeHg (Con/Con), 0ppm Isr/6.25ppm MeHg (Con/MeHg), 2ppm Isr/0ppm MeHg (Isr/Con), 2ppm Isr/6.25ppm MeHg (Isr/MeHg) for 6 or 12mo. Throughout the treatment period the extent of mouse hind limb cross was scored three times a week and their mean score per week was determined. The extent of hind limb cross was assigned a score based on severity. A score of 0, 1, or 2 were assigned to no cross, partial cross, and complete cross, respectively. **(A)** Mean limb cross test scores for six month treatment. Con/Con hind limb score is significantly different than Con/MeHg hind limb score on week 25. Con/Con hind limb score is significantly different than Isr/MeHg hind limb score during weeks 8 and 9. **(B)** Mean limb cross test scores for twelve month treatment. Con/Con hind limb score is significantly different than Isr/MeHg hind limb score during weeks 39 and 48. Treatment and time had a significant effect on mouse hind limb score (Two-Way ANOVA, Bonferonni post-test, $p < 0.05$). * = Con/Con is significantly different than Con/MeHg. # = Con/Con is significantly different than Isr/MeHg. Data are expressed as mean \pm SEM ($n \geq 12$).....87
- Figure 4.4** **Six and twelve month MeHg treatment caused blood Hg accumulation.** Male balb/c mice were treated with 0ppm Isr/0ppm MeHg (Con/Con), 0ppm Isr/6.25ppm MeHg (Con/MeHg), 2ppm Isr/0ppm MeHg (Isr/Con), 2ppm Isr/6.25ppm MeHg (Isr/MeHg) for 6 or 12mo. Following anaesthesia with isofluorane truck blood was collected and later analyzed for Hg content. MeHg

and Isr/MeHg caused significant Hg accumulation following (A) 6mo and (B) 12mo treatment (One-Way ANOVA, Tukey's post-test, $p < 0.05$) ($n = 4$).....90

- Figure 4.5 MeHg or Isr/MeHg treatment did not alter mitochondrial bioenergetics.** Mitochondrial bioenergetics of striatal synaptosomes was determined following treatment period. Oxygen consumption rate (OCR, pMoles/min) before and after the addition of oligomycin (1 μ M), Carbonyl cyanide 4-(trifluoromethoxy)phenylhydrazone (FCCP) (2 μ M), antimycin A (1 μ M), and rotenone (1 μ M). No differences were detected in OCR between treatment groups following (A) 6mo or (B) 12mo treatment period. Data are means \pm SEM ($n \geq 4$).92
- Figure 4.6 Mitochondrial function was unaltered following 6mo MeHg or Isr/MeHg co-treatment.** Quantification of mitochondrial basal respiration, ATP production, maximum respiration and spare capacity striatal synaptosomes. MeHg or Isr/MeHg co-treatment caused no significant differences in (A) basal respiration (B) ATP production (C) maximal respiration or (D) spare capacity. Data are means \pm SEM ($n \geq 5$).....93
- Figure 4.7 Mitochondrial function was unaltered following 12mo MeHg or Isr/MeHg co-treatment.** Quantification of striatal synaptosome mitochondrial basal respiration, maximum respiration, and spare capacity. MeHg or Isr/MeHg co-treatment caused no significant differences in (A) basal respiration (B) maximal respiration or (C) spare capacity. Data are means \pm SEM ($n \geq 5$).....95
- Figure 4.8 Twelve month Isr/MeHg treatment caused a significant increase in ATP production in both striatal and cortical synaptosome mitochondria.** Quantification of (A) striatal and (B) cortical synaptosome ATP production. 12mo Isr/MeHg treatment caused a significant increase in ATP production compared to both Isr/Con and Con/MeHg treatment groups. * = significant difference (One-Way ANOVA, Tukey's post-test, $p < 0.05$) ($n \geq 5$). Data are means \pm SEM.....97
- Figure 4.9 Twelve month MeHg or Isr/MeHg did not alter striatal response to KCl-induced $[Ca^{2+}]_i$ increase.** Striatal slices were loaded with fura-2AM and then exposed to 40mM KCl for 2min followed by 8min of ACSF. Fura-2 fluorescence was continuously monitored. Data are presented as relative fura-2 fluorescence (Fluorescence at time 0/fluorescence at time x). An increase in fura-2 fluorescence corresponds to an increase in $[Ca^{2+}]_i$. Time-to-peak fluorescence was determine for each treatment group. (A) Striatal $[Ca^{2+}]_i$ response to 40mM KCl.(B) Time-to-peak and (C) amplitude of response was quantified. No Differences were detected between treatment groups. Data are means \pm SEM ($n \geq 3$).....100

- Figure 4.10** **Twelve month MeHg or Isr/MeHg did not alter striatal response to NMDA-induced $[Ca^{2+}]_i$ increase.** Striatal slices were loaded with fura-2AM and then exposed to 50 μ M NMDA and 10 μ M glycine for 2min followed by 8min of ACSF. Fura-2 fluorescence was continuously monitored. Data are presented as relative fura-2 fluorescence (Fluorescence at time 0/fluorescence at time x). An increase in fura-2 fluorescence corresponds to an increase in $[Ca^{2+}]_i$. Time-to-peak fluorescence was determine for each treatment group. **(A)** Striatal $[Ca^{2+}]_i$ response to 50 μ M NMDA. **(B)** Time-to-peak and **(C)** amplitude of response was quantified. Many slices did not respond to NMDA application resulting in an n value less than 3.....102
- Figure 4.11** **Twelve month MeHg treatment caused a significantly decreased time-to-peak fluorescence following application of AMPA.** Striatal slices were loaded with fura-2AM and then exposed to 25 μ M AMPA for 2min followed by 8min of ACSF. Fura-2 fluorescence was continuously monitored. Data are presented as relative fura-2 fluorescence (Fluorescence at time 0/fluorescence at time x). An increase in fura-2 fluorescence corresponds to an increase in $[Ca^{2+}]_i$. Time-to-peak fluorescence was determine for each treatment group. **(A)** Striatal $[Ca^{2+}]_i$ response to AMPA **(B)** 12mo MeHg treatment caused a significantly faster time-to-peak fluorescence in response to AMPA ($p < 0.05$, unpaired student t-test, $n \geq 3$). **(C)** Amplitude of response was not affected by treatment. Data are means \pm SEM ($n \geq 3$).....104
- Figure 5.1** **A schematic representation of the effects of prolonged exposure to MeHg in differentiated SH-SY5Y cells.** Exposure of differentiated SH-SY5Y cells with 20nM MeHg resulted in a time- and VGCC subtype-dependent block of depolarization-dependent $[Ca^{2+}]_i$ increase. MeHg blocked KCl-induced Ca^{2+} increase through L-type VGCCs after a 48h exposure and through both L- and N-type VGCCs after 72h exposure. The resting $[Ca^{2+}]_i$ was also significantly increased following 72h MeHg exposure.....113
- Figure 5.2** **Schematic diagram of the effects of MeHg on the striatal circuit.** MeHg acts at striatal MSNs to causes increases in $[Ca^{2+}]_i$ as well as alter mitochondrial ATP production. It has also been shown to cause increase in both DA and glutamate release. These actions along with potential direct interactions with AMPA receptors results in altered post-synaptic Ca^{2+} response to AMPA receptor activation.....114

KEY TO ABBREVIATIONS

ACSF - Artificial cerebrospinal fluid

AM - Acetoxymethyl ester

AMPA - 2-Amino-3-hydroxy-5-methyl-5-isoxazole propionic acid

ANOVA - Analysis of variance

ATP - Adenosine 5'-triphosphate

BBB - Blood brain barrier

Ca^{2+} - Calcium

Ca^{2+}_e - Extracellular calcium

Ca^{2+}_i - Intracellular calcium

$[\text{Ca}^{2+}]_i$ - Intracellular calcium concentration

Ca^{2+}_m - Mitochondrial calcium

$[\text{Ca}^{2+}]_m$ - Mitochondrial calcium concentration

Con - Control

CNS - Central nervous system

DA – Dopamine

DAT – Dopamine transporter

DHP - Dihydropyridine

DMSO - Dimethyl sulfoxide

ECAR – Extracellular acidification rate

EGTA - Ethylene glycol tetraacetic acid

F - Fluorescence

FBS - Fetal bovine serum

FCCP - Cyanide 4-(trifluoromethoxy) phenylhydrazone

Fluo-4 NW - Fluo 4 no wash

Fura-2 AM - Fura-2 acetoxymethylester

GABA – Gamma-aminobutyric acid

GPe – External globus pallidus

GPI – Internal globus pallidus

GVIA - ω - Conotoxin GVIA

h - Hour(s)

HBS - HEPES buffered saline

HEPES - 4-(2-Hydroxyethyl)-1-piperazineethanesulfonic acid

HVA – High voltage activated

IP₃ - Inositol-1,4,5-triphosphate

Isr - Isradipine

LVA – Low voltage activated

M - Molar

MEM - Minimum essential medium

MeHg - Methylmercury

min - Minute(s)

mo - Month

MSN – Medium spiny neuron

μ – Micro

MIB – Mitochondrial isolation buffer

mo - Month

mPTP - Mitochondrial transition pore

Nif - Nifedipine

nm - Nanometer

nM - Nanomolar

NMDA - N-methyl-D-aspartate

NSDA - Nigrostriatal dopamine

NT - Neurotransmitter

OCR - Oxygen consumption rate

PCB – Polychlorinated biphenyl

PD – Parkinson's disease

PND - Postnatal day

ppm - Parts per million

RA - Retinoic acid

ROS - Reactive oxygen species

RT-PCR – Real time polymerase chain reaction

RyR - Ryanodine receptor

SEM - Standard error of the mean

SER - Smooth endoplasmic reticulum

SERCA - Smooth endoplasmic reticulum Ca^{2+} ATPase

SNC – Substantia nigra pars compacta

TPEN - N,N,N',N',-tertrakis-(2-pyridylmethyl)ethylenediamine

VGCC - Voltage-gated calcium channel

yr - Year

Zn²⁺ - Zinc

CHAPTER ONE: INTRODUCTION

A) Background

a. Methylmercury

i. Methylmercury in the environment

Mercury (Hg) is a persistent heavy metal that can be found in three forms: Hg^0 , Hg^+ and Hg^{2+} . Hg and its compounds are neurotoxic environmental contaminants of contemporary concern. Hg enters the environment from both natural and anthropogenic sources. Natural sources of Hg include degassing of the earth's crust, volcanic emissions, and soil erosion. Anthropogenic sources include coal burning, waste combustion, and gold mining (Clarkson and Magos, 2006; Wade, 2013). Mercury forms an amalgam with gold, creating an easy and affordable method for its extraction from lower-grade ore. Its heavy use with artisan gold mining has made it the world's leading source of mercury pollution, releasing more mercury into the environment than all of the world's coal plants combined (Wade, 2013). Once released into the atmosphere Hg is oxidized to Hg^+ and then returns to the earth's surface in rainwater. The majority of Hg^+ is reduced back to the vapor state and then returns to the atmosphere. However a portion is methylated by methanogenic bacteria to form MeHg. MeHg then bioaccumulates up the food chain, with the highest sources being piscivorous fish or marine mammals such as tuna and pilot whale, respectively. Consequently, humans are mainly exposed to MeHg through the consumption of fish and marine mammals. In an attempt to reduce Hg pollution many nations around the world came together to form the Minamata Convention. Their goal is to reduce anthropogenic Hg pollution up to 15% by the year 2020 (Lubick and Malakoff, 2013). Although

anthropogenic sources of Hg pollution can be reduced, Hg persists in the environment; it cannot be destroyed and it does not degrade.

ii. Mercury and human health

Hg and Hg compounds have been used in a number of different applications throughout history. The first known use dates back thousands of years. The Chinese used Hg to prepare red ink (Clarkson and Magos, 2006). Hg has been used as an important constituent of drugs for centuries. It has been used as an ingredient in many diuretics, antibacterials, ointments, and laxatives. Hg was also used as an antifungal agent on seed grain. The fluidity of Hg has led to its being used in thermometers, barometers, and on dynamic electrodes. As previously mentioned, Hg is commonly used in artisan gold mining, which is currently the largest source of anthropogenic pollution (Wade, 2013). Although it has been extensively used throughout history for a variety of applications its current usage is limited due to the known adverse human health effects.

Hg and Hg compounds are handled differently by the body, and clinical signs and symptoms associated with their poisoning differ. Exposure to Hg^0 is most commonly associated with occupational exposures. Signs and symptoms associated with Hg^0 poisoning include tremors, polyneuropathy, loss of memory, insomnia, and neurocognitive disorders. Exposure to Hg^{2+} was associated with its use in medical products. Hg^{2+} does not cross the blood brain barrier (BBB). However it is extremely toxic to the kidneys causing severe renal dysfunction (Ashner et al., 2013).

The primary target of MeHg is the central nervous system. When ingested MeHg is efficiently (90%) absorbed in the gastrointestinal tract. From there it enters the bloodstream where it primarily binds to hemoglobin in the red blood cells. MeHg then distributes throughout the body (Brunton et al., 2008). MeHg is highly reactive via oxidation with the amino acid cysteine. The MeHg-cysteine complex mimics methionine and is a substrate for the neutral amino acid transporter allowing it to enter into the cell (Yin et al., 2008). MeHg is also lipophilic, allowing it some ability to cross lipid membranes. MeHg is mainly eliminated through the liver via excretion to the bile and gut. However, it undergoes extensive enterohepatic circulation allowing reabsorption into the bloodstream (Brunton et al., 2008).

The neurotoxic impact of exposure to MeHg had not been understood until a seminal paper by Hunter and Russell (1954). In this paper they described a case study of a 23 yr old man exposed to MeHg dust for 4mo while working. Six mo after the exposure he presented to the hospital with paresthesia of his hands and forearms, ataxia, and constriction of the visual fields. Fifteen years after the exposure he died and an autopsy was performed. The most striking finding of the autopsy was gross atrophy of the cerebellum. Upon microscopic examination a loss of the cerebellar granule cells was evident while the neighboring purkinje cells were generally spared. Hunter and Russell's case report highlighted the latency between exposure and presentation of symptoms and the cell type-specific damage in the cerebellum associated with MeHg poisoning.

There have been two very well known episodes of mass MeHg poisonings; the first occurred in Minamata, Japan and the second occurred in Iraq. Although very unfortunate, these exposures allowed scientists to understand the pathophysiology of MeHg poisonings in humans. In the 1950's the Chisso factory in Mimamata, Japan was producing acetylaldehyle. Hg

was used as a catalyst in the production and discharged into Minamata Bay, a fertile fish spawning ground. Consequently people who lived near and around Minamata Bay were poisoned by the daily consumption of heavily contaminated fish from the bay. In Iraq, in 1971, wheat seed coated with a MeHg-containing fungicide that was meant to be used for planting was instead used to make bread. People who consumed the bread made with the MeHg-contaminated seed had MeHg poisoning (Bakir, 1973). Interestingly, victims of both chronic (Minamata) and acute (Iraq) MeHg poisonings presented with the same signs and symptoms. Following a characteristic latent period which can range from weeks to months, depending on the extent of exposure, signs and symptoms begin to appear. Characteristic signs and symptoms include paresthesia (loss of sensation in the extremities), ataxia (loss of coordination in gait), dysarthria (slurred speech), loss of hearing, and constriction of vision (Harada, 1968; Bakir, 1973). Several of the neurological signs presented by patients have plausible links to alterations in voltage-gated calcium channel (VGCC) function. The severity of symptoms depends of the exposure dose, the duration, and the stage of development that exposure takes place (for review see Castoldi, 2008). An example of this is the severe damage that occurs to the developing fetus when exposed to MeHg. MeHg crosses the BBB and placenta. The developing fetus can be adversely affected even when the mother has no symptoms of MeHg poisoning. Children exposed *in utero* during the mass poisoning in Minamata presented with severe cognitive and motor deficits (Harada et al., 1968).

Two unique populations which rely heavily on the daily consumption of fish or sea mammals as their main food source are inhabitants of the Faroe and Seychelles Islands. The Faroe Islands are located in the Arctic Ocean between Norway and Iceland. Inhabitants in the Faroe Islands consume both fish and marine mammals which may also accumulate other

environmental contaminants such as polychlorinated biphenyls (PCBs) (Weihe et al., 1996). The Seychelles Islands are located in the Indian Ocean off the eastern coast of Africa. Inhabitants of the Seychelles Islands consume only fish and not marine mammals. Scientists have studied these populations and focused on the impact of prenatal MeHg exposure and its association with adverse neurodevelopmental outcomes (Davidson et al., 2006, 2010, 2011; Debes et al., 2006; Stokes-Riner et al., 2011; Yorifuji et al., 2011; Grandjean et al., 2012; Strain et al., 2012; Karagas et al., 2012). Studies following inhabitants of the Faroe Islands found significant neurological deficits in children exposed prenatally to MeHg (Grandjean et al., 2012). In contrast, studies of inhabitants of the Seychelles, found no adverse outcomes due to long-term fish consumption (Davidson et al., 2011). The disparity between neurobehavioral outcomes may be due to the genetic differences between the two populations as well as the presence of other environmental contaminants such as PCBs present in marine mammals which exacerbate neuronal damage in the Faroe Island population.

The contemporary concern is for MeHg exposure which occurs over a lifetime. Long term exposure (lifetime or exposure during critical windows of development) could enhance processes associated with normal aging, thereby facilitating the onset of senescence-related neurodegeneration. This may ultimately lead to neuropathological changes associated with degenerative diseases. The role of environmental toxicants in neurodegenerative disease has long been speculated (Johnson and Atchison, 2009; Vance et al., 2010; Williams et al., 2010; Cannon and Greenamyre, 2011; Madison et al., 2012). The causative agent in the development of the sporadic form of many neurodegenerative diseases is unknown and researchers have speculated that environmental influences could play a role by altering neuronal function.

One such neurodegenerative disorder in which the environment is thought to play a role is Parkinson's disease (PD) (Landrigan et al., 2005). PD is strongly associated with aging and afflicts over one million people in the United States; that number is on the rise with an aging population (de Lau et al., 2004, Dorsey et al., 2007). During the development of PD the most severely afflicted neurons are the neurons of the nigrostriatal dopamine (NSDA) system (Braak and Braak, 2000). NSDA neuron cell bodies are located in the *substantia nigra pars compacta* (SNc) and project their axons to the striatum where they release dopamine (DA), which is involved in the regulation of the movement and coordination (Bergman, 1998). The severity of symptoms in PD is associated with the extent of SNc neuronal loss (Dauer and Przedborski, 2003; Fahn, 2003). PD has two forms - familial and sporadic. Increased risk for the development of the familial form of PD has been linked to mutations in a number of genes including, *DJ-1*, *PINK1* and *Parkin* (Schapira, 2008). The sporadic form of PD is the most common and the cause is unknown. As such, initiating or predisposing factors such as environmental exposure or lifestyle are thought to play a major role in sporadic PD. Post mortem autopsy reports from humans with PD present evidence of mitochondrial dysfunction and an increased production of reactive oxygen species (ROS) in the SNc of PD patients (Dexter et al., 1989). It has been postulated that exposure to an environmental toxicant which targets the mitochondria could be a factor in the development of the disease however the results are ambiguous. Development of the sporadic form has been associated with a high body burden of Hg (Ngim and Devathasan, 1989), however this was not the case in other studies (Ohlson and Hogstedt, 1981; Semchuk et al., 1993; Gorell et al., 1999). Epidemiological studies of the Faroe Island Inuits, a population with chronic environmental exposure to MeHg, report an increased (approximately 2-fold) prevalence

of PD compared to the general population (Wermuth et al., 1997; Wermuth et al., 2000; Wermuth et al., 2007). Studies of the association of PD and exposure to MeHg in these people have found that prenatal exposure to MeHg has no effect on the development of PD (Petersen et al., 2008b). However, long-term consumption of whale meat and blubber in adulthood increases is associated with the development of PD (Petersen et al., 2008a). The increased risk for the development of PD may be influenced by the presence of PCBs and other environmental contaminants in whale meat and blubber (Weihe et al., 1996; Petersen et al., 2008a). Although these studies have found an association with MeHg exposure and PD, it is not thought that MeHg exposure causes PD.

b. Neuronal calcium regulation

i. Calcium regulation

Ca^{2+} is a key regulator of a variety of neuronal processes such as neurotransmitter release, growth cone elongation, and gene transcription. Extracellular Ca^{2+} (Ca^{2+}_e) concentration is 10,000 higher than $[\text{Ca}^{2+}]_i$. Thus Ca^{2+}_e entry is a tightly regulated process. A neuron can utilize many different Ca^{2+} entry pathways, some of which are: VGCCs, glutamate receptors, store-operated Ca^{2+} channels, and transient receptor potential channels. VGCCs are intimately involved in the regulation of MeHg-induced toxicity and will be discussed in detail below.

VGCCs are the main entry portals for Ca^{2+}_e . They mediate Ca^{2+} influx as a result of depolarization of the plasma membrane, an energy-independent process. There are two classes of

Type	Channel Subtype	Antagonist	α_1 -Coding Gene	Cell/Tissue-Specific Expression	Function
HVA	L	Phenylalkylamines, dihydropyridines, benzothiazapines, and ω -agatoxin IIIA	α_{1S} (Ca _v 1.1)	Skeletal muscle	Excitation-contraction coupling
			α_{1C} (Ca _v 1.2)	CNS (dendrites and cell bodies)/cardiac muscle	Plasticity/cardiac muscle contraction
			α_{1D} (Ca _v 1.3)	Cochlea	Sensory transduction
				Striatal medium spiny neurons	Neurotransmitter release
				Substantia nigra pars compacta	Pacemaker activity
				Retina	Sensory transduction
	P/Q	ω -agatoxin IVA (P-type), ω -conotoxin MVIIC (Q-type)	α_{1A} (Ca _v 2.1)	Presynaptic terminals	Neurotransmitter release in neuromuscular junctions and CNS
				Purkinje neurons and cerebellar granule cells	Neurotransmitter release
				Thalamus	Involved in depolarization of thalamic neurons
	N	ω -conotoxin GVIA	α_{1B} (Ca _v 2.2)	Only expressed in neurons	Neurotransmitter release
				Nociceptive dorsal root ganglion neurons	Depolarization
	R	SNX 482	α_{1E} (Ca _v 2.3)	Presynaptic terminals	Neurotransmitter release
Hippocampus				Depolarization	
LVA	T	Kurtoxin, mibefradil, amiloride	α_{1G-I} (Ca _v 3.1-3.3)	Dendrites and cell bodies of some CNS neurons	Rhythmic burst firing and pacemaker activity

Table 1.1 Characteristics of HVA and LVA Ca²⁺ channels. Summary of the properties of HVA and LVA Ca²⁺ channels. Table from: Marrero et al., (2013).

VGCCs which are grouped according to the degree of depolarization from resting membrane potential that is needed for their activation: high-voltage activated (HVA) and low-voltage activated (LVA). Their properties are summarized in Table 1.1. HVA channels include L-, N-, P/Q-, and R-type VGCCs. They are separated based on their pharmacological and electrophysiological properties. HVA channels are multimeric proteins composed of one α_1 , β , $\alpha_2\delta$, and sometimes γ subunits. The pore-forming α_1 subunit confers the ion selectivity and pharmacological properties of the channels. The accessory subunits β , $\alpha_2\delta$, and γ modulate the voltage-dependence of activation and inactivation kinetics of the channel. Of particular importance to the work in this dissertation are L- ($\text{Ca}_v1.1-4$) and N- ($\text{Ca}_v2.2$) VGCCs. L-type VGCCs were named “L” because of their long lasting current (for review see: Catterall et al., 2005). L-type channels are antagonized by dihydropyridines (DHPs), such as nifedipine (Nif) and isradipine (Isr) (for review see: Kochegarov, 2003). Both of these antagonists were utilized in experiments described in this dissertation. N-type VGCCs were named “N” because they were first identified in neurons (for review see: Catterall et al., 2005). N-type channels are irreversibly antagonized by ω -conotoxin GVIA (GVIA), which is a snail toxin isolated from the *Conus geographus* snail (Kerr and Yoshikami, 1984; Olivera et al., 1984). The function of HVA VGCCs in response to MeHg is a primary focus of this dissertation.

The main sites of Ca^{2+} buffering are the Ca^{2+} buffering proteins, mitochondria, and smooth endoplasmic reticulum (SER). Maintenance of Ca^{2+} homeostasis is critical for neuronal and loss of Ca^{2+} buffering ability of either the mitochondria or SER could result in neuronal death (Bernardi et al., 1999). The role of the mitochondria in the maintenance of Ca^{2+}

homeostasis and adenosine 5'-triphosphate (ATP) production is central to this dissertation and is discussed in detail below.

Mitochondria have a very important role in the dynamic process of Ca^{2+} homeostasis. The mitochondria have a low affinity but high capacity for Ca^{2+} , thus they require a strong stimulus to induce Ca^{2+} uptake (Somlyo et al., 1985). Under basal conditions mitochondria do not serve as large Ca^{2+} stores however, mitochondrial Ca^{2+} ($[\text{Ca}^{2+}]_m$) levels do fluctuate in response to external stimuli such as neurotransmitter release (Denton and McCormac, 1980; Hansford and Castro, 1981). Ca^{2+} entry into the mitochondria is an energetically favorable process because the inner mitochondrial membrane has a negative membrane potential of approximately 140-180mV (Brand and Murphy, 1986; Bygrave, 1977; Hansford 1985; Reid et al., 1966; Senior, 1988). Ca^{2+} enters the mitochondria via the Ca^{2+} uniporter. The uniporter allows diffusion of Ca^{2+} down its electrochemical gradient from the cytosol, across the inner mitochondrial membrane, to be stored in the mitochondrial matrix (Gunter and Gunter, 1994). Small increases in $[\text{Ca}^{2+}]_m$ stimulate ATP production (Tarasov et al., 2012). However, when large amounts of Ca^{2+} enter the mitochondria it can result in mitochondrial membrane depolarization and an uncoupling of ATP synthesis (Sparagna et al., 1995; Wingrove and Gunter, 1986) demonstrating that there is a balance between Ca^{2+} entry and maintenance of the mitochondrial membrane potential. The main neuronal Ca^{2+} efflux pathway is the $\text{Na}^+/\text{Ca}^{2+}$

exchanger (Crompton et al., 1976). The mitochondria contain a Na^+/H^+ exchanger, which allows the efflux of Na^+ (Gunter and Gunter, 1994). Under conditions of extreme oxidative stress or $[\text{Ca}^{2+}]_m$ overload it can cause the opening of the mitochondrial permeability transition pore (mPTP). The mPTP is a non-selective pore that forms across the inner mitochondrial membrane which allows the passage of any molecule less than 1500 Da (Szabo and Zoratti, 1992; Chernyak and Bernardi, 1996; Pastorino et al., 1999; Szalai et al., 1999; He et al., 2000; Petronilli et al., 2001) and is linked to the induction of cell death (Fang et al., 2008; Gandhi et al., 2009). Acute MeHg exposure causes the opening of the mPTP (Polunas et al., 2011; Limke et al., 2001) and inhibition of its opening protects neurons against MeHg-induced cytotoxicity (Limke et al., 2001; Qu et al., 2013).

The mitochondria are known as the powerhouse of the cell because of their essential role in oxidative phosphorylation and production of ATP (for review see: Tarasov et al., 2012). They contain all of the necessary machinery for oxidative phosphorylation (ATP synthase and complexes I - IV) in their inner membrane. The mitochondrial intermembrane proton gradient drives ATP synthesis (Nelson and Cox, 2005). The rate of mitochondrial oxidative phosphorylation is a tightly regulated process adapting to the neuronal demand in order to maintain neuronal function. Exposure to MeHg places an increased ATP demand on the neuron. MeHg causes an increase in $[\text{Ca}^{2+}]_i$ which is buffered by the mitochondria in an energy-independent manner or by the SER via the smooth endoplasmic reticulum Ca^{2+} ATPase (SERCA). It could also be removed from the cytosol by the plasma membrane Ca^{2+} ATPase.

However, in aging, mitochondria are depolarized (Nicholls, 2002; Toescu, 2005) which causes them to buffer Ca^{2+} and produce ATP less efficiently. This could make them more vulnerable to MeHg.

ii. Calcium and aging

In trying to understand the cellular mechanisms that regulate the aging process Khachaturian (1987) hypothesized that neuronal aging was due to Ca^{2+} changes within the cytosol. This came to be known as the ‘ Ca^{2+} aging hypothesis’. The hypothesis has evolved with increased understanding of changes in the cellular processes during aging but the main premise has remained the same. It is now thought that the breakdown of cellular processes involved in Ca^{2+} homeostasis contributes to cellular dysfunction and ‘aging’ (Toescu and Vreugdenhil, 2010). Changes that occur in the mitochondria may have the most impact on neuronal aging. Mitochondria are instrumental in regulating $[\text{Ca}^{2+}]_i$ and are also large sources of Ca^{2+} . In aged neurons, the mitochondria are depolarized (Toescu, 2005). This results in a decreased Ca^{2+} gradient across the mitochondrial membranes resulting in a decreased ability to buffer changes in cytosolic Ca^{2+} and decreased capacity for ATP production. It has also been reported that aged neurons have a smaller number of larger mitochondrial that are less efficient in the production of ATP (Toescu, 2005). In aged neurons the ER has decreased expression of SERCA and releases larger amounts of Ca^{2+} through inositol-1,4,5-triphosphate receptors (IP_3) and ryanodine receptors (RyR) which contribute to the cytosolic Ca^{2+} load (Toescu, 2007; Toescu and

Vreugdenhil, 2010). Aged neurons also have decreased Ca^{2+} -ATPase expression at the plasma membrane (Toescu, 2007). All of these factors contribute to an inability of aged neurons to efficiently buffer changes in $[\text{Ca}^{2+}]_i$ as well as a decreased ability to respond to an increased demand for ATP. These changes influence an aged neuron's ability to respond to changes in $[\text{Ca}^{2+}]_i$, leaving them vulnerable to stressors and more susceptible to environmental toxicants that alter $[\text{Ca}^{2+}]_i$ such as MeHg.

iii. Methylmercury and calcium regulation

MeHg is a very promiscuous molecule which inhibits many different cellular processes simultaneously causing cellular dysfunction and damage. However, what is so intriguing about MeHg is that despite its promiscuity, it causes cell type-specific damage. The cell type specific damage is not due to the fact that MeHg only accumulates in those cells which have been found to die, such as the cerebellar granule cells. On the contrary, MeHg has been found to accumulate to a greater extent in the cerebellar purkinje cells than the cerebellar granule cells in the rat (Møller-Madson, 1991). Therefore, cells sensitive to MeHg must have unique targets or phenotypes which make them susceptible to MeHg-induced damage. Much of the work done in our and other labs has been aimed at understanding what makes certain cell types uniquely sensitive to MeHg.

Membrane proteins are the first to come in contact with exogenous compounds, so it is not surprising that MeHg alters the function of membrane ion channels. As an initial screen of potential ion channel targets of MeHg, the effects of acute application of MeHg on various ion channels on cerebellar granule cells was tested. It was found that $1\mu\text{M}$ MeHg significantly

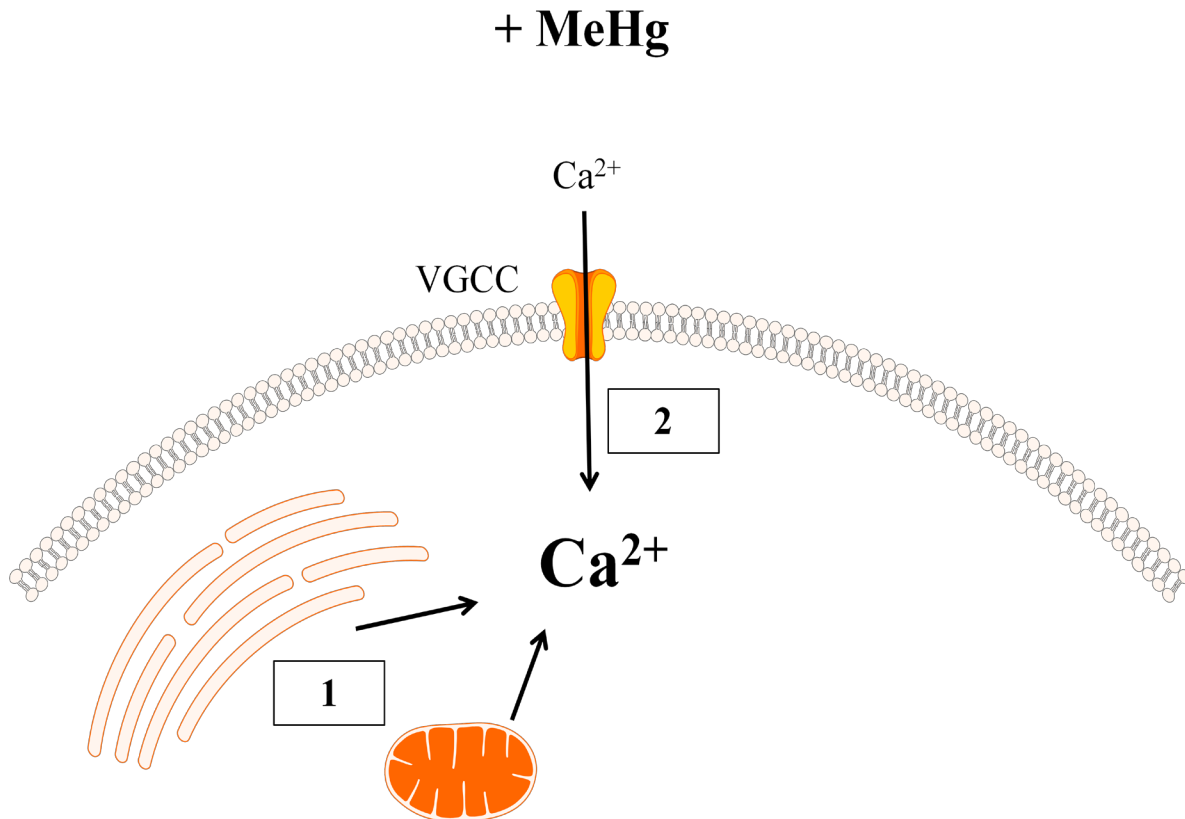


Figure 1.1. Acute MeHg exposure causes a biphasic increase in $[Ca^{2+}]_i$. (A) Diagram representing the MeHg-induced biphasic increase in $[Ca^{2+}]_i$. Acute MeHg exposure causes the release of Ca^{2+} from the SER and mitochondria followed by extracellular Ca^{2+} entry. For interpretation of the references to color in this and all other figures the reader is referred to the electronic version of this dissertation.

reduced current through GABA_A receptors and VGCCs but not inwardly rectifying or voltage-dependent potassium channels (Yuan et al., 2005). This study demonstrated that MeHg specifically targets certain ion channels. Acute application of MeHg in a number of different neuronal preparations has been shown to alter the function of VGCCs. MeHg inhibits the influx of ⁴⁵Ca²⁺ into synaptosomes (Atchison et al., 1986), and blocks dihydropyridine- (DHP) sensitive (L-type) and DHP-insensitive (N-type) Ca²⁺ channels in PC12 cells (Shafer et al., 1990). These effects on VGCCs are irreversible and occur irrespective of channel configuration (Sirois and Atchison, 1996). These studies have demonstrated that VGCCs are unique targets of MeHg.

MeHg also disrupts the dynamic Ca²⁺ homeostasis process (Komulainen and Bondy, 1987; Denny and Atchison, 1994; Marty and Atchison, 1997). Acute application of MeHg to cerebellar granule cells results in a concentration-dependent biphasic increase in [Ca²⁺]_i (Marty and Atchison, 1997). The first phase is due to release of Ca²⁺_i stores, of which a large component is due to release from the mitochondria (Limke, 2001). The second phase is due to Ca²⁺_e entry (Marty and Atchison, 1997). This is shown in Figure 1.1. Co-treatment with Nif or GVIA results in a significant delay in the time-to-onset of both phase 1 and phase 2, demonstrating that VGCCs are involved in MeHg-induced Ca²⁺ dysregulation (Marty and Atchison, 1997). VGCC antagonists have also been shown to delay the onset of behavior impairments and mortality in mice (Bailey et al, 2013; Sakamoto et al., 1996). These studies support the role of VGCCs in MeHg-induced neurotoxicity.

MeHg specifically targets mitochondrial regulation by causing a decrease in Ca^{2+} uptake and inducing its release (Levesque and Atchison, 1991). Activation of the mPTP (Limke and Atchison, 2002) leads to further Ca^{2+} -mediated damage, and is associated with MeHg-induced delayed cell death in cerebellar granule cells. Prevention of mPTP activation by cyclosporin reduces the extent of cerebellar granule cell cytotoxicity. MeHg also causes generation of reactive oxygen species (ROS) (LeBel et al., 1990; Sarafian and Verity, 1991; Yee and Choi, 1996) and induces a delayed-onset cell death (Sarafian et al., 1989; Marty and Atchison, 1998). Therefore any deficiency in Ca^{2+} buffering or extrusion pathways in a neuron may increase its sensitivity to MeHg-induced damage.

c. Striatal and nigrostriatal dopamine system

i. Neuronal organization

The neuronal circuit of the basal ganglia includes a highly organized group of subcortical nuclei involved in motor, associative, cognitive, and mnemonic functions (Bolam et al., 2000). The nuclei include the striatum, globus pallidus, subthalamic nucleus (STN), and SNc. The predominant input into the basal ganglia is from the cortex, and all of the output from the basal ganglia is directed through the thalamus back to the cortex. Diseases associated with the basal ganglia include both Huntington's and PD as well as obsessive-compulsive disorder (Kreitzer and Malenka, 2008). Thus understanding the structure and function of the basal ganglia has become important in understanding the pathology of these diseases. The research described in this thesis is focused on the effects of MeHg on neurons of the striatum and SNc.

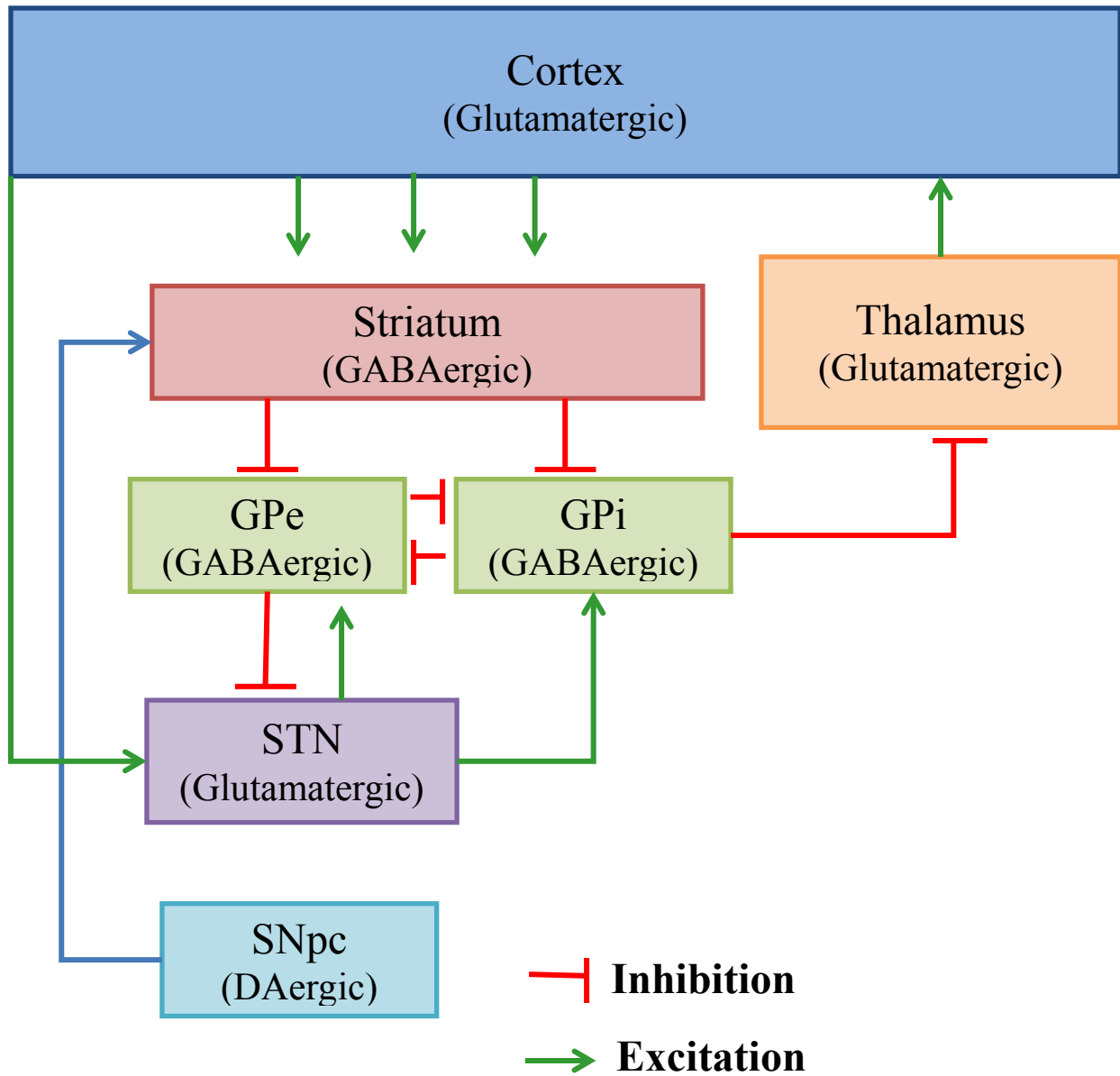


Figure 1.2. Organization of the basal ganglia. The basal ganglia is a highly organized circuit composed of multiple nuclei. GABAergic (inhibitory) projections are represented in red and glutamatergic (excitatory) projections are represented in green. This figure was modified from Obeso et al., (2008).

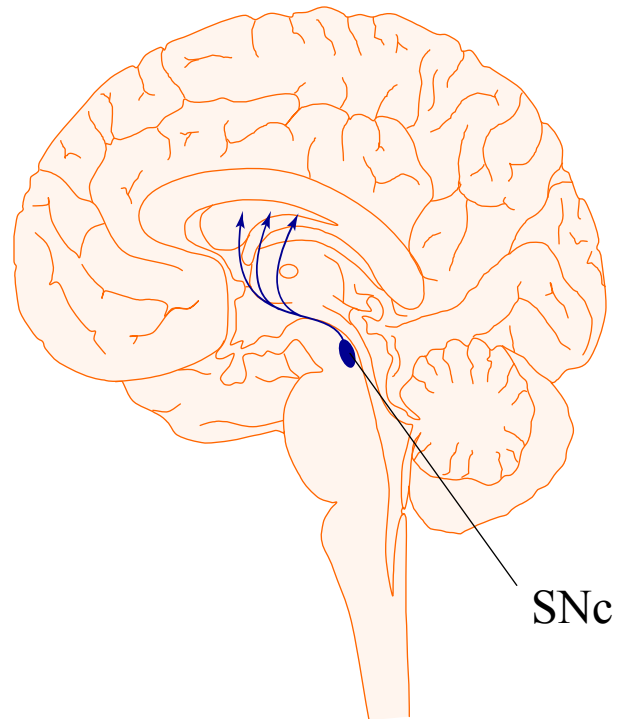


Figure 1.3. A graphic representation of the location of SNc neurons in the human brain. SNc cell bodies are located in the midbrain and their axons project to the striatum where they release DA.

The striatum plays a very important role in motor control, habit formation and motivated behavior. Its function is also altered in a number of neuropsychiatric disorders such as PD (Chuhma, et al., 2011). The striatum has a small population of interneurons: slow-firing large cholinergic neurons, fast-spiking parvalbumin expressing GABAergic neurons, and burst-firing somatostatin/nitric oxide expressing neurons (Bolam et al., 2000). The principal neurons of the striatum are the GABAergic medium spiny neurons (MSN) which make up 90-95% of all neurons in the striatum. MSNs receive glutamatergic input from the cortex and thalamus and dopaminergic input from SNc (Bolam et al., 2000). There are two classes of MSNs, which differ based on the type of DA receptor they express (Surmeier et al., 2007). The striatonigral MSNs express the DA D1 receptor and make up the direct-pathway. These neurons project to the internal globus pallidus (GPi) and substantia nigra pars reticula (Kreitzer and Malenka, 2008). The striatopallidal MSNs express the DA D2 receptor and make up the indirect-pathway. These neurons project to the external globus pallidus (GPe) neurons and which in turn project to the STN (Kreitzer and Malenka, 2008). A representation of this circuit is shown in Figure 1.2. DA plays an essential role in the modulation of the direct- and indirect-pathway. Activation of the D1 receptors activates MSNs while activation of D2 receptors inhibits MSN activity (Kreitzer and Malenka, 2008). Environmental toxicants such as MeHg, which alter neurotransmission or VGCC function, would alter MSN function, fundamentally altering the function of the basal ganglia circuit.

NSDA neuronal cell bodies are located in the SNc and project their axons to the striatum where they release DA, which is involved in the regulation of the movement and coordination (Bergman, 1998). This is shown in Figure 1.3. SNc neurons have a unique physiological

property, in that they autonomously generate action potentials in the absence of synaptic input (Grace and Bunney, 1983). These spontaneously occurring action potentials rely on the influx of Ca^{2+} through $\text{Ca}_v1.3$ channels, an L-type voltage-gated Ca^{2+} channel (Bonci et al, 1998; Ping and Shepard, 1996; Puopolo et al., 2007). As a result, during neuronal activity these neurons have much greater cytosolic Ca^{2+} fluctuations. This places a much higher demand on Ca^{2+} buffering organelles to maintain $[\text{Ca}^{2+}]_i$ at non-toxic levels (Wilson and Callaway, 2000; Chan et al., 2007). The elevated $[\text{Ca}^{2+}]_i$ and increased demand on Ca^{2+} buffering organelles leaves SNc neurons at an increased risk for damage by environmental toxicants that disrupt Ca^{2+} regulation.

ii. Methylmercury and the striatum and the NSDA system

Several studies have demonstrated that neurons of the basal ganglia are susceptible to the neurotoxic effects of MeHg. Lesions occur in the striatum following acute application of MeHg in rats (O’Kusky et al., 1988; O’Kusky and McGeer 1989; Wakabayashi et al., 1995; Sakamoto et al., 1998). Alterations in neuronal function of dopaminergic neurons has also been shown in cells in culture (Gotz et al., 2002; Tiernan et al., 2013), striatal synaptosomes (Komulainen and Tuomisto, 1982, 1985), striatal slices (Kalisch and Racz, 1996), and in *c. elegans* (Vanduyn et al. 2010; Vanduyn and Nass, 2013). A number of the earliest studies demonstrated that exposure to MeHg resulted in a concentration-dependent increase in DA release (Tsuzuki et al., 1982; Komulainen and Tuomisto, 1982; McKay et al., 1986; O’Kusky et al., 1988; Kalisch and Racz, 1996). Researchers went on to find that MeHg-induced increase in DA occurred independently of Ca^{2+}_e (Minnema et al., 1989; Kalisch and Racz, 1996; Faro et al., 2002). This suggests that

MeHg may act intracellularly to induce release of Ca^{2+} stores, which causes neurotransmitter release or it blocks DA uptake via the DA transporter (DAT). MeHg induces release of Ca^{2+} (Levesque and Atchison, 1991; Marty and Atchison, 1997) which may contribute to the increased DA release however, researchers also found that MeHg inhibits DA uptake (Bartolome et al., 1982; Rajanna et al., 1990; Faro et al., 2002). The extent of MeHg-induced DA release can be reduced though the addition of glutathione and cysteine which have free –SH groups which will bind MeHg and reduce its availability (Faro et al., 2005). NMDA receptor antagonists also reduce the extent of MeHg-induced DA release (Faro et al., 2002). Exposure of primary DA neuronal cultures to MeHg resulted in decreased neurite number and cell shrinkage (Gotz et al., 2002). Work in rat striatal synaptosomes suggest that MeHg induces mitochondrial dysfunction due to increased $[\text{Ca}^{2+}]_i$ (Dreiem and Seegal, 2007). This work supports the hypothesis that SNc neurons are susceptible to MeHg-induced toxicity. Increased release and reduced DA uptake in the striatum would result in prolonged exposure and activation of D1/D2 receptors on MSNs, this in combination with MeHg-induced $[\text{Ca}^{2+}]_i$ may result in increased susceptibility to MeHg-induced damage in MSNs.

B) Objectives and Rationale

a. Hypothesis and aims

We hypothesize that exposure to low-doses of MeHg throughout one's lifetime will reduce mitochondrial ATP production and alter Ca^{2+} regulation resulting in neuronal dysfunction; these effects will be exacerbated with aging. Previous studies have characterized the

effects of acute MeHg on mitochondrial function and $[Ca^{2+}]_i$ homeostasis (for review see: Limke and Atchison, 2004). However, the response of an aged animal to MeHg or the consequences of long-term exposure to MeHg on mitochondrial function or Ca^{2+} regulation have not been investigated. Three projects were designed to address these gaps in our knowledge. The first, presented in Chapter 2, uses differentiated SH-SY5Y cells as a model for dopaminergic neurons. Chapter 2 addresses the effects of acute and chronic MeHg treatment on $[Ca^{2+}]_i$ and VGCC function. The second project, presented in Chapter 3, uses Ca^{2+} imaging of striatal slices from young and aged animals to address the effects of aging in response to acute MeHg treatment. Finally, the effects of chronic exposure to a low-dose of MeHg on mitochondrial function and Ca^{2+} regulation is investigated in Chapter 4. Together these aims characterize the effects of aging in response to acute MeHg as well as the effects of chronic MeHg treatment on Ca^{2+} regulation.

b. Model systems

i. SH-SY5Y cell model

Although an *in vivo* system may better mimic what occurs in a human, they also introduce a number of factors that sometimes complicate your experiment making it difficult to interpret the data. A useful alternative is a human-derived cell line. *In vitro* studies allow for the investigation of mechanisms in an isolated system without the confounding factors present in animal studies. SH-SY5Y cells are an extensively characterized immortalized human neuroblastoma cell line that have been utilized as a model in toxicology, neuronal differentiation,

and to study different aspects of neurodegenerative diseases (Biedler et al., 1978; Pahlman et al., 1990; Wang et al., 2011; Noelker et al., 2012). SH-SY5Y cell line was sub-cloned from the SK-N-SH cell line, which was isolated from a bone marrow biopsy of a 4yr old female with a neuroblastoma (Bielder et al., 1973; Bielder et al., 1978; Ross et al., 1983). In the undifferentiated state these cells are proliferative and express low levels of neuronal markers. However, with the addition of all-*trans*-retinoic acid (RA) SH-SY5Y cells acquire a neuron-like phenotype they produce an extensive neuronal network and express neuronal markers such as tyrosine hydroxylase, neuron-specific enolase and neuronal nuclei protein (Nordin-Andersson et al., 1998; Lopes et al., 2010; Pahlman et al., 1990). In the differentiated state SH-SY5Y cells also express functional VGCCs primarily, N- and L-type Ca²⁺ channels (Morton et al., 1992; Reuveny and Narahashi, 1993).

SH-SY5Y cells are most commonly utilized as an *in vitro* model for neurodegenerative diseases (Agholme et al., 2013; Qualis et al., 2013; Yu et al., 2013), however they have also been used to study the toxic effects of MeHg. Some of the first studies demonstrated that SH-SY5Y cells are susceptible to MeHg-induced cytotoxicity following acute exposure (Nordin-Andersson et al., 1998; Sanfeliu et al., 2001; Toimela and Tahti, 2004). MeHg-induced cytotoxicity induces oxidative stress and cells can be protected with the addition of antioxidants (Kim et al., 2005; Toyama et al., 2007; Franco et al., 2009). MeHg also disrupts SH-SY5Y cell differentiation (Kim et al., 2007). Petroni et al., (2012, 2013) found that exposure to 100nM MeHg for 48h induced oxidative stress leading to cytotoxicity and this can be prevented by co-treatment with an NMDA receptor antagonist. Differentiated SH-SY5Y cells were used in Chapter 2 to study the effects of chronic MeHg treatment on VGCC function and Ca²⁺ regulation.

ii. Synaptosomes

Synaptosomes are isolated nerve endings prepared from the rodent brain. They are isolated using density gradient centrifugation of brain homogenate. Synaptosomes were first isolated in 1958 to identify the subcellular compartment of acetylcholine (Hebb and Whittaker, 1958). They have since been fully characterized and used extensively in neuroscience research (for review see: Whittaker, 1992). Synaptosomes are essentially nerve endings that are pinched off and then re-form their plasma membrane. They maintain a resting membrane potential, can regulate Ca^{2+} , produce ATP, and produce, store and release neurotransmitter (Whittaker, 1992; Whittaker et al., 1964). The main advantage of using synaptosomes is the ability to study nerve terminal function in isolation.

Synaptosomes have been extensively used to investigate alterations in presynaptic neuronal function following MeHg exposure. Many of the early studies utilized synaptosomes to characterize changes in neurotransmitter uptake and release due to MeHg exposure (Braken et al., 1981; Komulainen and Tuomisto, 1982; Komulainen and Tuomisto, 1985; Minnema et al., 1989; Rajanna et al., 1990). These studies demonstrated that MeHg induced DA release and inhibited its uptake in rat brain synaptosomes. Synaptosomes have been used in our lab to study the effects of MeHg on intracellular Ca^{2+} homeostasis, mitochondrial function and VGCC function (Atchison et al., 1986; Shafer and Atchison 1989; Shafer et al., 1990; Hare and Atchison, 1992; Levesque et al., 1992; Denny et al., 1993). Based on these studies we learned that acute MeHg treatment blocks Ca^{2+} influx through VGCCs, inhibits the binding of DHP-antagonists, interacts with nerve-terminal mitochondria causing a depolarization of the

membrane and Ca^{2+} release, and induces extracellular Ca^{2+} entry. These studies have been instrumental in furthering our understanding on the role of MeHg-induced Ca^{2+} dysregulation. As such, this model system was used to study the presynaptic effects of chronic MeHg treatment on mitochondrial function in striatal synaptosomes in chapter 4.

iii. Striatal Slice

One particularly useful model system is the acute live brain slice. This technique was developed to study the function of neurons in an environment similar to that *in vivo*, as some of the integrity of the neuronal network is preserved and neurons maintain some contacts present in the brain (Andersen et al., 1977; Schwartzkroin and Andersen, 1975; Skrede and Westgaard, 1971; Yamamoto and McIlwain, 1966). Thin slices (200 μm) of neuronal tissue are taken from the brain and are able to maintain viability for many hours when kept in an oxygenated artificial cerebrospinal fluid (ACSF) buffer. The effects of acute MeHg exposure on synaptic function have been studied in hippocampus and cerebellar brain slices in our laboratory (Yuan and Atchison, 1993, 1994, 1995, 1997, 2003). Cerebellar and brainstem slices have also been used to study the effects of $[\text{Ca}^{2+}]_i$ regulation using imaging techniques (Yuan and Atchison, 2007; Johnson et al., 2011). Live brain slices were utilized to study the $[\text{Ca}^{2+}]_i$ response of striatal MSNs from different age animals to acute MeHg treatment in Chapter 3 and to study the effects of chronic MeHg treatment on MSN Ca^{2+} regulation in Chapter 4.

c. Techniques

i. Calcium imaging

From the previous described background it is clear that MeHg alters neuronal Ca^{2+} regulation. There are a number of tools currently available to study changes in $[\text{Ca}^{2+}]_i$ (for review see: Paredes et al., 2008). We decided to utilize the fluorescent fluorophores fura-2 acetoxymethyl ester (fura-2AM) and fluo-4 no wash (Fluo-4NW). Both of these fluorophores have been extensively used to monitor MeHg-induced $[\text{Ca}^{2+}]_i$ changes (Hare et al., 1993; Marty and Atchison, 1997; Limke et al., 2002; Yuan and Atchison, 2007; Johnson et al., 2011).

The Ca^{2+} fluorophore fura-2AM was utilized for ratiometric $[\text{Ca}^{2+}]_i$ measurements in SH-SY5Y cells in Chapter 2 and in striatal slices in Chapter 4. Fura-2 has a high affinity for Ca^{2+} , however it will also bind other divalent cations such as zinc (Zn^{2+}). The use of a ratiometric fluorophore compensates for variability in fluorophore loading between cells, particularly when loading fluorophore in thick tissue slices. The -AM group confers fura-2 lipid solubility, allowing it to cross the cell membrane. During incubation the -AM group is cleaved by intracellular esterases. Subsequently fura-2 is trapped inside the cell where it preferentially binds to Ca^{2+} . Fura-2 is excited using 340nm and 380nm (corresponding to bound vs. unbound fura-2) and emits at 520nm. An increase in 340nm/380nm ratio corresponds to an increase in $[\text{Ca}^{2+}]_i$.

In addition to its use as continuously monitoring changes in $[Ca^{2+}]_i$, fura-2 can be used to determine the resting $[Ca^{2+}]_i$ of cells. Fura-2 fluorescence is continuously monitored under conditions of maximal fluorescence when fura-2 is saturated and under minimum fluorescence when there is zero Ca^{2+} present. Based on the fluorescence values under resting, maximum, and minimum fluorescence, the resting $[Ca^{2+}]_i$ can be determined. The mathematical relationship described by Grynkiewicz et al. (1985), states:

$$[Ca^{2+}]_i = K_d * Sf2/Sb2 * (R-R_{min})/(R-R_{max})$$

Where K_d (222nM) is equal to the dissociation constant for fura-2- Ca^{2+} binding. The values of Sf2 and Sb2 are equal to the value of 380nm fluorescence in Ca^{2+} -free and Ca^{2+} -saturating conditions, respectively. The values R , R_{min} , and R_{max} are equal to the ratio value under resting, Ca^{2+} -free, and Ca^{2+} -saturating conditions. It has been previously determined that MeHg induces Zn^{2+} release (Denny and Atchison, 1994), which can then be bound by fura-2 altering estimations of $[Ca^{2+}]_i$. Therefore the Zn^{2+} chelator TPEN was present during all of the experiments when $[Ca^{2+}]_i$ was determined.

Fluo-4NW was utilized in chapter 3 to monitor spatial changes in Ca^{2+}_i in striatal slices in response to acute MeHg treatment. Fluo-4 is a Ca^{2+} sensitive fluorophore commonly used to monitor changes in Ca^{2+}_i . Unlike fura-2, fluo4 is not a ratiometric fluorophore and cannot be

used to determine $[Ca^{2+}]_i$. Fluo-4 is excited at 485nm and emits at 520nm. An increase in fluo-4 fluorescence corresponds to an increase in Ca^{2+}_i .

ii. Mitochondrial function

The Extracellular Flux Analyzer (XF Analyzer, Seahorse Biosciences) was used to measure mitochondrial function of striatal synaptosomes described in chapter 4. The XF Analyzer provides real-time measurements of the extracellular flux of oxygen and protons in medium surrounding live cells, synaptosomes, or mitochondria. Addition of 4 different chemicals- oligomycin, carbonyl cyanide 4-(trifluoromethoxy) phenylhydrazone (FCCP), rotenone, and antimycin A- perturbs mitochondrial function and allows for the determination of the bioenergetic capacity of mitochondria. The use of each chemical provides information about different aspects of the bioenergetic capacity. Oligomycin inhibits ATP synthesis and allows for the determination of the oxygen consumption devoted to ATP synthesis. FCCP is an uncoupling agent and causes a collapse of the inner-mitochondrial membrane potential, its addition allows for the determination of the maximal respiration capacity. Finally, addition of a combination of antimycin A and rotenone which are inhibitors of complex I and III respectively, inhibit mitochondrial respiration and allows for the determination of the oxygen devoted to non-mitochondrial respiration. This is demonstrated in Figure 1.4. The XF Analyzer has been utilized to study changes in cellular metabolism in response to toxicants or disease states as well as a number of different physiologic changes (for review see: Brand and Nicholls, 2011).

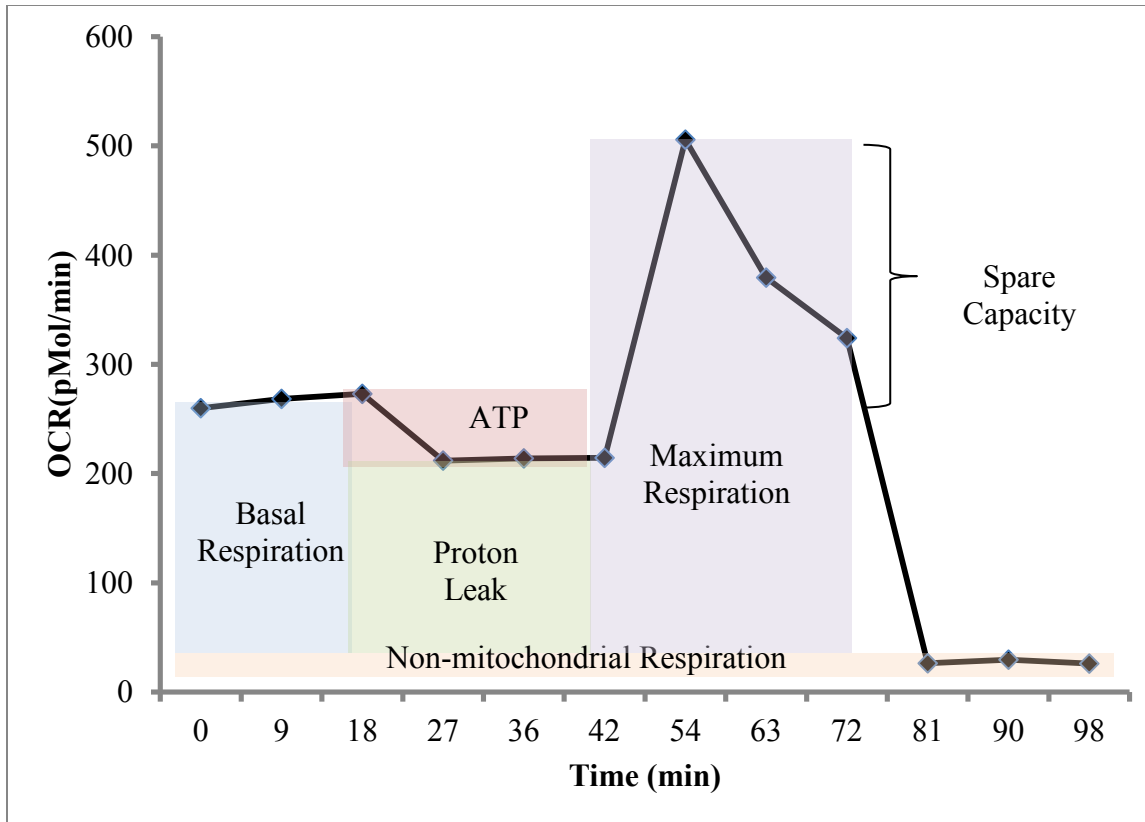


Figure 1.4. A depiction of an XF Analyzer experiment measuring mitochondrial OCR. Perturbation of mitochondrial oxidative phosphorylation allows for the determination of mitochondrial basal respiration, ATP production, maximal respiration, spare capacity, non-mitochondrial respiration, and proton leak.

CHAPTER TWO

PERTURBATION OF CALCIUM REGULATION FOLLOWING ACUTE AND CHRONIC METHYLMERCURY TREATMENT IN DIFFERENTIATED SH-SY5Y CELLS

A) Abstract

MeHg causes a loss of the cerebellar granule cells in the cerebellum in a Ca^{2+} dependent manner. *In vitro* studies have shown that acute MeHg treatment caused a biphasic increase in $[\text{Ca}^{2+}]_i$ which can be delayed by VGCC antagonists, demonstrating the role of VGCCs in MeHg-induced Ca^{2+} dysregulation. Others have shown effects of MeHg on DA release; numerous studies have addressed the acute effects of MeHg on cholinergic and dopaminergic cell lines and primary neurons. However, exposure to low levels of MeHg during lifetime are lacking. As such, our aim was to study effects of chronic MeHg treatment on VGCC function in differentiated SH-SY5Y cells, a dopaminergic cell line. These cells have not been extensively used to study MeHg neurotoxicity, so we first characterized the acute effects of MeHg on $[\text{Ca}^{2+}]_i$ in SH-SY5Y cells. Changes in $[\text{Ca}^{2+}]_i$ were measured using Fura-2; cells were perfused continuously with 1, 2, 5, or 10 μM MeHg. MeHg caused a biphasic, concentration-dependent increase in fura-2 fluorescence; the times to onset of both phases were inversely proportional to the [MeHg]. At 1 μM MeHg phase 1 and phase 2 occurred at ~11 and 49min respectively, whereas at 10 μM phase 1 occurred within 2 min and phase 2 within 16 min. Nif (5 μM) and GVIA (1 μM), L- and N-type antagonists respectively, delayed the onset of phase 2 but not phase 1. Effects of chronic MeHg treatment on VGCC function were subsequently characterized. Cells were treated with 0 or 20nM MeHg for 48 or 72h. Changes in $[\text{Ca}^{2+}]_i$ were monitored using fura-2, KCl-induced (40mM) Ca^{2+} influx was monitored as an index of VGCC function. Ca^{2+} influx through L- and N-type VGCCs was isolated using GVIA and Nif respectively. The 48h

treatment significantly decreased KCl-induced Ca^{2+} influx through L-type VGCCs; the 72h treatment significantly decreased KCl-induced Ca^{2+} influx through both L- and N-type VGCCs. The 72h treatment also caused a significant increase in resting $[\text{Ca}^{2+}]_i$. Thus chronic MeHg treatment significantly increases resting $[\text{Ca}^{2+}]_i$ and decreased KCl-induced Ca^{2+} increase.

B) Introduction

MeHg is an environmental neurotoxicant that causes cell-type specific damage in the central nervous system. Humans are most commonly exposed to MeHg through the consumption of contaminated seafood. The effects of both acute and long-term exposure to MeHg on humans results in cerebellar ataxia, paresthesia, and constriction of the visual field (Bakir, 1973; Harada, 1995). Development of these symptoms may be related to MeHg-induced alterations in VGCC function and $[Ca^{2+}]_i$ homeostasis. The effects of acute MeHg treatment on Ca^{2+}_i regulation and VGCC function have been characterized. However the effects of chronic MeHg are largely unknown.

Granule cells of the cerebellum are particularly sensitive to the effects of MeHg (Hunter and Russell, 1954). Acute MeHg treatment of primary cerebellar granule cells results in a biphasic increase in $[Ca^{2+}]_i$. The first phase is due to release of Ca^{2+}_i stores from the mitochondria and SER (Hare and Atchison, 1995; Limke and Atchison, 2001). The second phase is due to extracellular Ca^{2+} (Ca^{2+}_e) entering the cell (Marty and Atchison, 1997). Both phase 1 and phase 2 can be delayed through the use of the L- or N-type VGCC antagonists, Nifedipine and GVIA respectively (Marty and Atchison, 1997). This evidence demonstrates the role of VGCCs in MeHg-induced Ca^{2+} -dysregulation. Acute application of MeHg also alters function of VGCCs in a number of different neuronal preparations. MeHg inhibits the influx of $^{45}Ca^{2+}$ into neuronal synaptosomes (Atchison et al., 1986), and blocks DHP sensitive (L-type) and DHP-insensitive

(N-type) Ca^{2+} channels in PC12 cells (Shafer et al., 1990). These effects on VGCCs are irreversible and occur irrespective of channel configuration (Sirois and Atchison, 1996).

Changes in neurotransmission have also been associated with MeHg exposure. Acute MeHg treatment causes increased DA release. This has been demonstrated in cells in culture (Tiernan et al., 2013), striatal synaptosomes (Dreiem et al., 2009), striatal slices (Kalisch and Racz, 1996), and *in vivo* (Faro et al., 2000, 2003, 2007). Acute MeHg exposure causes an increase in $[\text{Ca}^{2+}]_i$ so it is not surprising that it also causes increased neurotransmitter release in DA neurons. Taken together, the data support the hypothesis that DA neurons are susceptible to MeHg-induced Ca^{2+} dysregulation.

Long-term exposure to low levels of MeHg throughout ones lifetime are of contemporary concern. The goal of this study was to determine the effects of chronic MeHg exposure on VGCC function in differentiated SH-SY5Y cells, KCl-induced Ca^{2+} influx was used as an index of VGCC function and membrane integrity. Chronic treatment could result in no change, increased Ca^{2+} influx, or decreased Ca^{2+} influx upon KCl-induced VGCC activation. Acute treatment with MeHg blocks Ca^{2+} current through VGCCs (Shafer et al., 1990; Sirois and Atchison, 2000). However, MeHg also mediates a biphasic increase in $[\text{Ca}^{2+}]_i$, which can be delayed with an L- or N-type Ca^{2+} channel antagonist (Marty and Atchison, 1997). These data seem to be contradictory. However one explanation may be that MeHg uses VGCCs for entry into the cell, which competitively blocks the channel. Once inside the cell, MeHg interacts with

the channel to enhance extracellular Ca^{2+} influx. We expect that at least initially MeHg will block VGCCs causing decreased Ca^{2+} influx. These changes will be time-dependent.

SH-SY5Y cells are a well characterized immortalized human neuroblastoma cell line, which can be differentiated with the addition of RA. Upon differentiation they produce an extensive neural network, express tyrosine-hydroxylase, and functional L- and N-type VGCCs (Nordin-Andersson et al., 1998; Lopes et al., 2010; Pahlman et al., 1990; Morton et al., 1992; Reuveny and Narahashi, 1993). Very limited work has been done to characterize the effects of acute MeHg treatment in SH-SY5Y cells. It has been shown that they are susceptible to MeHg-induced ROS production and cytotoxicity (Petroni et al., 2010 and 2011). Changes in $[\text{Ca}^{2+}]_i$ following acute MeHg treatment have not been characterized in differentiated SH-SY5Y cells.

The goals of this study were two fold. The first was to characterize the $[\text{Ca}^{2+}]_i$ response to acute MeHg treatment and determined the contribution of VGCCs in the SH-SY5Y cell response. The second goal was to determine the effects of chronic MeHg treatment on VGCC function in differentiated SH-SY5Y cells. The results of this study demonstrate that acute MeHg treatment causes the characteristic biphasic increase in $[\text{Ca}^{2+}]_i$ in differentiated SH-SY5Y cells. The time-to-onset of phase 2 can be delayed with Nif or GVIA. Chronic MeHg treatment causes a time- and subtype specific block of VGCCs. These data demonstrate that acute and chronic MeHg treatment alters VGCC function in a similar manner.

C) Materials and methods

Chemicals and solutions

Methylmercuric (II) chloride was obtained from Aldrich Chemical (Milwaukee, WI). Fura-2AM, minimum essential medium (MEM), F12, antibiotic/antimycotic, collagen I- rat tail, ionomycin, and tetrakis-(2-pyridylmethyl)ethylenediamine (TPEN) were obtained from Life Technologies (Carlsbad, CA). RA and Nif were obtained from Sigma-Aldrich (St. Louis, MO). Fetal bovine serum (FBS) was obtained from Atlanta Biologicals (Flowery Branch, GA). GVIA was obtained from Alamone Labs (Jerusalem, Israel).

HEPES buffered saline (HBS) contained (mM) 135 NaCl, 5 KCl, 1 MgCl₂, 2 CaCl₂, 20 d-glucose and, 20 HEPES, pH 7.3. The 40mM KCl solution contained the same components as HBS except that the NaCl was lowered to 115.4 mM. R_{min} solutions contained (mM) 130 NaCl, 5.4 KCl, 0.8 MgSO₄, 20 d-glucose, 20 HEPES and, 10 EGTA. R_{max} solutions contained (mM) 150 NaCl, 5.4 KCl, 8 CaCl₂, 0.8 MgSO₄, 20 d-glucose and, 20 HEPES. Both R_{min} and R_{max} solutions contained 10μM ionomycin and 35μM TPEN. Ionomycin is a Ca²⁺ ionophore. It was added to the solutions to facilitate Ca²⁺ transport across the plasma membrane. MeHg treatment alters intracellular [Zn²⁺] (Denny and Atchison, 1994) which can bind to fura-2 and skew Ca²⁺ measurements. TPEN was added to the loading solution to chelate Zn²⁺ prior to initiating Ca²⁺ recording.

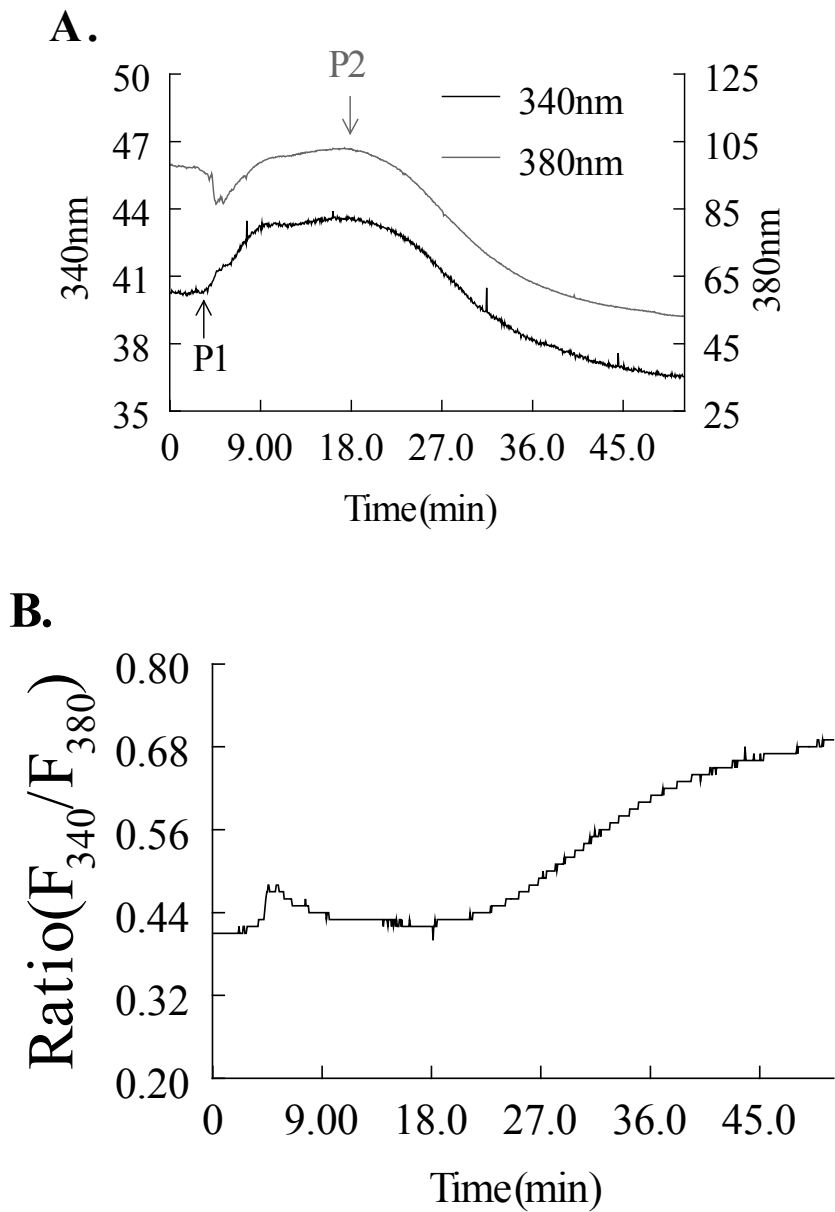


Figure 2.1. Acute MeHg treatment in differentiated SH-SY5Y cells caused a biphasic increase in $[\text{Ca}^{2+}]_i$. (A-B) Representative 340nm, 380nm, and ratio of ($F_{340\text{nm}}/F_{380\text{nm}}$) fura-2 tracings from a single differentiated SH-SY5Y cell treated acutely with $5\mu\text{M}$ MeHg. (A) Representative 340nm tracing is shown in black. 340nm fluorescence corresponds to changes in Ca^{2+} -bound fura-2. The onset of phase 1 was the time at which the 340nm tracing increases from baseline. Representative 380nm tracing is shown in grey. 380nm fluorescence corresponds to changes in unbound fura-2. The onset of phase 2 was the time at which the 380nm tracing had a sustained decrease from baseline. (B) Representative ratio of ($F_{340\text{nm}}/F_{380\text{nm}}$). An increase in fluorescence of the ratio corresponds to an increase in $[\text{Ca}^{2+}]_i$. Acute $5\mu\text{M}$ MeHg treatment caused a biphasic increase in $[\text{Ca}^{2+}]_i$.

Cell Culture

SH-SY5Y cells (ATCC #CRL-2266) used in these studies were from passages 3-10 from our receipt. Cells were grown in 1:1 MEM/F12 (v/v) medium plus 10% (v/v) FBS and antibiotic/antimycotic (SH-SY5Y medium). For all experiments, 2.5×10^5 cells/mL were seeded on collagen (250 μ g/ml)- coated glass coverslips. Twenty-four hours after plating, the medium was replaced with SH-SY5Y medium containing 10 μ M RA (differentiation medium). Cells were grown for 5 days in differentiation medium with a medium exchange every 48h.

Single-cell microfluorimetry

Microfluorimetry experiments were performed using a IX-70 microscope (Olympus, Tokyo, Japan) coupled to an IonOptix (Milton, MA) system with a heated perfusion system (37°C, 3ml/min). Alterations in $[Ca^{2+}]_i$ were monitored through the use of the Ca^{2+} -sensitive ratiometric fluorophore fura-2. SH-SY5Y cells were loaded with 3 μ M fura-2AM in HBS for 45m at 37°C. During incubation the -AM group of fura-2 is cleaved by esterases in the cell. Subsequently, ionized fura-2 is trapped inside the cell where it binds preferentially to Ca^{2+} . Prior to initiating recording, cells were washed with HBS for 10m to remove excess unbound fura-2 and allow the cells to reach homeostasis. Cells were then depolarized with 40mM KCl to check cell viability and assure they are able to buffer increases in $[Ca^{2+}]_i$. If cells did not respond to KCl, they were not used for data analysis. Fura-2 was excited at 340 and 380nm (bound and unbound fura-2, respectively). Changes in fura-2 fluorescence ratio were recorded at 510nm. An increase in the 340nm/380nm ratio corresponds to an increase in $[Ca^{2+}]_i$.

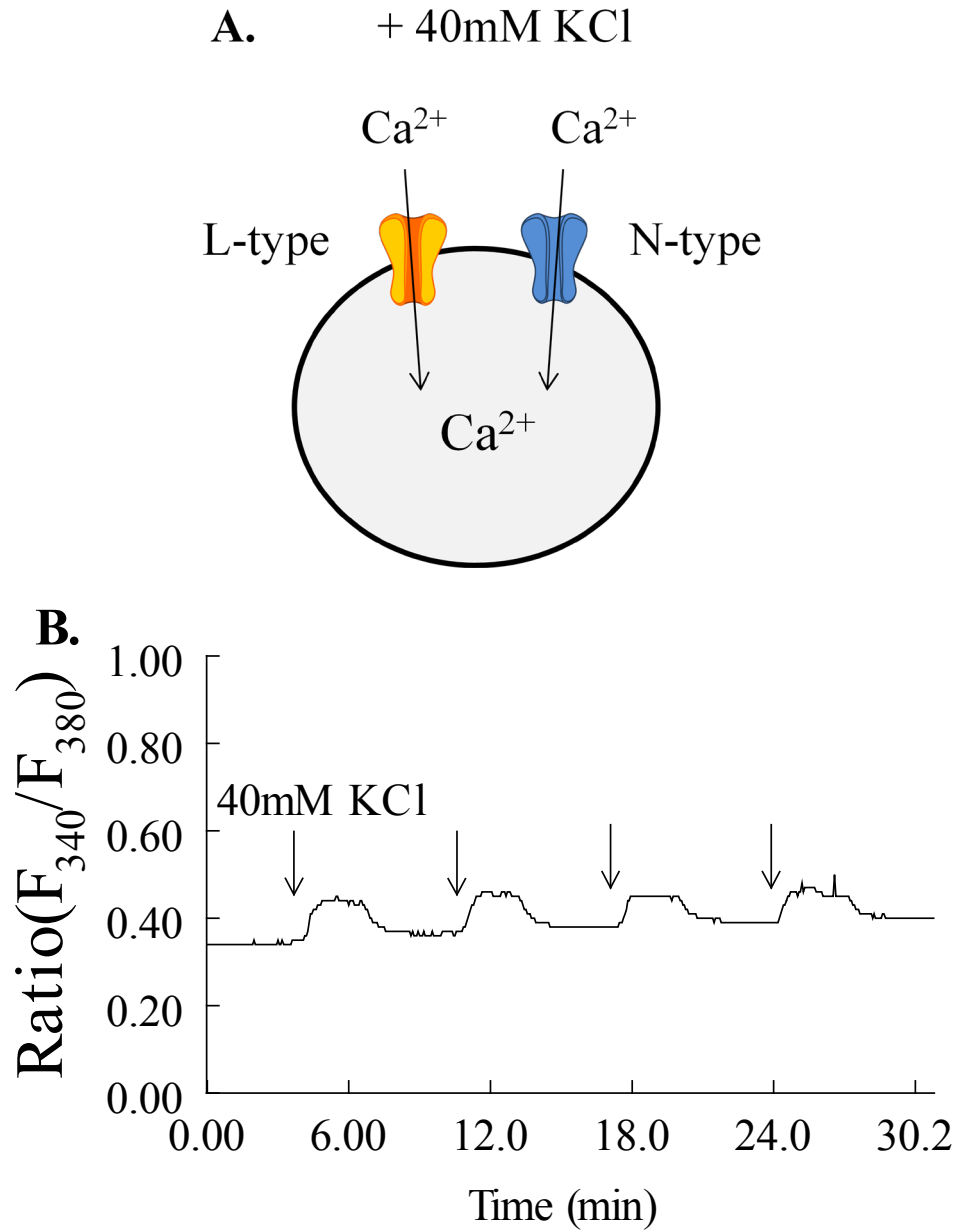


Figure 2.2. Measurement of VGCC function. (A) Schematic diagram of how VGCC function was measured. VGCCs were activated by depolarizing the cell membrane with 40mM KCl which activated VGCCs and allowed Ca^{2+} influx through L- and N-type channels. (B) Representative fura-2 tracing from a single differentiated SH-SY5Y cell treated with 0nM MeHg for 48h. Application of 40mM KCl is indicated by the arrows. The amplitude of KCl-induced Ca^{2+} influx was measured for each depolarization and averaged to determine a mean amplitude for each experiment (n=1).

MeHg treatments

Cells were loaded with fura-2 and then superfused with 1, 2, 5, or 10 μ M MeHg. All MeHg solutions were prepared on the day of experiment from a 10mM stock solution. The contribution of N- or L-type VGCC's in MeHg-induced $[Ca^{2+}]_i$ increases were determined through the use of VGCC antagonists. The contribution of N-type VGCC's was determined by pre-treating cells with 1 μ M GVIA. The contribution of L-type VGCC's was determined by the co-treatment with 5 μ M nifedipine. The onset of the first phase was measured manually by determining the time at which the 340nm tracing rose irreversibly from baseline (Figure 2.1a). The onset of the second phase was determined as the time at which the 380 tracing had an irreversible decrease from baseline (Figure 2.1a). The ratio of these tracing demonstrates that acute MeHg treatment results in a biphasic increase in $[Ca^{2+}]_i$ (Figure 2.1b).

To determine the effects of prolonged MeHg treatment on VGCC function, differentiated SH-SY5Y cells were treated with 0 or 20nM MeHg for 48 or 72h. MeHg treatment medium contained no FBS or antibiotic/antimycotic. Medium was exchanged every 24h. Upon completion of the treatment period, cells were loaded with fura-2AM using the method that was described previously. VGCC function was measured by depolarizing the cell membrane using 40mM KCl, which activated VGCCs and allowed Ca^{2+} influx (Figure 2.2a,b). Using the 340nm/380nm tracing the maximum amplitude of KCl-induced Ca^{2+} influx was measured for each depolarization and averaged to determine a mean amplitude for each plate (n=1). The function of L- and N-type VGCCs was determined through the use of Nif and GVIA. Cells were depolarized 4 times with 40mM KCl. The first depolarization was considered the control and

occurred with no antagonist present. The following 3 depolarizations occurred in the presence of an antagonist (Figure 2.3a,b). The amplitude of KCl-induced Ca^{2+} influx was quantified for each depolarization. The mean amplitude of the depolarizations in the presence of antagonist was divided by the amplitude of the control depolarization to determine the percent of control. KCl-induced Ca^{2+} influx through L-type VGCCs was isolated by blocking N-type VGCCs. Cells were incubated with $1\mu\text{M}$ GVIA for 5m prior to the application of KCl. KCl-induced Ca^{2+} influx through N-type VGCC's was isolated by blocking L-type VGCCs with $5\mu\text{M}$ Nif. Nif was present in HBS and KCl solutions throughout the experiment.

Determination of $[\text{Ca}^{2+}]_i$

Fura-2 was used to determine the $[\text{Ca}^{2+}]_i$ of treated and untreated cells. The mathematical relationship of fura-2 fluorescence and $[\text{Ca}^{2+}]_i$ was described by Grynkiewicz et al. (1985), it states:

$$[\text{Ca}^{2+}]_i = K_d * \text{Sf2/Sb2} * (R - R_{\min}) / (R_{\max} - R)$$

Calculating the resting $[\text{Ca}^{2+}]_i$ is possible by controlling the $[\text{Ca}^{2+}]_i$ of cells. This is done by removing essentially all Ca^{2+} (R_{\min}) and saturating fura-2 (R_{\max}). The value used for the dissociation constant for fura-2- Ca^{2+} binding (K_d) was 225nM (Ionoptix, Tools for Cardiovascular Research). R is equal to the resting ratio value. The ratio of Sf2 and Sb2 is equal to the value of the denominator (380nm) under zero Ca^{2+} conditions (Sf2) and saturating Ca^{2+}

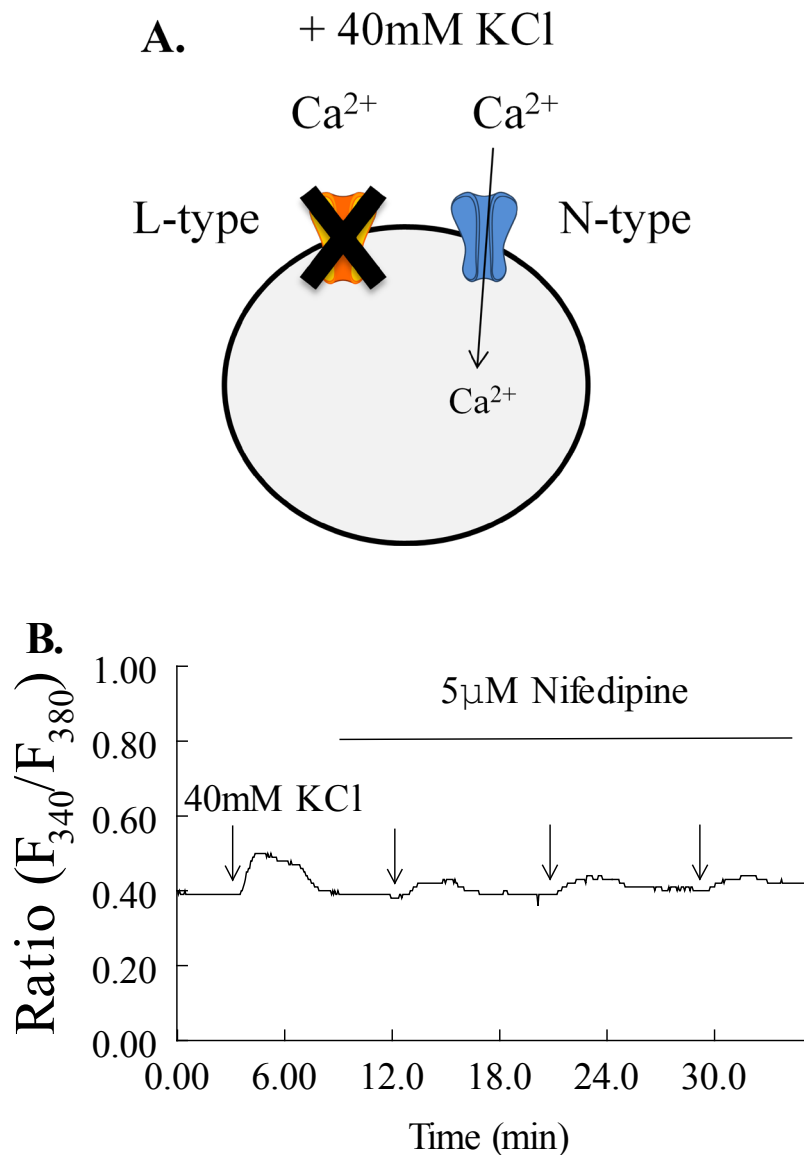


Figure 2.3. Determination of VGCC subtype sensitivity to chronic MeHg treatment. (A) Schematic diagram of how VGCC function was measured. SH-SY5Y cells were pretreated with either 1 μ M GVIA or 5 μ M nifedipine (as shown in diagram) and then depolarized with 40mM KCl. Subsequent Ca²⁺ influx was due solely to flow through the unblocked channel resulting in decreased Ca²⁺ influx. **(B)** Representative fura-2 tracing from a single differentiated SH-SY5Y cell treated with 0nM MeHg for 48h. Application of 40mM KCl is indicated by the arrows. The (Figure 2.3 cont'd) first depolarization was considered the control and occurred with no antagonist present. The following 3 depolarizations occurred in the presence of antagonist. The amplitude of KCl-induced Ca²⁺ influx was quantified for each depolarization. The mean amplitude of the depolarizations in the presence of antagonist was divided by the amplitude of the control depolarization to determine the percent of control.

conditions (Sb2). SH-SY5Y cells were treated with 0 or 20nM MeHg for 72h and then loaded with fura-2 as previously described. Cells were washed for 5min with normal HBS to allow establishment of a baseline. Next cells were perfused with R_{\min} solution for 5min. The R_{\min} solution contains no Ca^{2+} and EGTA, a Ca^{2+} chelator. Perfusion with this solution will remove all Ca^{2+} present and the 340nm/380nm will reach its minimum value. The R_{\min} solution is followed by perfusion with the R_{\max} solution for 5min. The R_{\max} solution contains 8mM Ca^{2+} which will saturate fura-2 and the 340nm/380nm will reach its maximum value.

Statistics

Comparisons of mean time-to-onset were made using One-Way ANOVA followed by Tukey-Kramer multiple comparisons *post hoc* test, $p < 0.05$. Comparisons of 2 means were made using an unpaired two-tailed student t-test, $p < 0.05$.

D) Results

a. Acute methylmercury treatment

Events that occur over a prolonged period of time, such as chronic treatment, can result in direct as well as secondary or tertiary results that may be far-removed consequences of prolonged exposure. As such, the first crucial step in determining the chronic effects of MeHg on differentiated SH-SY5Y cells is to parse out the initiating events. This was achieved by characterizing the Ca^{2+} response to acute MeHg treatment. Differentiated SH-SY5Y cells were loaded with fura-2AM and then superfused with 1, 2, 5, or 10 μM MeHg until P2 was reached and the 340nm/380nm tracing plateaued (there was no further increase in intracellular calcium) (Figure 2.1A,B). Acute MeHg treatment caused a biphasic increase in $[\text{Ca}^{2+}]_i$ (Figure 2.1B). The time-to-onset of phase 1 was the time at which the 340nm fluorescence tracing increased and the time-to-onset of phase 2 was the time that the 380nm fluorescence tracing irreversibly decreased from baseline (Figure 2.1A). The time-to-onset of phase 1 and phase 2 was inversely related to $[\text{MeHg}]$ with a decrease in the time-to-onset with increasing $[\text{MeHg}]$ (Figure 2.4). At 1 μM MeHg phase 1 and phase 2 occurred in approximately 11min and 49min respectively. When cells were treated with 5 and 10 μM MeHg there was a statistically significant hastening in the time-to-onset of phase 2 compared to 1 μM MeHg. These results are consistent with work done in rat cerebellar granule cells (Marty and Atchison, 1997).

The next step was to determine if L- or N-type VGCCs contribute to the biphasic increase in $[\text{Ca}^{2+}]_i$ in differentiated SH-SY5Y cells. This was investigated by antagonizing L- or N-type

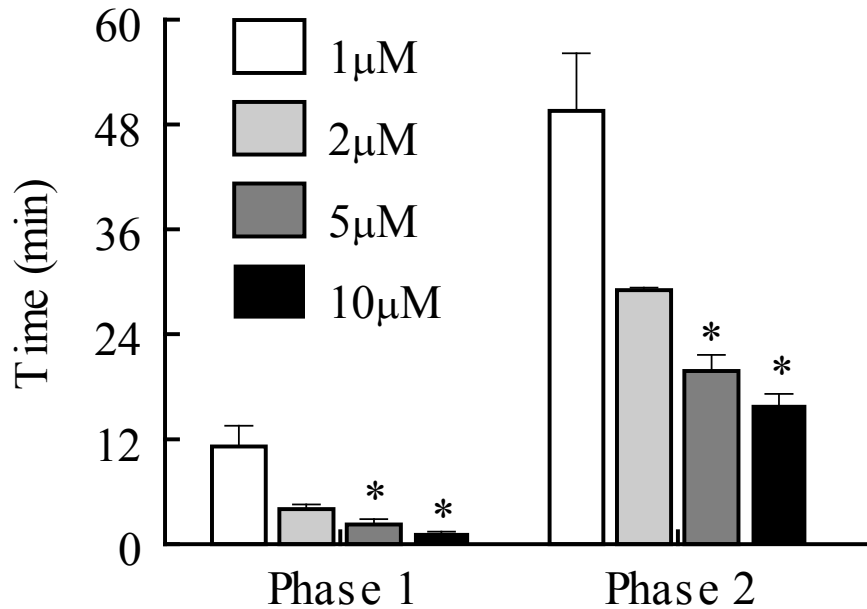


Figure 2.4. Acute MeHg caused a concentration-dependent decrease in the time-to-onset of Phase 1 and Phase 2 in differentiated SH-SY5Y cells. Differentiated SH-SY5Y cells were superfused with 1, 2, 5, or 10 μM MeHg and changes in $[Ca^{2+}]_i$ were continuously monitored. MeHg caused a concentration dependent decrease in the time-to-onset of phase 1 and phase 2. Acute treatment with 5 and 10 μM MeHg resulted in a significant decrease in the onset of phase 1 and 2 compared to 1 μM MeHg. Data are expressed as mean \pm SEM. * = significant difference compared to 1 μM MeHg (One-Way ANOVA, $p < 0.05$, $n \geq 4$).

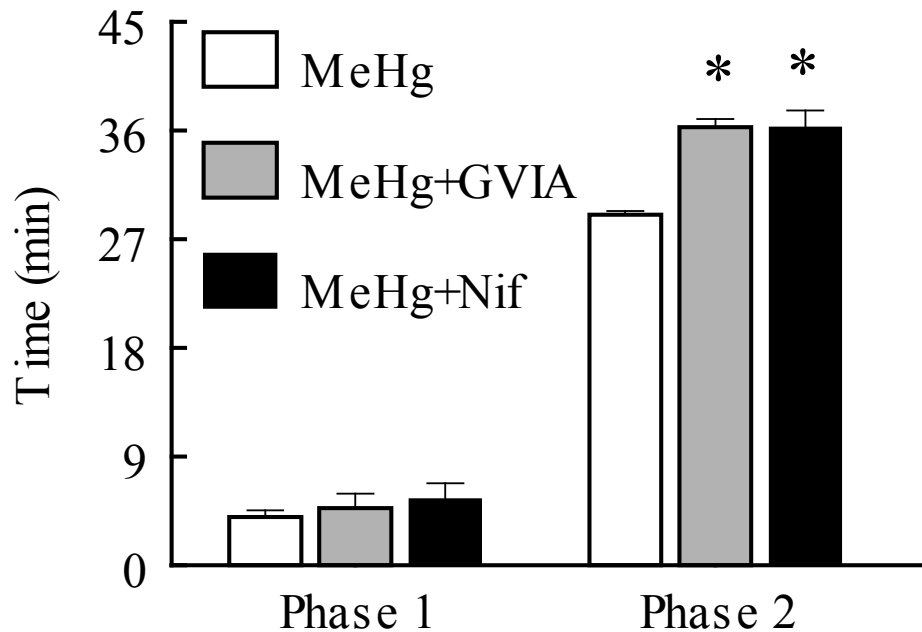


Figure 2.5. N- or L-type VGCC antagonists delay the onset of phase 2. Differentiated SH-SY5Y cells were superfused with 2 μ M MeHg alone, 2 μ M MeHg + 1 μ M GVIA, or 2 μ M MeHg + 5 μ M Nif and changes in $[Ca^{2+}]_i$ were continuously monitored. VGCC antagonists did not delay the onset of phase 1. Co-treatment with GVIA or Nif significantly delayed the onset of phase 2. Data are expressed as mean \pm SEM. * = significant difference compared to 2 μ M MeHg alone (One-Way ANOVA, $p < 0.05$, $n \geq 3$).

VGCC with nifedipine (5 μ M) or GVIA (1 μ M) respectively prior to the application of 2 μ M MeHg. Cells were loaded with fura-2AM and pretreated with Nif or GVIA and then superfused with 2 μ M MeHg. Treatment with 2 μ M MeHg alone resulted in the onset of phase 1 and phase 2 at approximately 4min and 30min respectively. Application of Nif or GVIA statistically significantly delayed the time-to-onset of phase 2 to approximately 36min (Figure 2.5). These data are similar to work completed in rat cerebellar granule cells (Marty and Atchison, 1998). However in granule cells VGCC antagonists delay the onset of phase 1 and phase 2 indicating that these two cell types may differ in the intracellular events that initiate the onset of phase 1.

b. Chronic methylmercury treatment

Acute MeHg exposure clearly alters intracellular Ca²⁺ homeostasis in differentiated SH-SY5Y cells as well as primary neuronal cultures and immortalized cell lines (Denny and Atchison, 1996; Marty and Atchison, 1997; Limke and Atchison, 2001). Yet the effects of prolonged exposure to low-level MeHg on Ca²⁺ regulation have been largely ignored. To begin to fill this gap in our knowledge, experiments were designed to assess the effects of chronic MeHg treatment on VGCC function. Previous studies have utilized a long-term treatment paradigm in undifferentiated SH-SY5Y cells (Petroni et al., 2011) and PC12 cells (Shafer et al., 2002). Shafer et al., (2002) utilized low (10-50) nM MeHg to study MeHg-induced cell death and MeHg effects on voltage-sensitive sodium (Na⁺) and Ca²⁺ currents. Because cells were treated for a prolonged period of time (48 or 72h) we chose to utilize 20nM MeHg, which did not induce a significant level of cell detachment, neurite retraction, or cell death. Differentiated SH-SY5Y cells were treated with 0 or 20nM MeHg for 48 or 72h and then loaded with fura-2AM, KCl- (40mM) induced Ca²⁺ influx was monitored as a measure of VGCC function (Figure 2.2A,

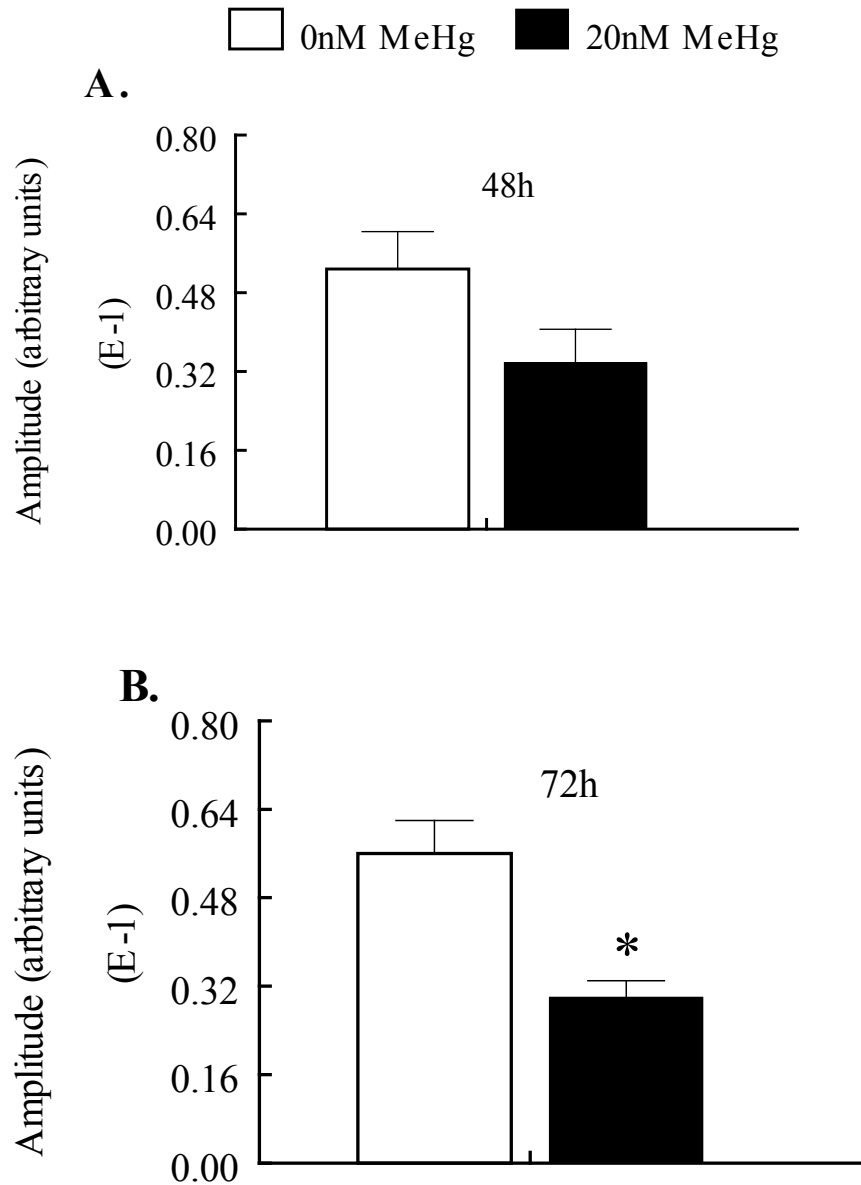


Figure 2.6. Chronic MeHg caused decreased KCl-induced Ca^{2+} influx. Differentiated SH-SY5Y cells were treated with 0 or 20nM MeHg for 48 or 72h. Following MeHg treatment cells were loaded with fura-2AM and KCl-induced Ca^{2+} influx was measured. **(A)** Forty-eight hour 20nM MeHg treatment caused a slight reduction in the maximum amplitude of KCl-induced Ca^{2+} influx. **(B)** Seventy-two hour 20nM MeHg caused a significant decrease in the maximum amplitude of KCl-induced Ca^{2+} influx (Unpaired t-test, $p = 0.018$, $n \geq 4$).

B). Cells were depolarized 4 times with KCl; the maximum amplitude of each depolarization was measured and then averaged for cell. A mean amplitude for each plate was determined (n=1). The maximum amplitude of KCl-induced Ca^{2+} influx was decreased in cells treated with 20nM MeHg compared to cells treated with 0nM MeHg (Figure 2.6A). Seventy-two hour treatment with 20nM MeHg caused a significant decrease in the maximum amplitude of KCl-induced Ca^{2+} influx compared to cells treated with 0nM MeHg (Figure 2.6B). These experiments demonstrate that long-term MeHg treatment disrupts VGCC function in a time-dependent manner.

We next determined if decreased Ca^{2+} influx was due to decreased influx through L- or N-type channels, or both. A similar experimental design was used as described in the previous experiments except the L- and N-type VGCC antagonists Nif and GVIA were utilized to isolate current through specific subtypes of VGCC. Cells were treated for 48 or 72h and then loaded with fura-2AM and KCl-induced Ca^{2+} influx was used as an indirect measure of VGCC function. Cells were depolarized with 40mM KCl 4 separate times. The first depolarization was considered the control and occurred with no antagonist present. The following 3 depolarizations occurred in the presence of antagonist. Ca^{2+} influx through N-type VGCCs were isolated by antagonizing L-type VGCCs with Nif and Ca^{2+} influx through L-type VGCCs was isolated by antagonizing N-type VGCCs with GVIA. The amplitude of KCl-induced Ca^{2+} influx was quantified for each depolarization. The mean amplitude of depolarizations in the presence of antagonist was divided by the amplitude of the control depolarization to determine the percent of control. Forty-eight hour 20nM MeHg treatment caused a statistically significant decrease in

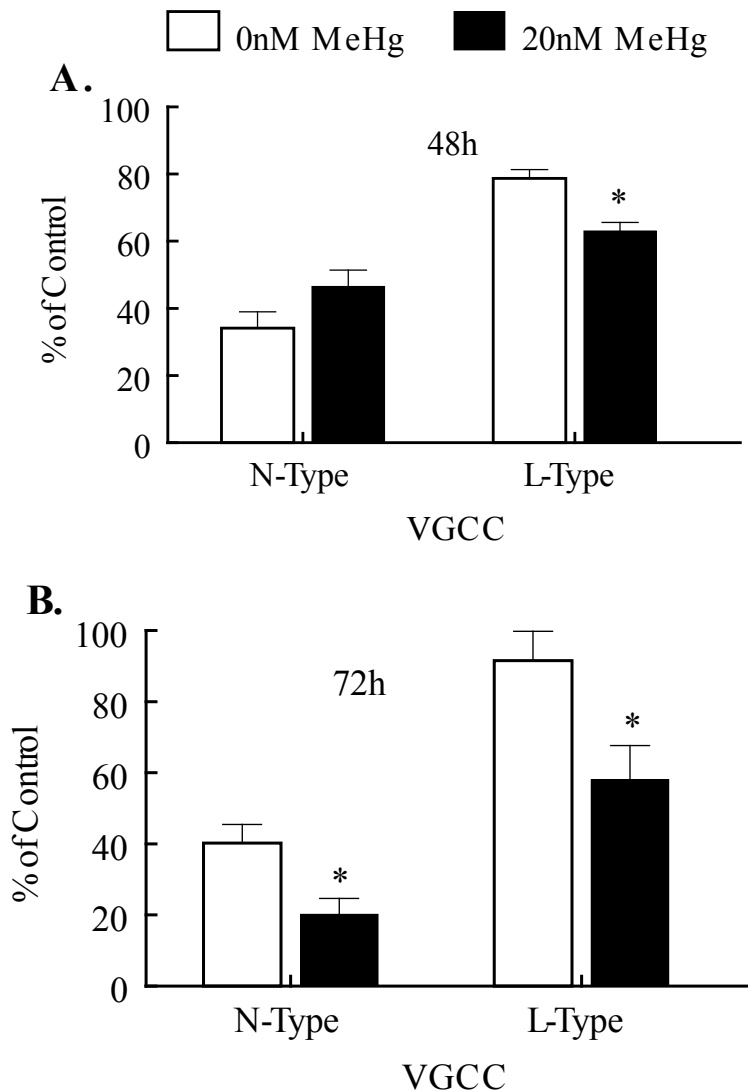


Figure 2.7. Chronic MeHg treatment caused a time- and subtype specific block of VGCCs.

The maximum amplitude of KCl-induced Ca^{2+} influx was measured in cells treated with 0 or 20nM MeHg for 48 or 72h. Cells were depolarized 4 times using 40mM KCl. The first depolarization was performed with KCl alone (control depolarization) the following 3 were performed in the presence of a VGCC antagonist. The amplitude of KCl-induced Ca^{2+} influx was quantified for each depolarization. The mean amplitude of depolarizations in the presence of antagonist was divided by the amplitude of control depolarization to determine percent (%) of control. Data are represented as percent (%) of control depolarization. **(A)** Forty-eight hour 20nM MeHg treatment, caused a significant decrease in Ca^{2+} influx through L-type VGCCs and no change in KCl-induced Ca^{2+} influx through N-type channels (Unpaired t-test, $p = 0.0122$, $n=3$). **(B)** Seventy-two hour 20nM MeHg treatment caused a significant decrease in KCl-induced Ca^{2+} influx through N - and L-type VGCCs (Unpaired t-test, $p<0.05$, $n\geq 3$). * = significantly different than the 0nM MeHg group. Data are expressed as mean \pm SEM.

KCl-induced Ca^{2+} influx through L-type VGCCs and had no effect on Ca^{2+} influx through N-type VGCCs (Figure 2.7A). Seventy-two hour 20nM MeHg treatment caused a statistically significantly decrease in KCl-induced Ca^{2+} influx through both N and L-type VGCCs compared to cells treated with 0nM MeHg (Figure 2.7B). These data demonstrate that prolonged MeHg treatment alters L- and N-type VGCC function in a subtype- and time-dependent manner. Based on our previous experiments which demonstrated that acute MeHg exposure caused a biphasic increase in $[\text{Ca}^{2+}]_i$ we hypothesized that chronic MeHg treatment may increase resting $[\text{Ca}^{2+}]_i$. To test this hypothesis, differentiated SH-SY5Y cells were treated with 0 or 20nM MeHg for 72h and the resting $[\text{Ca}^{2+}]_i$ was measured using fura-2. Seventy-two hour 20nM MeHg treatment resulted in a statistically significant increase in resting $[\text{Ca}^{2+}]_i$ (Figure 2.8).

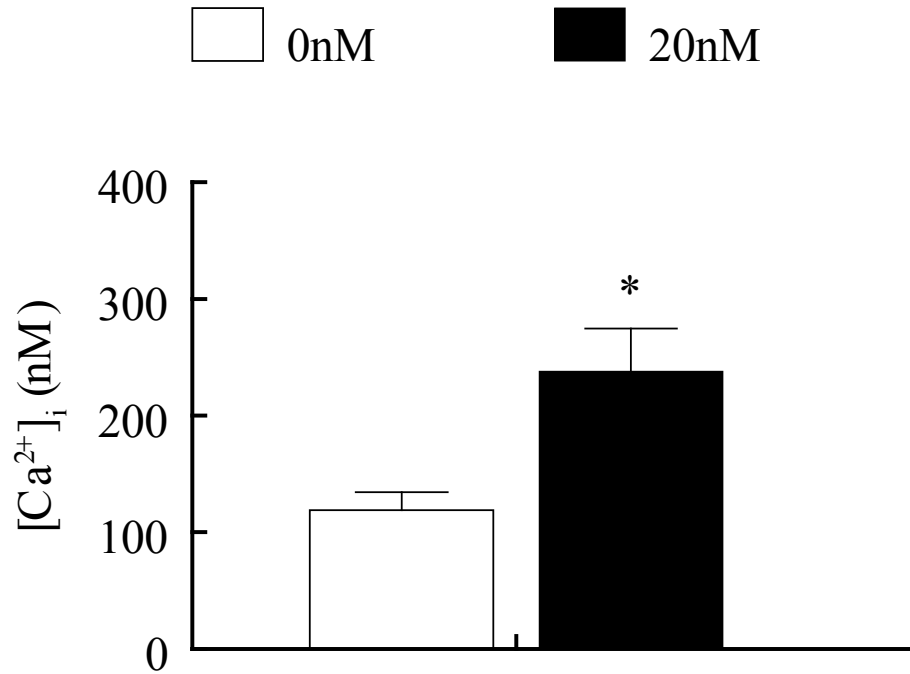


Figure 2.8. Chronic MeHg treatment caused a significant increase in resting $[Ca^{2+}]_i$. Differentiated SH-SY5Y cells were treated with 0 or 20nM MeHg for 72h and the resting $[Ca^{2+}]_i$ was calculated. Cells treated with 20nM MeHg had a significant increase in mean resting $[Ca^{2+}]_i$ compared to 0nM MeHg treated cells.* = significant difference compared to 0nM MeHg group (Unpaired t-test, $p < 0.05$, $n = 3$).

E) Discussion

Disruption of Ca^{2+} homeostasis appears to be a central event in MeHg-induced toxicity. Both primary cells in culture and acute live brain slices from rodents respond to acute MeHg treatment with an increase in $[\text{Ca}^{2+}]_i$ (Hare and Atchison, 1994; Marty and Atchison, 1997; Edwards et al., 2005; Yuan and Atchison, 2007; Ramanathan and Atchison, 2011) for cells in culture this can be differentiated kinetically into two distinct phases. Acute MeHg in differentiated SH-SY5Y cells causes a biphasic increase in $[\text{Ca}^{2+}]_i$ and the time-to-onset is inversely related to $[\text{MeHg}]$. Nif or GVIA delay the onset of phase 2. Our results are consistent with previous reports (Marty and Atchison, 1997). However, the characteristics of the biphasic response appear to differ between cell types. Cerebellar granule cells are a known target of MeHg and the occurrence of phase 1 is highly dependent on release of mitochondrial Ca^{2+} (Limke and Atchison, 2001), it can be delayed by VGCC antagonists. In contrast, the rat neuroblastoma cell line NG108-15 responds to acute MeHg with 3 distinct phases. Phase 1 is primarily due to Ca^{2+} release from the SER this is followed by a non- Ca^{2+} phase due to Zn^{2+} and finally the 2nd Ca^{2+} phase due to Ca^{2+} entry. The SH-SY5Y cell response is similar to that seen in the NG108-15 cell line. This insinuates that phase 1 in SH-SY5Y cells is due to Ca^{2+} release from the SER which cannot be delayed with the addition of Nif or GVIA. Therefore the initiation of phase 1 is mediated differently in cerebellar granule cells. Characterizing the source of Ca^{2+} release of phase 1 or the involvement of other divalent cations was beyond the scope of this dissertation. However, those studies could be completed in the future and modeled after work done by Denny and Atchison (1994).

Understanding the consequences of long-term exposure to low-doses of environmental toxicants is critical in advancing the field of toxicology. Humans are most commonly exposed to low doses of a toxicant throughout their lifetime. Therefore studies must be designed to begin to parse out the health impact(s) of such exposures. In this study our goal was to understand the effects of long-term exposure to MeHg on VGCC function. We found that 72h exposure to 20nM MeHg caused a statistically significant decrease in KCl-induced Ca^{2+} influx. Twenty four hour MeHg treatment (30nM) in PC12 cells caused the block of both peak and end type Ca^{2+} current (Shafer et al., 2002). Our data support these findings and suggest that prolonged exposure to nanomolar concentrations of MeHg results in the blockade of VGCCs. Acute MeHg treatment has been shown to block Ca^{2+} current through L- and N-type VGCCs in PC12 cells (Shafer et al., 1990) as well as block of KCl-induced $^{45}\text{Ca}^{2+}$ influx in neuronal synaptosomes (Atchison et al., 1986; Shafer and Atchison, 1989). The similarity in response suggests that MeHg acts in the same way to block VGCCs in both acute and chronic treatments. Upon further investigation, we found that L-type VGCCs are more vulnerable to MeHg-induced block than were N-type VGCCs. Following 48h MeHg treatment L-type VGCCs had significantly decreased Ca^{2+} influx, whereas N-type VGCCs were only affected following a 72h MeHg exposure. MeHg blocks VGCCs in a time- and subtype-specific manner. L-type VGCCs must have a unique characteristic(s) that makes them vulnerable to block by MeHg such as the amino acid composition or duration of channel opening.

Acute MeHg treatment increases $[\text{Ca}^{2+}]_i$ in SH-SY5Y cells. We wanted to determine if prolonged MeHg exposure caused increased resting $[\text{Ca}^{2+}]_i$. Following a 72h MeHg treatment,

differentiated SH-SH5Y cells had significantly higher resting $[Ca^{2+}]_i$ than did untreated cells.

The source of excess cytosolic Ca^{2+} is unknown, but we hypothesize that it is due to intracellular Ca^{2+} release from the SER or mitochondria, similar to what occurs in phase 1 of acute treatment. Increased resting $[Ca^{2+}]_i$ may result in depolarization of the mitochondria causing reduced ATP production. This would further hinder the neurons ability to handle Ca^{2+} via ATP-dependent pathways such as SERCA and the plasma membrane Ca^{2+} -ATPase. These events may lead to cell death.

This study demonstrated that acute MeHg treatment causes a biphasic increase in $[Ca^{2+}]_i$ differentiated SH-SY5Y cells similar to what occurs in NG108-15 cells. VGCCs contribute to the onset of phase 2 in SH-SY5Y cells. In support of our hypothesis long-term exposure caused decreased KCl-induced Ca^{2+} influx in a time- and VGCC subtype-dependent manner and caused increased resting $[Ca^{2+}]_i$. This work supports previous findings that MeHg causes a block of VGCCs (Atchison et al., 1986; Shafer et al., 1990). Ca^{2+} signaling plays a critical role in numerous neuronal processes. Disruption of VGCC function as well as mitochondrial function due to increased $[Ca^{2+}]_i$ might explain known cellular susceptibilities which lead to the characteristic cell-type specific damage following MeHg exposure.

CHAPTER 3

STRIATAL SLICES FROM AGED ANIMALS ARE MORE SUSCEPTIBLE TO METHYLMERCURY-INDUCED CALCIUM INCREASE THAN YOUNG ANIMALS

A) Abstract

MeHg is a potent environmental neurotoxicant that impairs several neurological functions upon short and long term exposure. Disruption of $[Ca^{2+}]_i$ homeostasis is an early and crucial event in MeHg induced cytotoxicity. The cerebellum is a primary target of MeHg-induced cytotoxicity resulting in loss of the granule cell layer. The striatum is another potential target due to high expression of $Ca_v1.3$, an L-type Ca^{2+} channel. The developmental effects of MeHg are well established, however the effects on aged individuals have not been characterized. As neuronal $[Ca^{2+}]_i$ homeostasis is significantly altered during aging, aged neurons may be particularly susceptible to MeHg. The objective of this study was to examine MeHg-induced $[Ca^{2+}]_i$ dysregulation in striatal MSNs of aged mice. Changes in the relative fluorescence (RF) of Fluo4, a $[Ca^{2+}]_i$ indicator, were measured by laser scanning confocal microscopy every 5 min during 45 min of perfusion with $20\mu\text{M}$ MeHg, or every 3 min during a 21 min treatment with $100\mu\text{M}$ MeHg from striatal slices from male ICR mice aged 1 month (mo), 9 mo or 20.5 mo. Striatal slices from 9 and 21mo mice treated with $20\mu\text{M}$ MeHg had a significantly hastened time-to-maximum fluorescence compared to 1mo. There was no difference in response when slices were treated with $100\mu\text{M}$ MeHg. We also compared the time-to-peak fluorescence between cerebellar granule cells and striatal medium spiny neurons and found no difference between their responses. This study is the first to demonstrate that aged mice are more susceptible to MeHg-induced Ca^{2+} -dysregulation than young animals.

B) Introduction

Methylmercury is an environmental neurotoxicant that causes cell type specific damage to the CNS upon short and long term exposure. There have been two well-known catastrophic MeHg poisonings that have contributed to our knowledge about MeHg poisoning. The first occurred in Minamata, Japan in the 1950's and the second in Iraq in 1973. In Minamata, industrial waste that contained MeHg was dumped into the nearby bay where it accumulated in the fish, which lived in the bay. Fishermen and their families who consumed the contaminated seafood were consequently exposed to MeHg over a period on many years. In Iraq, wheat seed which was coated with a MeHg containing fungicide that was supposed to be planted was instead used to make bread. In this exposure people who consumed the bread were exposed to a high concentration of MeHg. Victims of both occurrences presented with the same signs and symptoms: cerebellar ataxia, parasthesia, constriction of the visual field, dysarthria, and loss of hearing (Bakir, 1973; Harada, 1968).

Cerebellar granule cells are a very sensitive target for MeHg-induced cytotoxicity (Hunter and Russel, 1954) and the disruption of $[Ca^{2+}]_i$ is an early and crucial event in that process. Acute MeHg treatment causes a biphasic increase in $[Ca^{2+}]_i$. The first phase is due to release of intracellular stores of Ca^{2+} and the second phase is due to extracellular Ca^{2+} entry (Hare and Atchison, 1995; Marty and Atchison, 1997; Limke and Atchison, 2002). Cotreatment with L- or N-type VGCC antagonists will delay the onset of phase 1 and 2 and delay cytotoxicity (Marty and Atchison, 1997; Marty et al., 1998). VGCC antagonists have also been shown to delay the onset of behavioral deficits (Bailey et al., 2013) induced by MeHg and mortality *in vivo*

(Sakamoto et al., 1996). These data demonstrate the modulation of Ca^{2+} -homeostasis is a central event in MeHg-induced neuronal dysfunction and subsequent cytotoxicity.

MSNs are the principal neuron of the striatum. They play a very important role in modulating the activity of the basal ganglia. Their main inputs come from the cortex (glutamatergic) and the midbrain (dopaminergic) (Smith and Bolam, 1990). Altered function of the basal ganglia is associated with a number of disease states including Parkinson's and Huntington's disease (Chuhma, et al., 2011). Proper functioning of the MSNs rely on their ability to modulate both the glutamatergic and dopaminergic signals they receive. Changes in neurotransmission of their primary inputs would result in altered function and output of the basal ganglia (Giraultm, 2012; Kreitzer and Malenka, 2008). MeHg alters neurotransmission of both dopaminergic and glutamatergic neurons. Acute exposure to dopmaminergic neurons causes increased dopamine release (Dreiem et al., 2009; Tiernan et al., 2013). The same has been shown for glutamatergic neurons (Farina et al., 2011). Lesions occur in the striatum following acute application of MeHg in rats (O'Kusky et al., 1988; O'Kusky and McGeer 1989; Wakabayashi et al., 1995; Sakamoto et al., 1998). A combination of MeHg-induced $[\text{Ca}^{2+}]_i$ -increase and altered neurotransmission in the striatum may induce neuronal dysfunction resulting in cytotoxicity in the striatum.

As neuronal $[\text{Ca}^{2+}]_i$ homeostasis is significantly altered during aging, aged neurons may be particularly susceptible to MeHg. During the aging process many changes occur that alter a neurons ability to efficiently produce ATP (Toescu, 2005) and buffer changes in $[\text{Ca}^{2+}]_i$ (Toescu, 2007; Toescu and Vreugdenhil, 2010). These changes influence an aged neuron's ability to respond to changes in $[\text{Ca}^{2+}]_i$ leaving them vulnerable to stressors that alter $[\text{Ca}^{2+}]_i$

homeostasis such as MeHg. The objective of this study was to examine the responses of striatal MSNs from 1mo (young), 9mo (adult), and 21mo (aged) animals to acute MeHg treatment. We hypothesized that aging will increase the striatum's susceptibility to MeHg-induced Ca^{2+} dysregulation.

C) Materials and methods

Chemicals and solutions

Methylmercuric (II) chloride was obtained from Aldrich Chemical (Milwaukee, WI). Fluo4-NW was obtained from Invitrogen (Carlsbad, CA). TPEN was obtained from Sigma Aldrich (St. Louis, MO). Slicing solution contained (in mM): 222.5 sucrose, 2.5 KCl, 1.25 KH₂PO₄, 26 NaHCO₃, 25 D-glucose, 5 MgCl₂, and 0.5 CaCl₂ (pH 7.3-7.4 upon aeration with 95% O₂/5% CO₂). ACSF contained the following changes in salt composition (in mM): 125 NaCl, 1 MgCl₂, and 2 CaCl₂. Alternative ACSF contained the following changes in salt composition (in mM): 110 sucrose, 62.5 NaCl, and 20 D-glucose.

Slice preparation

All animal procedures adhered to NIH guidelines and were approved by the MSU institutional animal use and care committee. Adult male ICR (Harlan Laboratories) 1mo, 9-9.5 mo and 21-21.5 mo mice were utilized for this study. Following anesthesia with isoflurane, mice were perfused intra-cardially with ice-cold slicing solution. Mice were decapitated, and the whole brain was removed and placed in ice-cold slicing solution. The forebrain was sliced into 200µm coronal sections using a Leica VT100S vibratome (Leica Microsystems Inc., Bannockburn, IL). Slices were transferred to an incubation chamber containing oxygenated alternative ACSF and incubated for 30min at 37°C and then at 23-25°C until use.

Methylmercury treatment

All MeHg solutions were prepared on the day of experiment from a 10mM stock solution. MeHg concentrations of 20 and 100µM were chosen based on the acute in vivo exposure to MeHg in Iraq where 90% of the patients who presented with cerebellar ataxia had a blood [Hg] of 19µM

(Bakir et al., 1973). Also, previous work from our lab demonstrated that acute exposure to MeHg causes a concentration-dependent increase in $[Ca^{2+}]_i$ in a cerebellar slice (Yuan and Atchison, 2007). Relatively high MeHg concentrations are needed in acutely isolated brain slices compared to cells in culture because of the extensive ability of MeHg to bind to the slice non-specifically thereby reducing its effective concentration.

Confocal imaging

Slices were loaded for >30min at 23-25°C in 1x Fluo4-NW with 2.5 mM probenecid and 5µM TPEN. Probenecid was added to the loading solution to inhibit organic-anion transporters, which can extrude dye. MeHg treatment alters intracellular $[Zn^{2+}]$ (Denny and Atchison, 1994) which can bind to fura-2 and skew Ca^{2+} measurements. TPEN was added to the loading solution to chelate Zn^{2+} prior to initiating Ca^{2+} recording. Immediately following loading imaging commenced. Intracellular Ca^{2+} imaging was performed on a Leica confocal microscope. A region containing at least 10 fluo-4 loaded cells was located to perform imaging. The z-series was optimized and a 3µm step size was used. A pretreatment z-series was recorded at time - 5min. Confocal images of Fluo-4 ($[Ca^{2+}]_i$) fluorescence (excited at 488nm, emission >512nm) were obtained with a 40x water immersion objective (numerical aperture 0.75) fitted to a Leica DM LFSA (Leica Optics, Bannockburn, IL). Images (512x512 pixels, xyz or xyzt scan mode) were collected before and during exposure to 20µM MeHg (scanned every 5m for 45m) or 100µM MeHg (scanned every 3m for 21m). All experiments were completed at room temperature (23-25°C). Changes in Fluo4 fluorescence were analyzed using Leica software. Fluorescence intensity data from several regions of interest in the same slice were averaged.

Background fluorescence was then subtracted and normalized to the pre-treatment control (n=1).

The time-to-peak fluorescence for each region of interest was determined, and averaged to determine the mean time-to-peak fluorescence for each slice.

Statistics

Comparisons of mean time-to-peak fluorescence were made using one-way ANOVA followed by Tukey-Kramer multiple comparisons *post-hoc* test, $p < 0.05$.

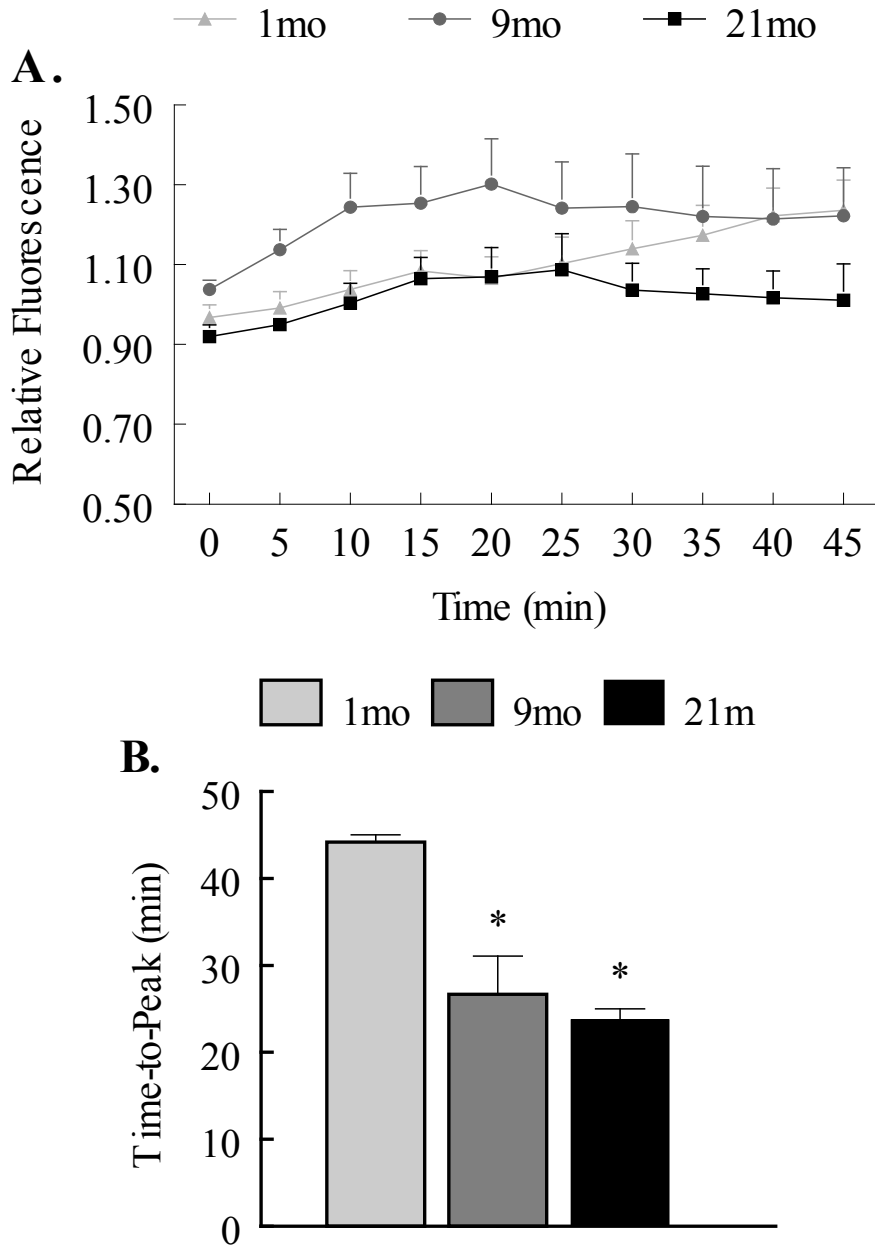


Figure 3.1. Striatal slices from aged animals are more susceptible to 20µM MeHg than slices from 1mo animals. Striatal slices from 1mo, 9mo, and 21mo mice were loaded with Fluo4 and superfused with 20µM MeHg for 45min. **(A)** Relative Fluo4 fluorescence (F/F₀) of striatal slices from 1mo, 9mo, and 21mo mice to 20µM MeHg treatment. **(B)** The time-to-peak fluorescence was quantified for each group. Striatal slices from 9 and 21mo mice had a significantly decreased time-to-peak compared to slices from 1mo animals. Data are means ± SEM (n≥4) * = significantly different than 1mo animals (p<0.05, One-Way ANOVA, Tukey's post-test).

D) Results

a. Confocal recordings

The influence of age on the susceptibility to MeHg-induced Ca^{2+} dysregulation was investigated by performing acute MeHg treatment on striatal slices from different age mice and monitoring changes in $[\text{Ca}^{2+}]_i$ with Fluo-4. Striatal slices from 1, 9, and 21mo mice were superfused with $20\mu\text{M}$ MeHg for 45min. Images were recorded every 5 min for 45min (Figure 3.1A). Responses from multiple cells in each slice were recorded, and the time-to-peak fluorescence was determined. Slices from 9 and 21mo old mice had statistically significant faster time-to-peak fluorescence than did those slices from 1mo old mice (Figure 3.1B). Because there was no difference in response between the striatal slices from 9 and 21mo old animals we compared the response striatal slices from 1 and 9mo animals to $100\mu\text{M}$ MeHg. Striatal slices from 1 and 9mo old animals were superfused with $100\mu\text{M}$ MeHg for 21min (Figure 3.2A). There was no difference in the time-to-peak fluorescence between 1 and 9mo animals (Figure 3.2B). These data demonstrate that the susceptibility of striatal MSNs to MeHg-induced Ca^{2+} -dysregulation increases with age. However, when striatal MSNs are exposed to a very high [MeHg] age does not influence their response.

b. Comparative responses of striatal and cerebellar slices to acute methylmercury

Cerebellar granule cells are among the most sensitive cell types to MeHg cytotoxicity (Hunter and Russell, 1954). To determine if striatal MSNs were more or less sensitive to MeHg-induced Ca^{2+} dysregulation than cerebellar granule cells, we compared the time-to-peak fluorescence. Confocal recordings of cerebellar granule cells was completed by a former member of the Atchison lab (Dr. Erin Wakeling). Treatments, recordings, and data analysis were

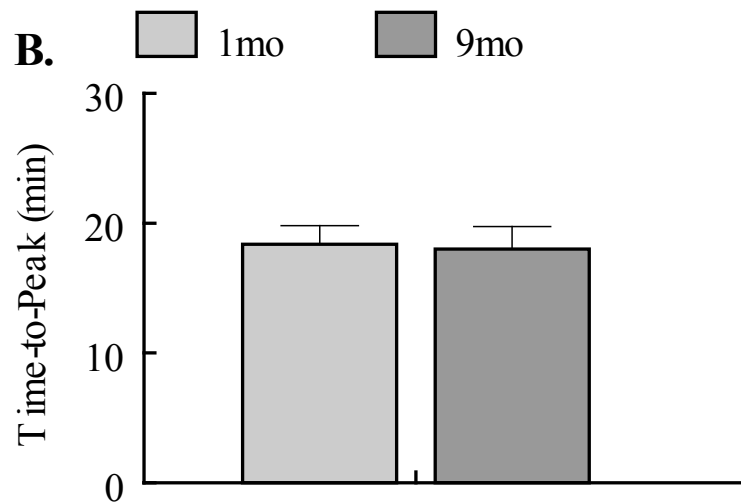
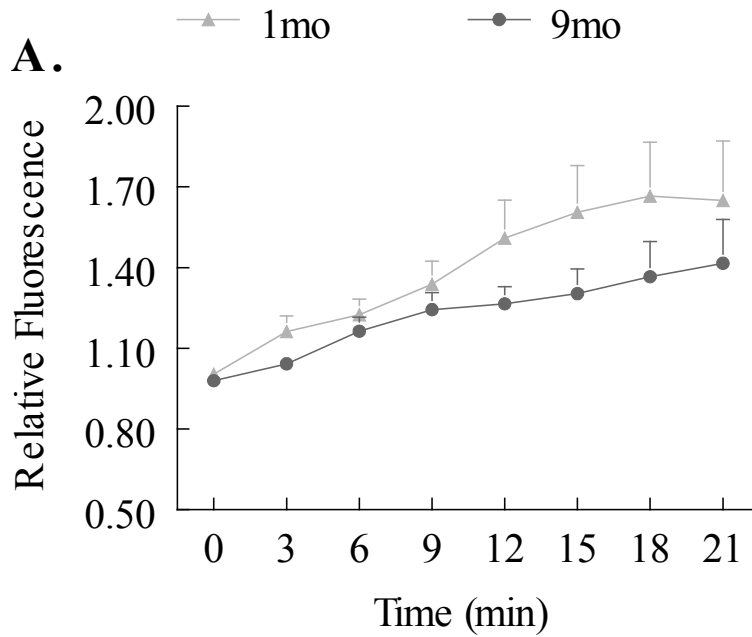


Figure 3.2. Age had no effect on the response of striatal slices to 100 μ M MeHg treatment. Striatal slices from 1 and 9mo animals were loaded with Fluo4 and superfused with 100 μ M MeHg for 21min. **(A)** Relative Fluo4 fluorescence (F/F_0) response of striatal slices from 1 and 9mo mice to 100 μ M MeHg treatment. **(B)** There was no difference in the time-to-peak effect between 1 and 9mo striatal slices to 100 μ M MeHg treatment. Data are means \pm SEM ($n \geq 4$).

completed in the same manner allowing for comparison between the two regions. The time-to-peak fluorescence of striatal and cerebellar slices to 20 and 100 μ M were compared and no differences were detected (Table 3.1). This study was the first to compare the relative susceptibility of cerebellar granule cells and striatal MSNs at different ages to acute MeHg treatment. We demonstrated that 1) MeHg disrupts intracellular calcium statistically significantly faster in aged animals compared to young and 2) striatal MSNs and cerebellar granule cells are equally sensitive to MeHg-induced $[Ca^{2+}]_i$ changes in 1, 9, and 21mo animals when they are treated with 20 or 100 μ M MeHg .

	Cerebellar Granule Cells	Striatal Medium Spiny Neurons
20μM MeHg		
1mo	42.5 \pm 1.4	43.8 \pm 1.3
9mo	29.3 \pm 4.5	27.2 \pm 2.2
21mo	21.3 \pm 5.2	27 \pm 2.7
100μM MeHg		
1mo	18 \pm 1.2	18.6 \pm 1.7
9mo	11.1 \pm 2.6	18 \pm 1.7

Table 3.1. No difference in time-to-peak fluorescence between cerebellar granule cells and striatal medium spiny neurons. The time-to-peak fluorescence was determined for cerebellar granule cells and striatal medium spiny neurons in response to 20 μ M and 100 μ M MeHg. No differences were detected between the time-to-peak fluorescence (min) in the cerebellum and striatum at any age. Data are expressed as means \pm SEM. (n \geq 4).

D) Discussion

Disruption of $[Ca^{2+}]_i$ is an early event in neuronal MeHg toxicity (Hare et al., 1993; Marty and Atchison, 1997). An inability to regulate changes in $[Ca^{2+}]_i$ may increase a neuron's susceptibility to MeHg-induced damage. The breakdown of cellular processes involved in maintaining neuronal Ca^{2+} homeostasis is associated with aging (Toescu and Vreugdenhil, 2010). Results of this study indicate that adult and aged neurons are more susceptible to MeHg-induced Ca^{2+} -dysregulation than young neurons. Striatal slices from 1, 9, and 21mo old animals were treated with 20 μ M MeHg and changes in $[Ca^{2+}]_i$ were monitored using Fluo4. The time-to-peak fluorescence of striatal slices from 9 and 21mo old animals occurred approximately 20min faster for than 1mo old animals. These data indicate that as animals age the striatal MSNs are more sensitive to MeHg-induced Ca^{2+} -dysregulation. However when striatal slices were treated with 100 μ M MeHg there was no difference in response. These data demonstrate that when exposed to a very high [MeHg] striatal MSNs respond the same, no matter their age.

This study was the first to compare the Ca^{2+}_i response of young and aged animals to acute MeHg exposure. Neuronal aging has been associated with the breakdown of numerous cellular processes involved with Ca^{2+} regulation and ATP production. Due to these changes, aged neurons are less able to respond to neuronal stressors (Toescu, 2005; Toescu and Vreugdenhil, 2010). Thus, it is not surprising that aged neurons are more sensitive to MeHg-induced Ca^{2+} -dysregulation. Acute exposure to MeHg triggers a series of events that neurons with an impaired ability to buffer changes in $[Ca^{2+}]_i$ would not be able to withstand. Acute

treatment has been shown to cause release of intracellular stores of $[Ca^{2+}]_i$ (Hare and Atchison, 1995; Limke and Atchison, 2002). In order to recover from this first MeHg-induced increase in $[Ca^{2+}]_i$, the neuron would need to be able to use energy-dependent pathways to pump Ca^{2+} into the SER via the smooth endoplasmic reticulum ATPase (SERCA) or out of the cell via the plasma membrane ATPase. Aged neurons have decreased expression of both of these ATPases (Toescu, 2007; Toescu and Vreugdenhil, 2010) and their mitochondria are depolarized. This would decrease their ability to produce ATP and buffer increases in $[Ca^{2+}]_i$ (Toescu, 2005). It may be that the inability of aged neurons to respond to the increased need for ATP to handle large fluxes in $[Ca^{2+}]_i$ is what makes them more sensitive to MeHg.

We also compared the time-to-peak fluorescence of striatal MSNs and cerebellar granule cells to 20 μ M and 100 μ M MeHg and found no differences in response. Cerebellar granule cells are a sensitive target of MeHg-induced cytotoxicity (Hunter and Russell, 1954). It was surprising to find no differences in the response time between the MSN and granule cells. This indicates that MSNs are a sensitive target of MeHg-induced cytotoxicity. Although we found no differences in response time, more comparative studies need to be completed to fully understand if MSNs are also a sensitive target or if this was just a circumstance of the system used in this study. We monitored changes in Ca^{2+} every 3min or 5min using the Ca^{2+} sensitive fluorophore Fluo4. This method is effective to determining spatial changes in Ca^{2+} , however we are not able to continuously monitor local changes in Ca^{2+} in a cell by cell manner. Continuously monitoring changes in Ca^{2+} throughout the entire treatment period may have parsed out temporal changes in

Ca^{2+} , and differences may have been found between brain regions. However, based on this study cerebellar granule cells and striatal MSNs are equally sensitive to 20 μM and 100 μM MeHg.

This study was the first to demonstrate an age-dependent effect on neuronal susceptibility to MeHg-induced Ca^{2+} -dysregulation. We also compared the Ca^{2+} responses of striatal MSNs and cerebellar granule cells to acute MeHg treatment and found them to be equally sensitive to MeHg-induced Ca^{2+} -dysregulation. We have demonstrated the need to characterize responses of not only young animals but aged animals to toxicants that disrupt Ca^{2+} -regulation to make decisions about safe exposure levels in all ages of the population. These results imply that interaction of the natural aging process with exposure to environmental toxicants is a potential concern for public health, particularly for a society with increasing life-span.

CHAPTER 4

CHRONIC METHYLMERCURY TREATMENT ALTERS STRIATAL CALCIUM

REGULATION AND SYNAPTOSOME MITOCHONDRIAL FUNCTION

A) Abstract

The acute effects of MeHg have been investigated extensively however the effects of chronic low-dose exposure have not been characterized. The data presented in this chapter are part of a comprehensive study of the behavioral, molecular, and neurophysiological effects of chronic MeHg exposure in male Balb/c mice. The ability of an L-type VGCC blocker isradipine (Isr), to prevent or delay MeHg-induced toxicity was also investigated. The objective of this study was to investigate the effects of chronic low-dose MeHg treatment on mitochondrial function of NSDA neuron synaptosomes and Ca^{2+} regulation of striatal MSNs and whether co-treatment with the VGCC antagonist, Isr, would prevent MeHg-induced neuronal dysfunction. Male Balb/c mice were given free access to 0 or 6.25 ppm Hg as MeHg in their drinking water and 0 or 2 ppm isradipine in their feed. Treatments did not alter mouse weight and caused no overt toxicity. Twelve mo MeHg treatment resulted in a small decrease in striatal synaptosome mitochondrial ATP production and a significantly faster $[\text{Ca}^{2+}]_i$ -increase in response to AMPA receptor activation. Co-treatment with the VGCC antagonist Isr resulted in a significant increase in ATP production compared to Isr or MeHg treatment alone. Together these results suggest a role for MeHg-induced disruption of striatal synaptosome mitochondrial function and MSN AMPA receptor function. These results will be integrated with other results from this project to provide a more comprehensive understanding of the effects of long-term exposure to low-dose MeHg on neuronal function.

B) Introduction

Previous chapters established that MeHg is an environmental neurotoxicant of contemporary concern, due to the exposure to low levels of MeHg throughout one's lifetime. Our current understanding of MeHg-induced toxicity has largely been derived from acute treatment studies (for review see: Atchison and Hare, 1994; Limke et al., 2004; Farina et al., 2011). While these studies have discovered many of the targets of MeHg following acute treatment we do not know if the same series of events occur following chronic exposure to MeHg. Therefore, the effects of chronic exposure to MeHg are not well understood. A limited number of studies have investigated changes in neuronal function following prolonged exposure to MeHg (Bourdineaud et al., 2008; Huang et al., 2008; Cambier et al., 2009; Sokolowski et al., 2011). These studies support previous work demonstrating that long-term exposure to MeHg decreases mitochondrial respiration resulting in decreased ATP production (Bourdineaud et al., 2008; Cambier et al., 2009) as well as induces oxidative stress (Huang et al., 2008) and mitochondrial dependent apoptosis (Sokolowski et al., 2011).

In the adult brain SNc neurons are spontaneously active, firing action potentials in the absence of synaptic input. The generation of action potentials is reliant on the opening of $\text{Ca}_v1.3$ channels to allow Ca^{2+} influx as opposed to the usual reliance on Na^+ entry (Chan et al., 2009). The autonomous firing of action potentials in SNc neurons results in repeated fluctuations of $[\text{Ca}^{2+}]_i$ which is then buffered by the SER or mitochondria or removed from the cytosol via the plasma membrane $\text{Na}^+/\text{Ca}^{2+}$ exchanger or Ca^{2+} -ATPase. MeHg disrupts L-type VGCC function (shown in Chapter 2; Peng and Atchison, 2002; Hajela et al., 2003), $[\text{Ca}^{2+}]_i$ regulation (Marty and Atchison, 1997) and Ca_m^{2+} and SER Ca^{2+} regulation (Levesque and Atchison, 1991; Hare

and Atchison, 1995; Limke and Atchison 2002). The reliance of SNc neurons on Ca^{2+} entry via L-type Ca^{2+} channels and resultant continuous stress on Ca^{2+} buffering organelles SNc neurons may make them a sensitive target of MeHg toxicity.

Striatal MSNs are also potential sensitive targets for MeHg-induced Ca^{2+} -dysregulation. They serve an important role in modulating the activity of the basal ganglia and alterations in the function of VGCCs or glutamate receptors, specifically AMPA and NMDA, could significantly alter the output of the basal ganglia. MeHg-induced disruption of VGCC function was discussed in the previous chapter. It also modifies glutamate receptor function and expression. The overstimulation of glutamate receptors has been implicated in MeHg-induced excitotoxicity (Aschner et al., 2000; Liu et al., 2012). Exposure to MeHg sensitizes AMPA receptors resulting in increased Ca^{2+} influx upon receptor activation (Johnson et al., 2011). Antagonism of NMDA receptors protects primary motor (Ramanathan and Atchison, 2011) and cortical neurons (Xu et al., 2013) as well as SH-SY5Y (Petroni et al., 2011) cells from MeHg-induced Ca^{2+} dysregulation and cell death. A reduction of NMDA receptor expression in mouse cortical neurons (Xu et al., 2013) and in the basal ganglia, cerebellum, brain stem and occipital cortex of wild mink (Basu et al., 2007) was associated with exposure to MeHg. MeHg clearly disrupts VGCC and glutamate receptor function. We expect that MeHg will interact with VGCCs to reduce KCl-induced Ca^{2+} influx; this will be prevented by co-treatment with Isr. Chronic MeHg treatment will also alter AMPA and NMDA receptor function causing increased Ca^{2+} influx upon channel activation.

The goal of the work described here was to expose mice to an environmentally relevant [MeHg] and investigate MeHg-induced changes in Ca^{2+} regulation, neurotransmission, mitochondrial function, and gene expression in susceptible brain regions. We also sought to determine whether co-treatment with Isr prevents or delays MeHg-induced toxicity. This was a highly collaborative study performed in our laboratory and involving multiple measures. The data presented in this chapter are solely the work investigating the effects of chronic MeHg treatment on striatal synaptosome mitochondrial function and striatal Ca^{2+} regulation. We report that chronic exposure to MeHg sensitizes AMPA receptors on MSNs resulting in a faster response time. We also found striatal synaptosomal mitochondria increased ATP production in response to chronic exposure to Isr and MeHg.

C) Materials and methods

Chemicals and solutions

Methylmercuric (II) chloride was obtained from Aldrich Chemical (Milwaukee, WI). Fura-2AM, TPEN, AMPA, NMDA, and pluronic acid were obtained from Sigma-Aldrich (Milwaukee, WI). Probenecid was obtained from Molecular Probes (Eugene, OR). Oligomycin, FCCP, antimycin A, and rotenone were obtained from Seahorse Biosciences (North Billerica, MA). Percoll was obtained from GE Healthcare (Pittsburg, PA).

Animal care and treatments

All animal procedures complied with the National Institute of Health guidelines on animal care and are approved by Michigan State University Institutional Animal Use and Care Committee. Male Balb/c mice (Harlan, Frederick, MD) were utilized for this study. The use of only male mice simplified the study; gender-specific differences between adult-onset neurotoxicity are currently unknown. Animals arrived at 8wks of age and were allowed to acclimate to their new environment for 1wk. Mice were housed in pairs and fed standard feed (Harlan, Teklab 18% Protein Global Rodent Diet). They were randomly assigned a treatment group; Con/Con (No isradipine/No MeHg), Con/MeHg (No isradipine/6.25ppm MeHg), Isr/Con (2ppm Isr/No MeHg), or Isr/MeHg (2ppm Isr/6.25ppm MeHg). MeHg and Isr treatments started when animals were 12 wks old. Mice had free access to 6.25ppm MeHg in their drinking water and food pellets, which contained 0 or 2ppm Isr for a period of 6 or 12mo. Isr was purchased from VWR (Chicago, IL) and sent to Harlan to be mixed with standard feed. An inert yellow dye was added to the Isr diet to distinguish it from the standard feed. Animal cages were coded with colors to blind experiments. All mice were monitored 7 days a week. Mice were weighed and their extent of hind limb cross was assessed 3 times a week (M-W-F). The mean body weight

and hind limb cross score per week was determined and then averaged with all mice within the same treatment group. The extent of hind limb cross was assigned a score based on severity. A score of 0, 1, or 2 were assigned to no cross, partial cross, and complete cross, respectively. The animal's ability to remain on an accelerating rotarod was tested 3 times a week (T-W-Th) every 4wks for the first 6mo of treatment and then every 2wks for the duration of the treatment. The rotarod was programmed as a continuously accelerating ramp: 1 - 40 rpm in 120 sec. The latency to fall for each mouse was recorded and the best time per week was selected for each mouse and then averaged for each treatment group.

Tissue collection

Upon completion of each treatment period, mice were anaesthetized with isoflurane. To ensure that mice were under anesthesia their blink reflex was checked, and when they no longer blinked they were determined sufficiently unconscious for intra-cardiac perfusion. The chest cavity was opened and 1mL of trunk blood was collected for Hg analysis. Then the mouse was perfused with ice-cold slicing solution, which contained (in mM): 222.5 sucrose, 2.5 KCl, 1.25 KH_2PO_4 , 26 NaHCO_3 , 25 D-glucose, 5 MgCl_2 , and 0.5 CaCl_2 (pH 7.3-7.4 upon aeration with 95% O_2 /5% CO_2). The mouse was then decapitated and the whole brain removed and placed in ice-cold slicing solution. Blood samples were stored at -80°C until analysis. Total Hg concentration was determined using cold-vapor atomic absorption spectrometry by the Diagnostic Center for Population and Animal Health at Michigan State University.

Striatal synaptosome isolation

Striatal synaptosome isolation protocol was adapted from Dunkley et al. (2008). The striatum was dissected from the whole brain and placed in cold mitochondrial isolation buffer (MIB). MIB contained in mM: 300 sucrose, 10 HEPES, 1 EGTA, pH 7.4. The striatum was

homogenized in 2mL of MIB using a Teflon homogenizer. Following homogenization, the tissue was placed in a centrifuge tube and 6mL of MIB was added bringing the volume to 8mL. The homogenized tissue was spun at 20,890 x g for 10 min at 4°C using a Sorval SM-24 rotor. The supernatant was removed and pellet resuspended in 3mL of 3% (v/v, Percoll/Percoll Buffer) Percoll. Percoll buffer contained (in mM): 300 sucrose, 10 HEPES, 1 EGTA, pH 7.4. This was carefully added on top of a Percoll gradient of 10% (v/v) and 23% (v/v) Percoll. The gradient was centrifuged at 31,650 x g for 10m at 4°C. This resulted in the production of 4 bands. Band 3, which contained the synaptosomes, was removed and added to 8mL of MIB and then spun at 17,800 x g for 10m at 4°C. The supernatant was removed and the pellet was resuspended in sucrose buffer. The synaptosomes were placed in a 2ml tube and spun using a microcentrifuge at 10,000 x g for 5m at 4°C. The supernatant was removed and protein content determined using the Bradford Assay.

Mitochondrial function analysis

Mitochondrial function was assessed using the extracellular flux analyzer (XF-24) (Seahorse Biosciences, North Billerica, MA). The XF-24 simultaneously measures extracellular flux of oxygen (oxygen consumption rate (OCR)) and protons (extracellular acidification rate (ECAR)) of striatal synaptosomes. The synaptosome plating density and chemical concentrations were optimized before starting the experiments. Synaptosomes (10µg/well) were plated in XF-24 plates using ionic buffer which contained (in mM): 20 HEPES, 10 D-glucose, 1.2 Na₂HPO₄, 1 MgCl₂, 5 NaHCO₃, 5 KCl, 140 NaCl, pH 7.4. In order to assure that synaptosomes remained attached to the plate throughout the duration of the mitochondrial function assay the plate was centrifuged at 3,400 x g for 1h at 4°C. Ionic buffer was then removed and replaced with 750µL

incubation buffer which contained: 3.5mM KCl, 120mM NaCl, 1.3mM CaCl₂, 0.4mM KH₂PO₄, 1.2mM Na₂SO₄, 2mM MgSO₄, 15mM D-glucose, 10μM pyruvate, 4mg/ml bovine serum albumin, pH 7.4. The plate was then placed in a CO₂ free incubator at 37°C for 10m prior to the start of assay. The plate was then placed in the XF-24 and mitochondrial function assessed. The sequential application of 1μM oligomycin, 2μM FCCP, 1μM rotenone and 1μM antimycin A metabolically perturbs mitochondrial function. Basal respiration, ATP production, maximum respiration and spare capacity can be subsequently determined, respectively. This is demonstrated in Figure 1.4. Oligomycin inhibits ATP synthase resulting in a reduction of mitochondrial OCR by the fraction used to produce ATP. FCCP is an oxidative phosphorylation uncoupling agent and forces the mitochondria to reach their maximum respiration rate. The difference between maximum respiration and ATP production is considered the spare mitochondrial capacity. Antimycin A and rotenone inhibit complexes I and III respectively, which inhibits all mitochondrial respiration, allowing for determination of the small fraction of non-mitochondrial respiration. Subtraction of the non-mitochondrial respiration from basal, maximum, spare, and ATP production allows for a more accurate calculation of mitochondrial respiration. Data are expressed as OCR (pMol/min).

Striatal slice Preparation

Slices were prepared in the same manner as described in Chapter 3. The forebrain was glued on the cutting stage and placed in a chamber containing oxygenated sucrose-based slicing solution. Coronal slices (200μm) containing the striatum were collected. Slicing solution contained (in mM): 222.5 sucrose, 2.5 KCl, 1.25 KH₂PO₄, 26 NaHCO₃, 25 D-glucose, 5 MgCl₂, and 0.5 CaCl₂ (pH 7.3-7.4 upon aeration with 95% O₂/5% CO₂). Following slicing brain slices

were allowed to recover in oxygenated alternative solution for 30 min at 37°C. Alternative ACSF contains the following changes in salt composition (in mM): 110 sucrose, 62.5 NaCl, and 20 D-glucose. After the 30min incubation in alternative solution slices were placed in ACSF until used for an experiment. ACSF contains the following changes in salt composition (in mM): 125 NaCl, 1 MgCl₂, and 2 CaCl₂.

High speed calcium imaging

Images were collected using an inverted Nikon Eclipse TE 2000-U microscope coupled to a Polychrome V light source (Till Photonics) and a high-speed electron multiplying CCD camera (Ixon EM+, Andor, South Windsor, CT). Slices were loaded in 2mL of ACSF with 10µM Fura-2AM, 2.5mM probenecid, 5µM TPEN and 0.002% (v/v) pluronic acid for 45m in a 5% CO₂, 37°C incubator. Probenecid was added to the loading solution to inhibit organic-anion transporters, which can extrude dye. Pluronic acid was added to facilitate Fura-2AM entry into cells. MeHg treatment alters intracellular [Zn²⁺] (Denny and Atchison, 1994) which can bind to fura-2 and skew Ca²⁺ measurements. TPEN was added to the loading solution to chelate Zn²⁺ prior to initiating Ca²⁺ recording. Following incubation, slices were washed with Mg⁺-free ACSF for 10m. Mg⁺-free ACSF had all of the same components of ACSF except with no MgCl₂. Fura-2 is a Ca²⁺ sensitive fluorophore which we utilized for ratiometric microscopy. Fura-2 was excited at 340nm and 380nm (bound vs. unbound fura-2) and emits at 515nm. Following the wash, regions of interest were selected in the plane of view and treatments began. Slices were exposed to 25µM AMPA, 50µM NMDA + 10µM glycine and 40mM KCl. Each treatment lasted for 2min followed by 8min of ACSF. Agonist concentrations were selected

based on previous work completed in our laboratory (Johnson et al., 2011). Fura-2 fluorescence was continuously monitored. Image series were exported and then processed using Image J. In Image J, background was subtracted using a 50 pixel rolling ball subtraction, and images were registered to reduce movement between images. Regions of interest were then selected. Ratiometric values were produced from individual 340nm and 380nm values. Only ratiometric traces with a value less than 1 were used for data analysis. Ratiometric values greater than one indicate a dead or damaged cell. All data are represented as relative fluorescence (fluorescence at time 0/fluorescence at time x). Time-to-peak fluorescence was determined for each slice (n=1) and then averaged to determine a mean time-to-peak for each treatment group.

Statistics

Statistical analysis of all behavior data was done using a Two-Way ANOVA followed by Bonferonni post-test, $p < 0.05$. All other comparisons were made using One-Way ANOVA followed by Tukey-Kramer multiple comparisons *post-hoc* test, $p < 0.05$.

—●— Con/Con —■— Con/MeHg —▲— Isr/Con —◆— Isr/MeHg

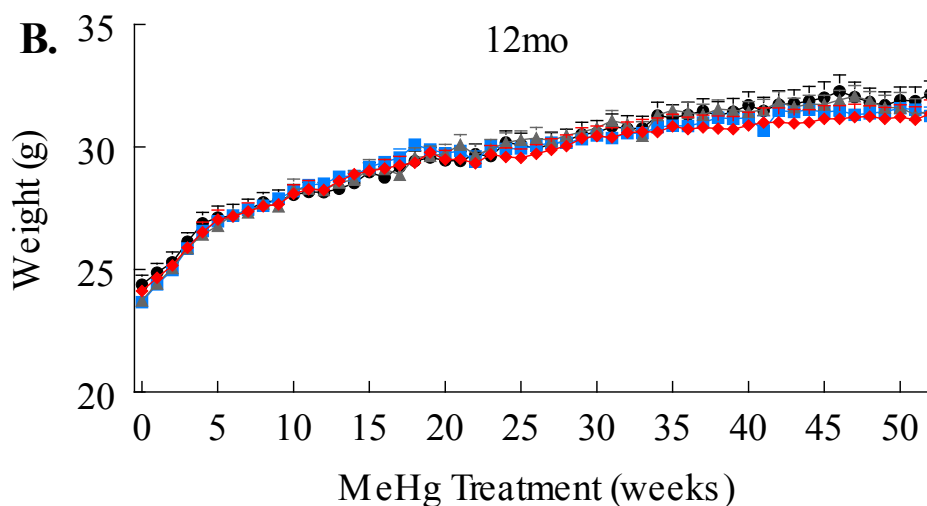
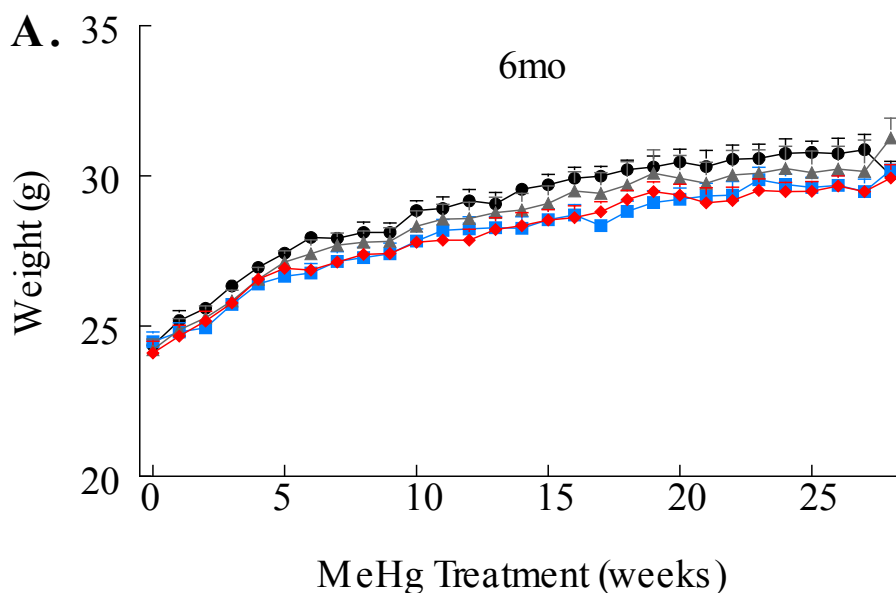


Figure 4.1. Six or twelve month MeHg or Isr/MeHg treatments did not alter mouse weight. Male balb/c mice were treated with 0ppm Isr/0ppm MeHg (Con/Con), 0ppm Isr/6.25ppm MeHg (Con/MeHg), 2ppm Isr/0ppm MeHg (Isr/Con), 2ppm Isr/6.25ppm MeHg (Isr/MeHg) for 6 or 12mo. Throughout the treatment period mice were weighed three times a week and their mean weight per week was determined. (A) Six or (B) twelve month treatments did not alter mouse weight. Treatment and time had a significant effect on mouse weight following 6 and 12mo treatments (Two-Way ANOVA, Bonferroni post-test, $p < 0.05$) ($n \geq 12$). Data are expressed as mean \pm SEM.

—●— Con/Con —■— Con/MeHg —▲— Isr/Con —◆— Isr/MeHg

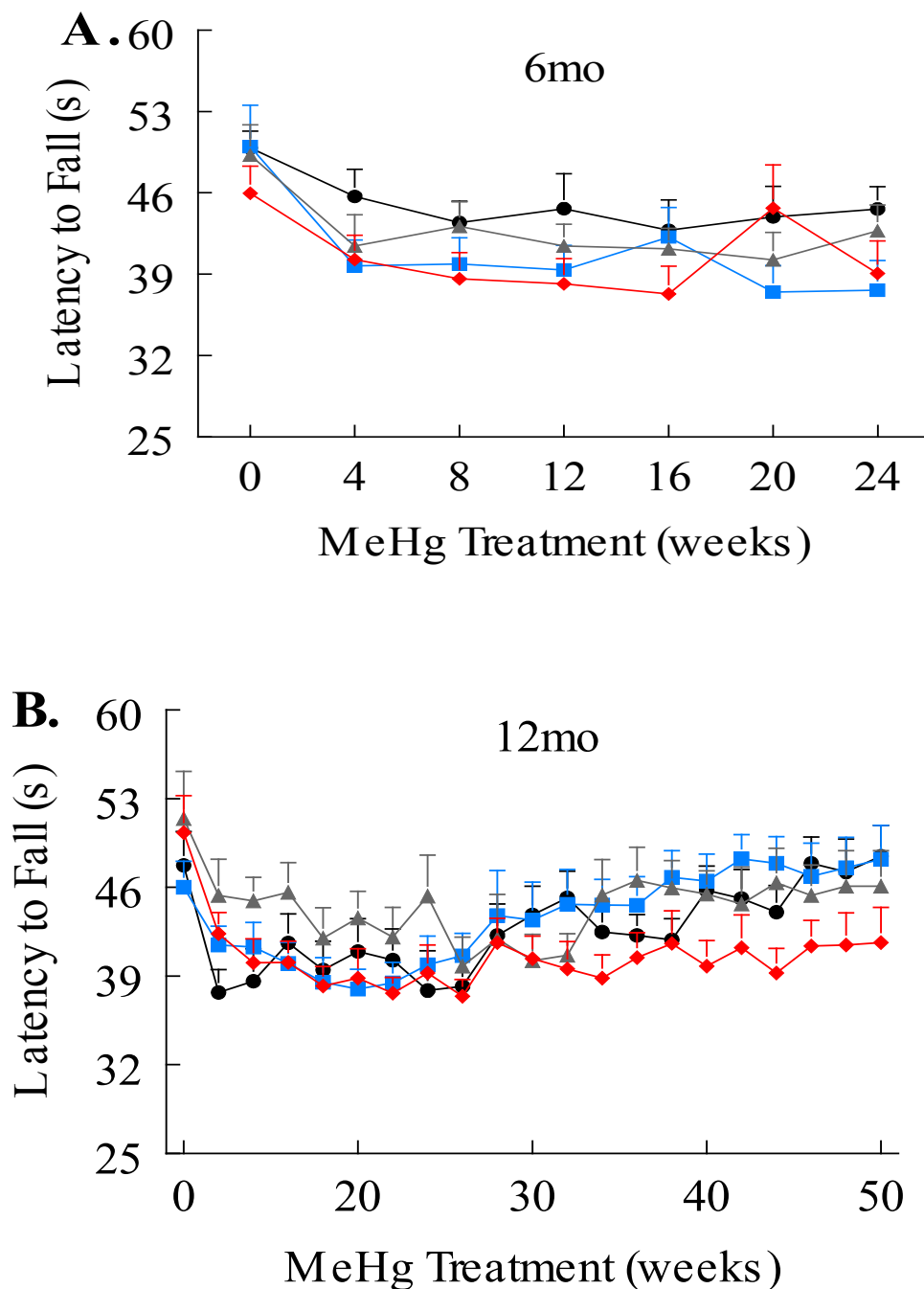


Figure 4.2. Six or twelve month MeHg or Isr/MeHg treatments did not alter mouse performance on the rotarod. Male balb/c mice were treated with 0ppm Isr/0ppm MeHg (Con/Con), 0ppm Isr/6.25ppm MeHg (Con/MeHg), 2ppm Isr/0ppm MeHg (Isr/Con), 2ppm

(Figure 4.2 cont'd) Isr/6.25ppm MeHg (Isr/MeHg) for 6 or 12mo. During the first 6mo of treatment mouse ability to remain on an accelerating rotarod was tested every 4wks and then every 2wks for the duration of the treatment. **(A)** Six or **(B)** twelve month treatments did not alter mouse ability to remain on an accelerating rotarod. Treatment and time had a significant effect on mouse ability to remain on the accelerating rotorod following 6 and 12mo treatments (Two-Way ANOVA, Bonferroni post-test, $p < 0.05$) ($n \geq 12$). Data are expressed as mean \pm SEM.

—●— Con/Con —■— Con/MeHg —▲— Isr/Con —◆— Isr/MeHg

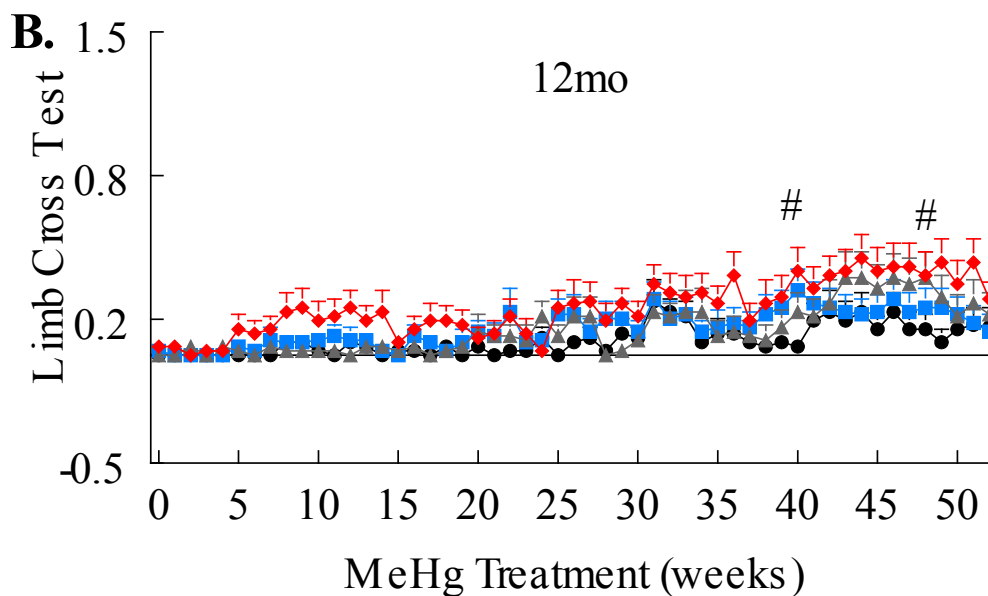
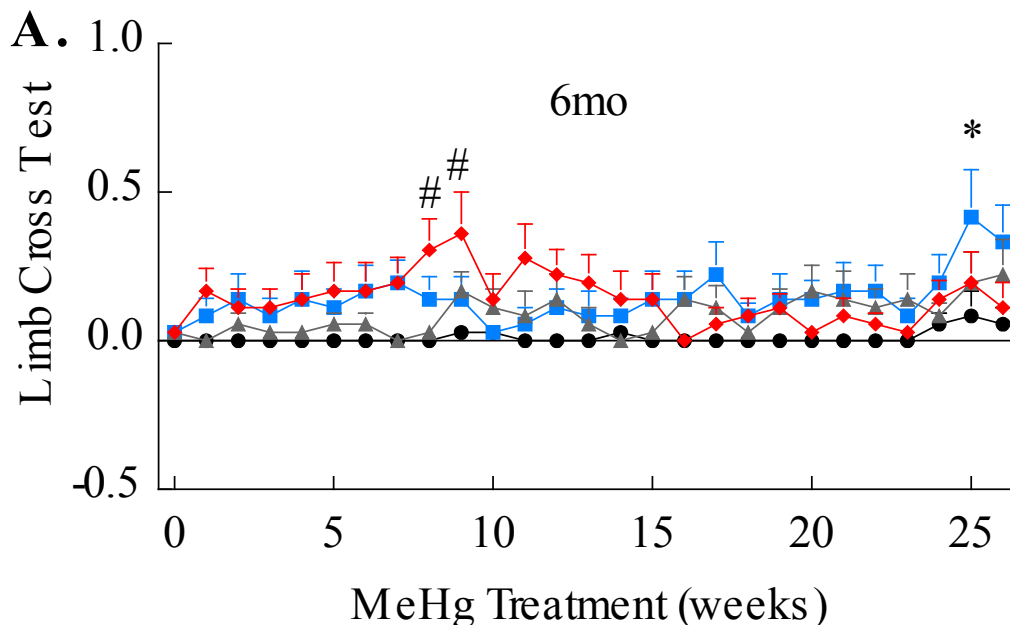


Figure 4.3. Six or twelve month MeHg or Isr/MeHg treatments did cause a consistent pattern of altered mouse limb cross. Male balb/c mice were treated with 0ppm Isr/0ppm MeHg (Con/Con), 0ppm Isr/6.25ppm MeHg (Con/MeHg), 2ppm Isr/0ppm MeHg (Isr/Con), 2ppm Isr/6.25ppm MeHg (Isr/MeHg) for 6 or 12mo. Throughout the treatment period the extent of

(Figure 4.3 cont'd) mouse hind limb cross was scored three times a week and their mean score per week was determined. The extent of hind limb cross was assigned a score based on severity. A score of 0, 1, or 2 were assigned to no cross, partial cross, and complete cross, respectively. **(A)** Mean limb cross test scores for six month treatment. Con/Con hind limb score is significantly different than Con/MeHg hind limb score on week 25. Con/Con hind limb score is significantly different than Isr/MeHg hind limb score during weeks 8 and 9. **(B)** Mean limb cross test scores for twelve month treatment. Con/Con hind limb score is significantly different than Isr/MeHg hind limb score during weeks 39 and 48. Treatment and time had a significant effect on mouse hind limb score (Two-Way ANOVA, Bonferonni post-test, $p < 0.05$). * = Con/Con is significantly different than Con/MeHg. # = Con/Con is significantly different than Isr/MeHg. Data are expressed as mean \pm SEM.($n \geq 12$)

D) Results

a. Animal health and behavior

The goal of this study was to mimic a lifetime exposure to low levels of MeHg in the diet and assess alterations in striatal synaptosome mitochondrial function and striatal MSN Ca²⁺ regulation. Our collaborators at Auburn University performed pilot studies to determine both [MeHg] and [Isr]. Mouse weights were monitored to determine if the treatments altered mouse growth or weight gain and no differences were found (Figure 4.1A,B). This indicates that animals from all treatment groups were eating and drinking similar amounts regardless of their treatment. Previous work has demonstrated that adult exposure to MeHg alters motor coordination and hind limb strength as assessed by the animal's ability to remain on a rotarod and extent of hind limb cross (Kobayashi et al., 1981; Bellum et al., 2007; Huang et al., 2008; Johnson et al., 2011). Six or twelve mo treatments did not alter mouse performance on the accelerating rotarod (Figure 4.2A, B). Following the 6mo treatment there was no consistent pattern of effect as assessed by the hind limb cross test. However significant differences were found between Con/Con and Con/MeHg groups on week 25 and between Con/Con and Isr/MeHg groups on weeks 8 and 9 (Figure 4.3A). Following the 12mo treatment there was no consistent pattern of treatment effects. There were significant differences found between Con/Con and Isr/MeHg on weeks 39 and 48 (Figure 4.3B). Taken together these data indicate treatments caused no overt toxicity or behavioral deficits.

b. Trunk blood Hg concentration

Trunk blood Hg content was analyzed to determine if Con/MeHg and Isr/MeHg mice accumulated Hg throughout the treatment period. Following the 6mo and 12mo treatment period

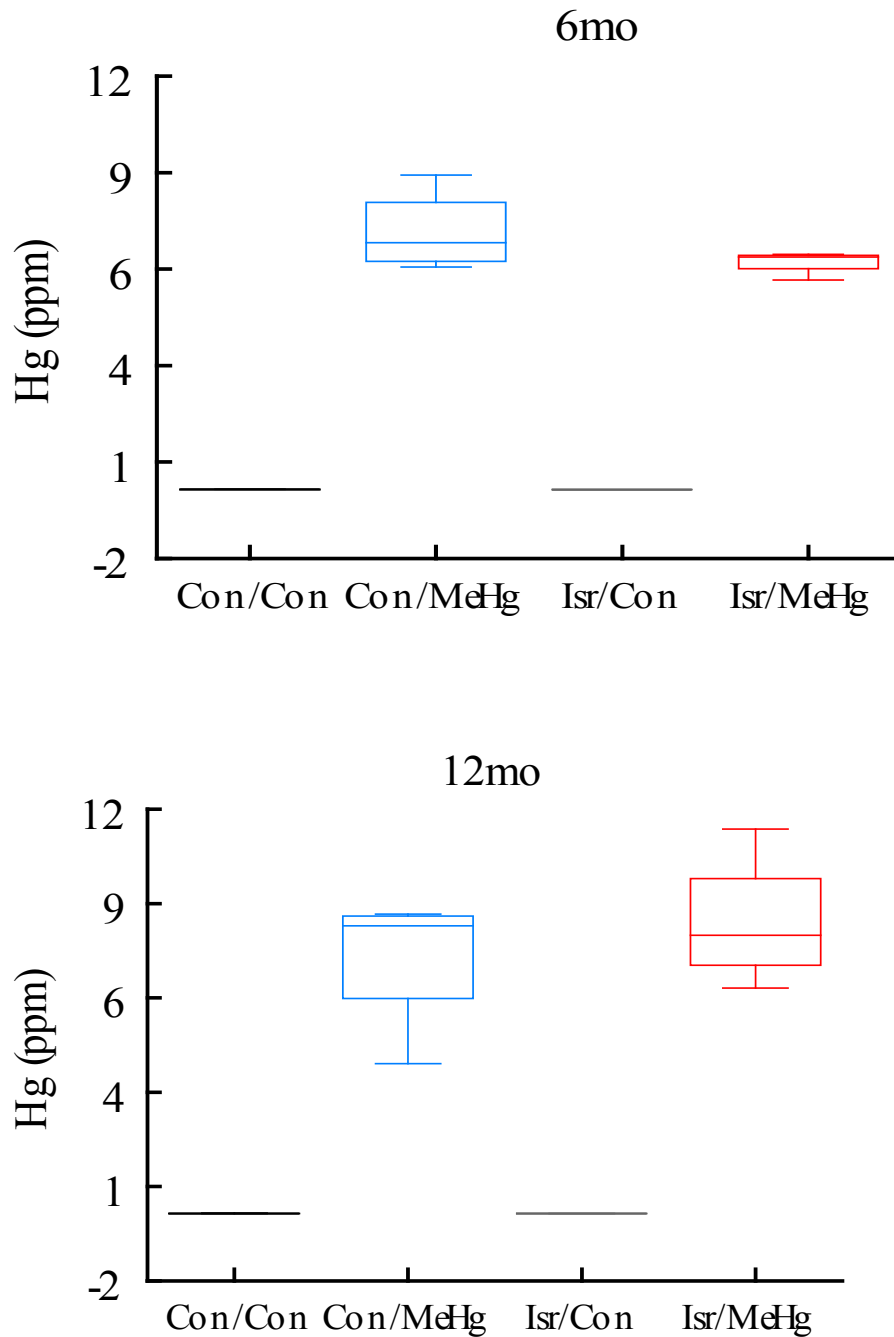


Figure 4.4. Six and twelve month MeHg treatment caused blood Hg accumulation. Male balb/c mice were treated with 0ppm Isr/0ppm MeHg (Con/Con), 0ppm Isr/6.25ppm MeHg (Con/MeHg), 2ppm Isr/0ppm MeHg (Isr/Con), 2ppm Isr/6.25ppm MeHg (Isr/MeHg) for 6 or 12mo. Following anaesthesia with isoflurane truck blood was collected and later analyzed for Hg content. MeHg and Isr/MeHg caused significant Hg accumulation following (A) 6mo and (B) 12mo treatment (One-Way ANOVA, Tukey's post-test, $p < 0.05$) ($n = 4$).

Con/MeHg mice had a trunk blood Hg level of 7.5ppm and 7.6ppm, respectively. Similarly, the Isr/MeHg mice had a trunk blood Hg level of 6.6ppm and 8.7ppm following the 6 and 12mo treatment period (Figure 4.4A,B). Trunk blood Hg concentrations from mice treated with MeHg in their drinking water have been found to be similar with levels of Hg in the brainstem (Johnson et al., 2011). A similar study treating mice for 7 wks with MeHg via oral gavage demonstrated that trunk blood Hg levels were similar to those found in the cerebral cortex, cerebellar cortex, and brainstem (Huang et al., 2008). Based on these studies we predict that similar levels of Hg would be found in the striatum.

c. Mitochondrial function

Chronic MeHg treatment had no effect on striatal synaptosome mitochondrial bioenergetics following 6 or 12mo treatment (Figure 4.5). Addition of oligomycin, FCCP, and antimycin A/rotenone allowed for the determination of mitochondrial basal respiration, ATP production, maximum respiration, and spare capacity. Six-mo treatment did change any of these measures of mitochondrial function (Figure 4.6A-D). This length of MeHg treatment may not have been long enough to induce mitochondrial dysfunction or striatal synaptosome mitochondria are not a sensitive target of MeHg-induced dysfunction. Similarly following the 12mo treatment no changes occurred between groups in their basal respiration, maximum respiration, or spare capacity (Figure 4.7A-C). However, the 12mo Con/MeHg treatment caused a small decrease in ATP production while the Isr/MeHg treatment caused a significant increase in ATP production compared to the Isr/Con and Con/MeHg groups (Figure 4.8A). To determine if this change in ATP production was specific to striatal synaptosome the mitochondrial function of cortical synaptosomes was also measured. The same increase in ATP production was seen in the Isr/MeHg group (Figure 4.8B) indicating that it was not a region-specific effect. MeHg

● Con/Con ■ Con/MeHg ▲ Isr/Con ◆ Isr/MeHg

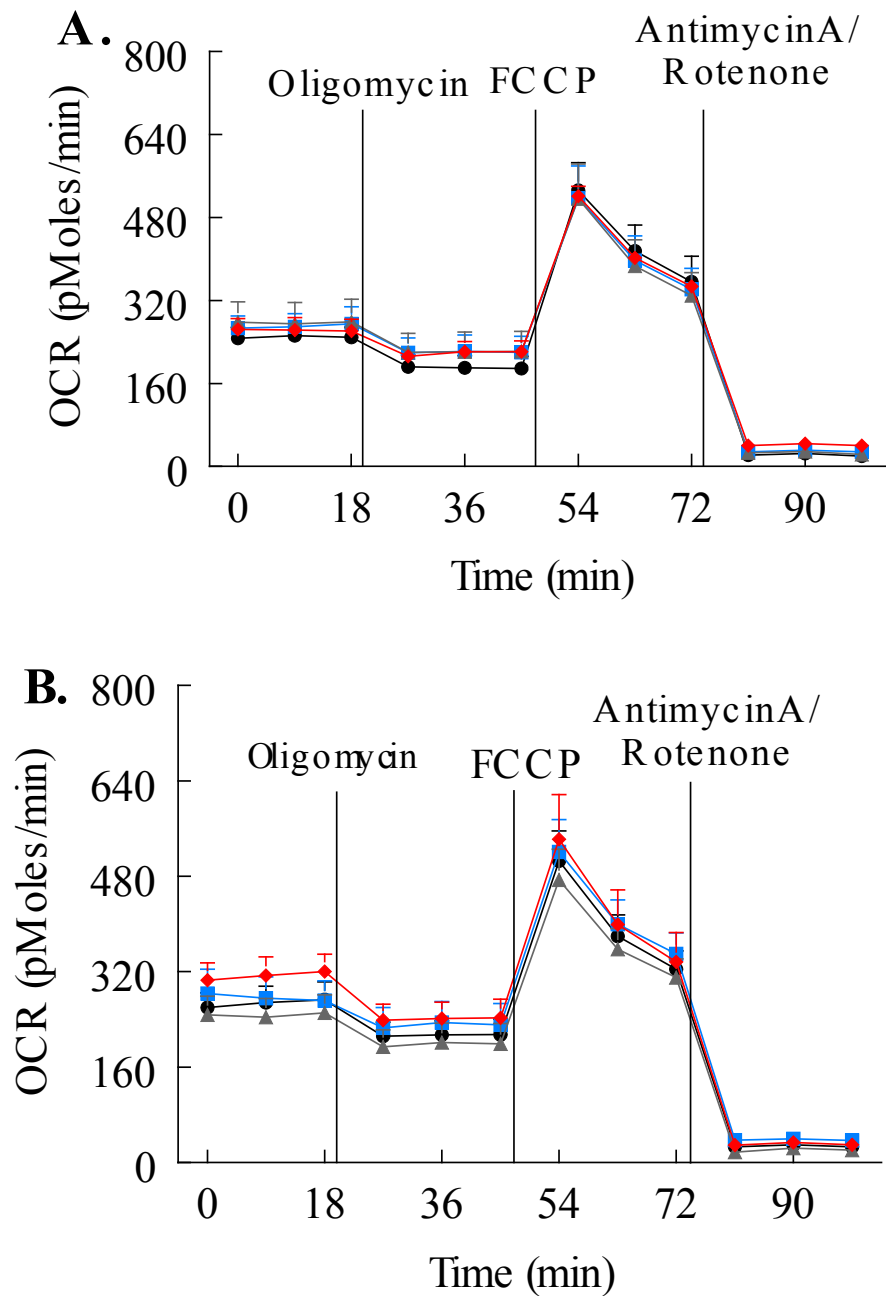


Figure 4.5. MeHg or Isr/MeHg treatment did not alter mitochondrial bioenergetics.

Mitochondrial bioenergetics of striatal synaptosomes was determined following treatment period. Oxygen consumption rate (OCR, pMoles/min) before and after the addition of oligomycin (1 μ M), Carbonyl cyanide 4-(trifluoromethoxy)phenylhydrazine (FCCP) (2 μ M), antimycin A (1 μ M), and rotenone (1 μ M). No differences were detected in OCR between treatment groups following (A) 6mo or (B) 12mo treatment period. Data are means \pm SEM (n \geq 4).

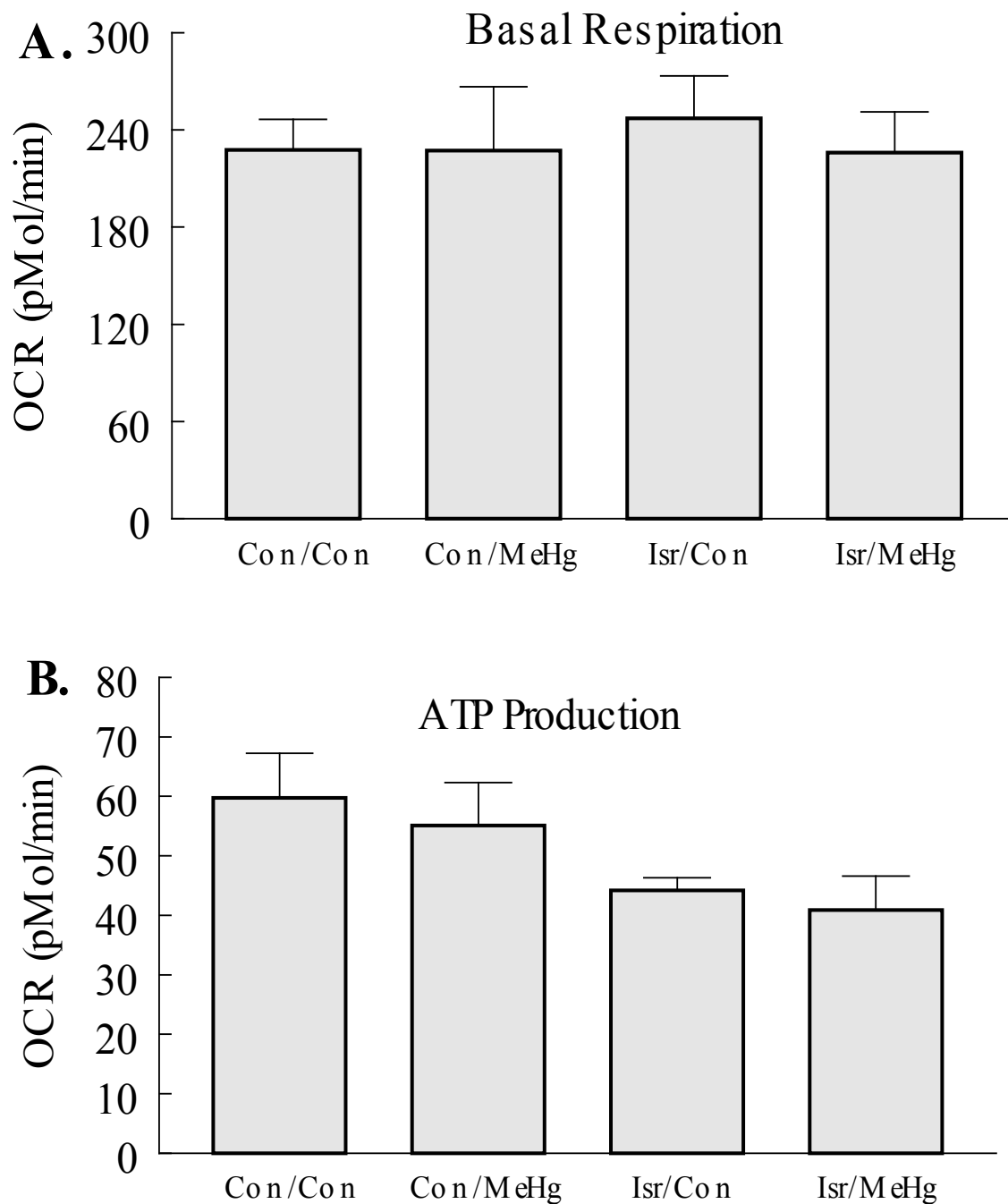
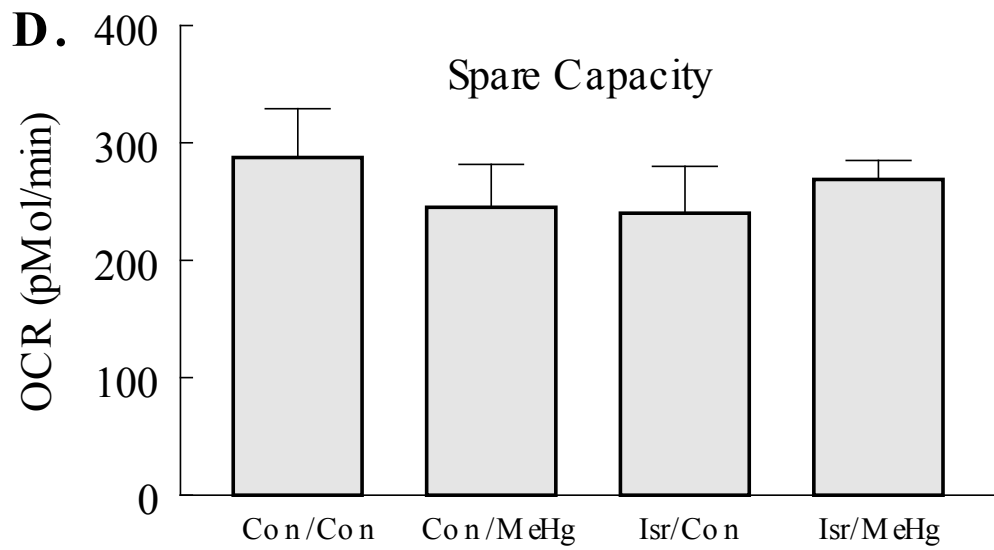
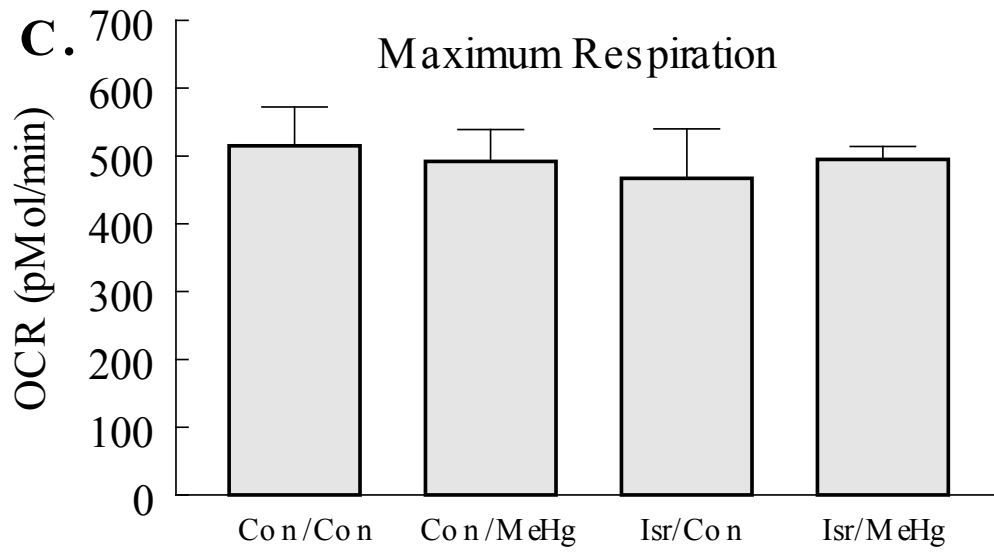


Figure 4.6. Mitochondrial function was unaltered following 6mo MeHg or Isr/MeHg co-treatment. Quantification of mitochondrial basal respiration, ATP production, maximum respiration and spare capacity striatal synaptosomes. MeHg or Isr/MeHg co-treatment caused no significant differences in **(A)** basal respiration **(B)** ATP production **(C)** maximal respiration or **(D)** spare capacity. Data are means \pm SEM ($n \geq 5$).

(Figure 4.6 cont'd)



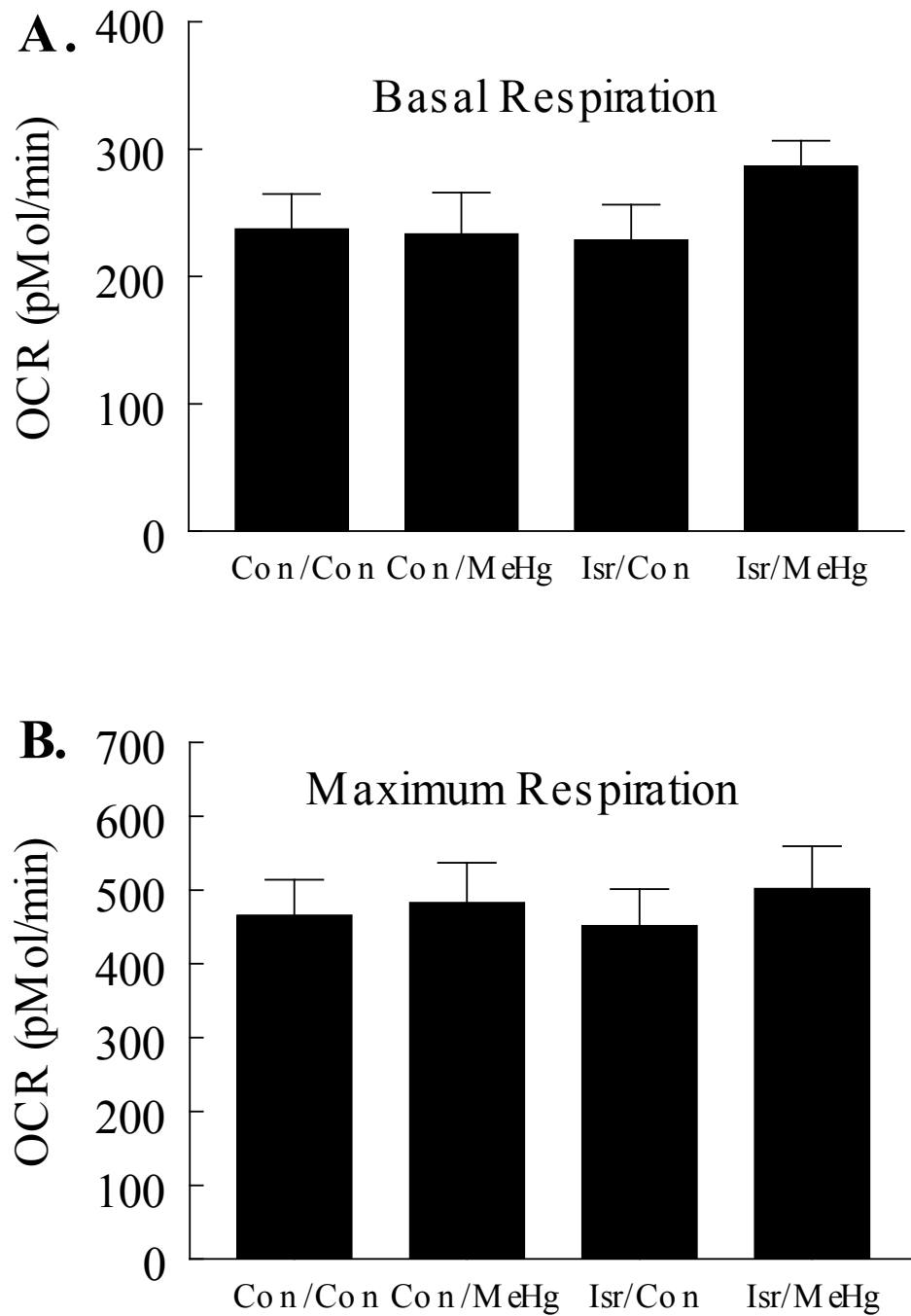
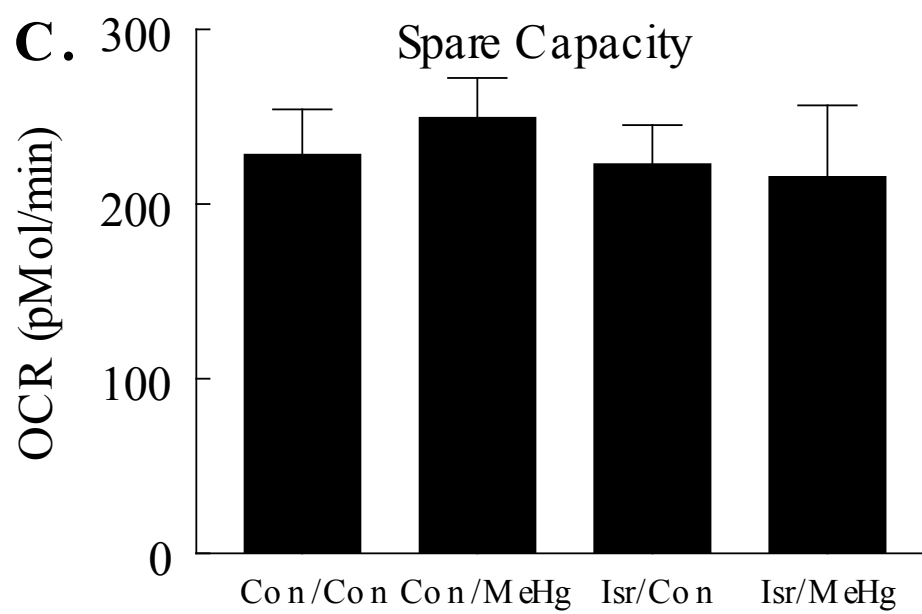


Figure 4.7. Mitochondrial function was unaltered following 12mo MeHg or Isr/MeHg co-treatment. Quantification of striatal synaptosome mitochondrial basal respiration, maximum respiration, and spare capacity. MeHg or Isr/MeHg co-treatment caused no significant differences in (A) basal respiration (B) maximal respiration or (C) spare capacity. Data are means \pm SEM ($n \geq 5$).

(Figure 4.7 cont'd)



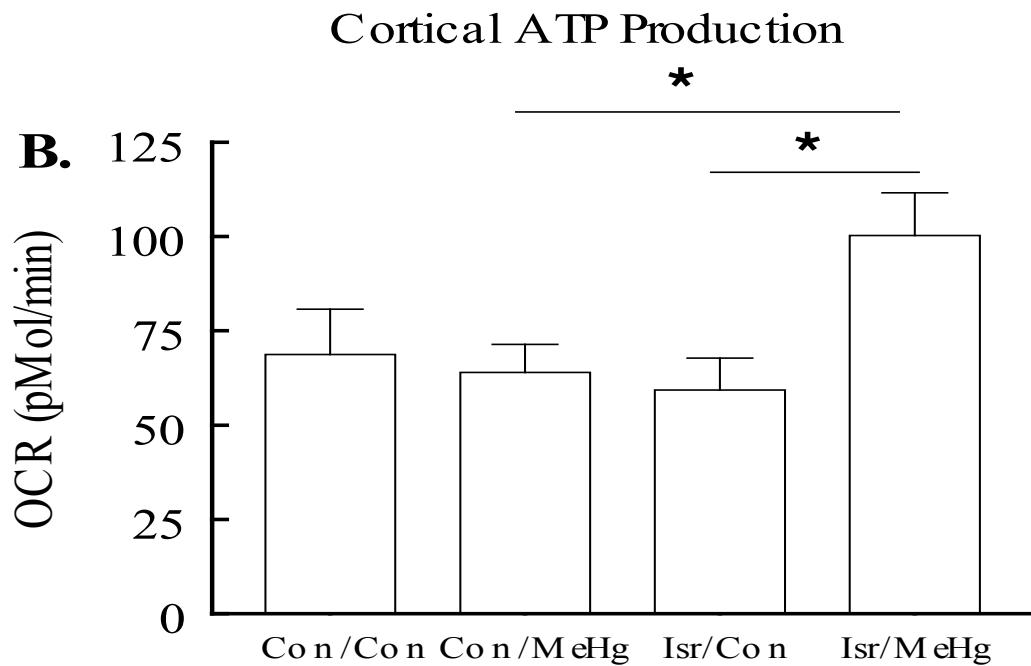
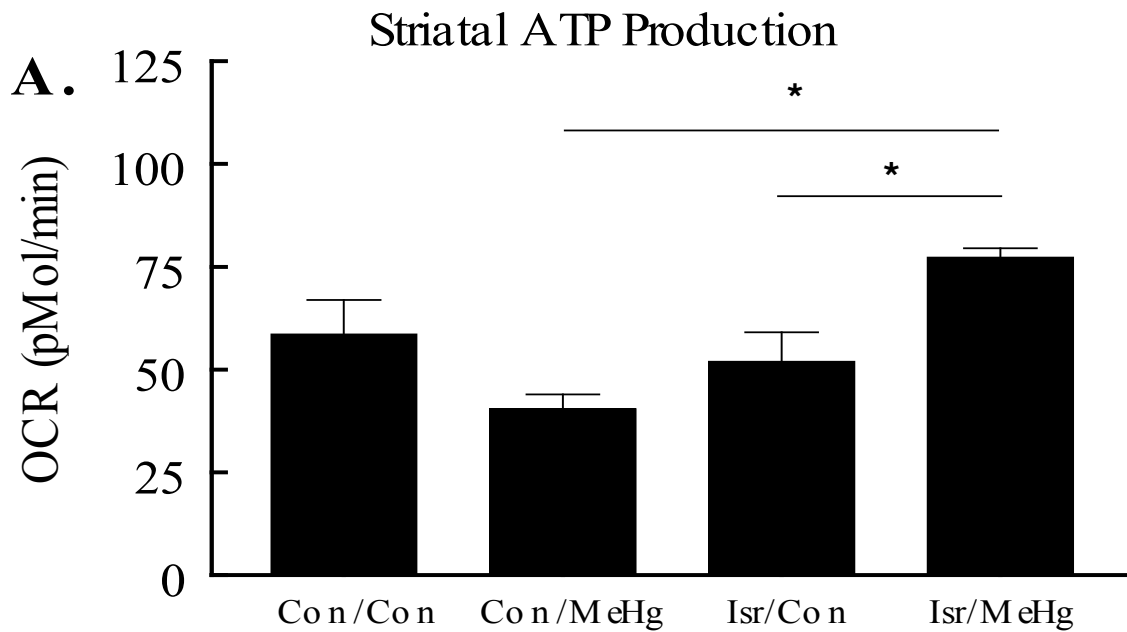


Figure 4.8. Twelve month Isr/MeHg treatment caused a significant increase in ATP production in both striatal and cortical synaptosome mitochondria. Quantification of (A) striatal and (B) cortical synaptosome ATP production. 12mo Isr/MeHg treatment caused a significant increase in ATP production compared to both Isr/Con and Con/MeHg treatment groups. * = significant difference (One-Way ANOVA, Tukey's post-test, $p < 0.05$) ($n \geq 5$). Data are means \pm SEM.

treatment may induce mitochondrial dysfunction in specific cell types as seen in the decrease in ATP production of striatal synaptosomes following 12mo treatment. However, when animals are co-treated with Isr the mitochondria are able to meet the increased ATP demand that accounts for the increased ATP production.

d. High speed $[Ca^{2+}]_i$ imaging

To determine if chronic MeHg treatment altered Ca^{2+} entry pathways, striatal slices from 12mo treated animals were exposed to high [KCl] (40mM) and the glutamate receptor agonists, NMDA and AMPA. Slices from all treatment groups responded similarly to 40mM KCl; there was no difference between the fura-2 response, time-to-peak, or amplitude of response (Figure 4.9A-C). These data are in contrast to what was seen in Chapter 2 in which prolonged MeHg treatment inhibited KCl-induced Ca^{2+} influx in SH-SY5Y cells. This may be due to a compensatory mechanism that increases VGCC expression in striatal neurons in order to account for blocked VGCCs. The striatal response to NMDA was variable between treatments groups and amongst striatal slices within the same treatment group. Many times slices did not respond to NMDA, which resulted in an 'n' value less than 3. No differences were found between the time-to-peak or amplitude of response to NMDA (Figure 4.10A-C). The response of striatal slices to AMPA was also recorded (Figure 4.11A). The Isr/Con and Isr/MeHg groups appeared to respond in a biphasic manner with a first phase being a fast low amplitude response followed by a more prolonged high amplitude response. All treatment groups responded to AMPA and had a sustained increase in $[Ca^{2+}]_i$ that did not return to baseline. AMPA receptors desensitize quickly, which should result in an increase in $[Ca^{2+}]_i$ followed by a decrease in $[Ca^{2+}]_i$ resulting in a return to baseline. This did not occur in any treatment group. The Con/Con group began to return

to baseline, however that was never reached. Work done by Tseng et al. (2007) demonstrated that a sustained depolarization in striatal MSNs could be mediated by Ca^{2+} influx through NMDA receptors. Taken together this suggests that application of AMPA is sufficient to depolarize the MSN membrane and cause activation of NMDA receptors resulting in a sustained increase in $[\text{Ca}^{2+}]_i$. There was no difference between treatment groups in their amplitude of response (Figure 4.11C). However, the time-to-peak fluorescence of the Con/MeHg group was significantly faster than the Con/Con group (Figure 4.11B). This suggests that 12mo MeHg treatment causes an increase in AMPA receptor expression or causes a sensitization of AMPA receptors to AMPA resulting in a faster response time.

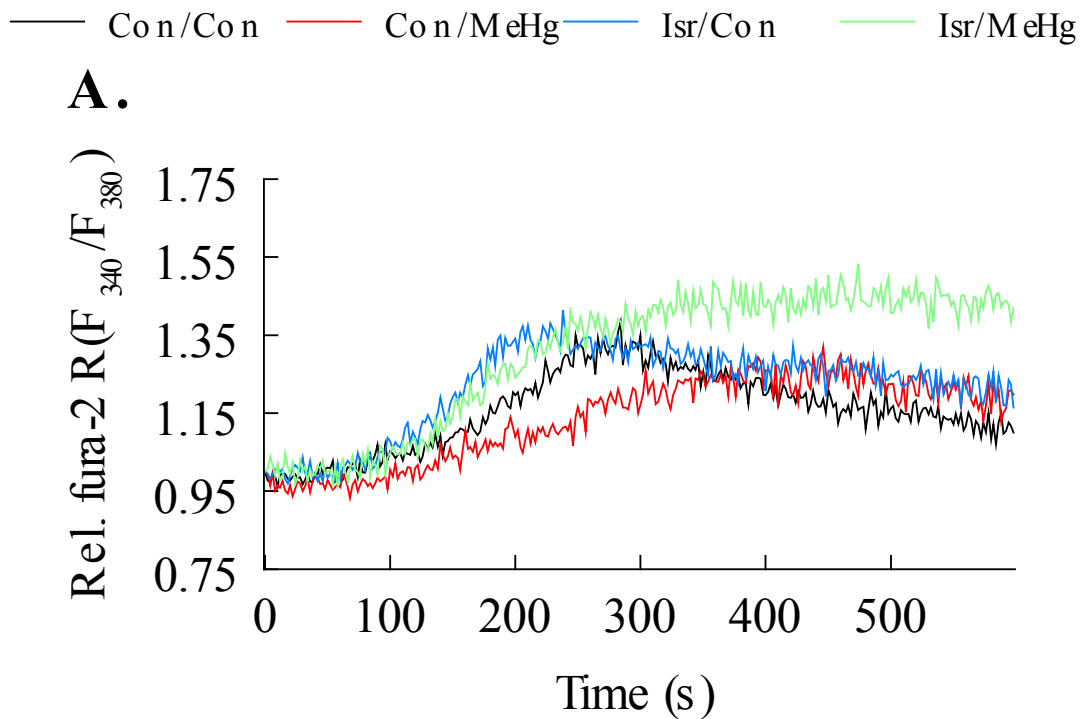
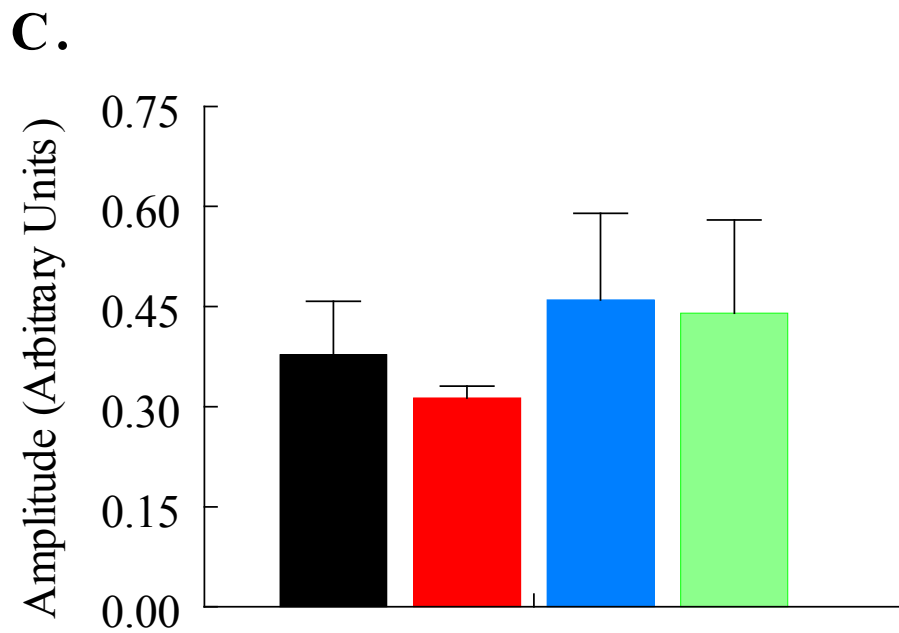
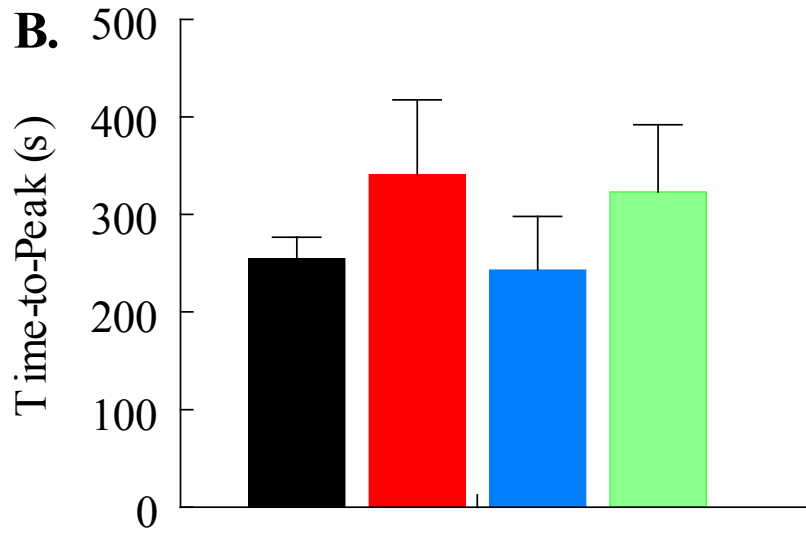


Figure 4.9. Twelve month MeHg or Isr/MeHg did not alter striatal response to KCl-induced $[Ca^{2+}]_i$ increase. Striatal slices were loaded with fura-2AM and then exposed to 40mM KCl for 2min followed by 8min of ACSF. Fura-2 fluorescence was continuously monitored. Data are presented as relative fura-2 fluorescence (Fluorescence at time 0/fluorescence at time x). An increase in fura-2 fluorescence corresponds to an increase in $[Ca^{2+}]_i$. Time-to-peak fluorescence was determined for each treatment group. **(A)** Striatal $[Ca^{2+}]_i$ response to 40mM KCl. **(B)** Time-to-peak and **(C)** amplitude of response was quantified. No Differences were detected between treatment groups. Data are means \pm SEM ($n \geq 3$).

(Figure 4.9 cont'd)

■ Con/Con ■ Con/MeHg ■ Isr/Con ■ Isr/MeHg



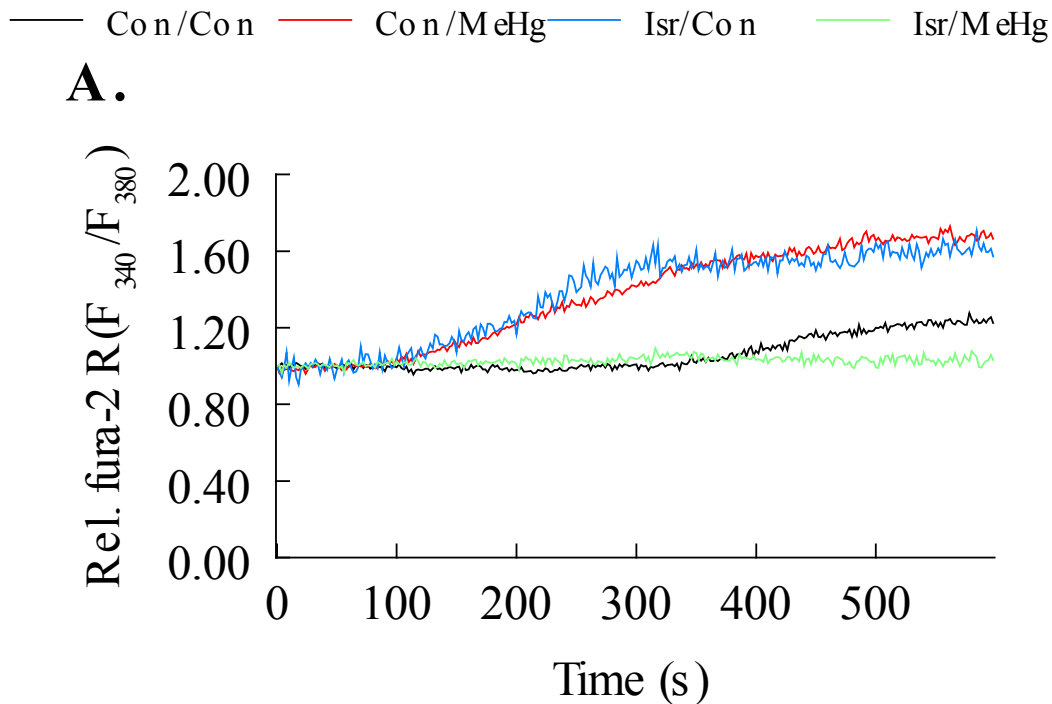
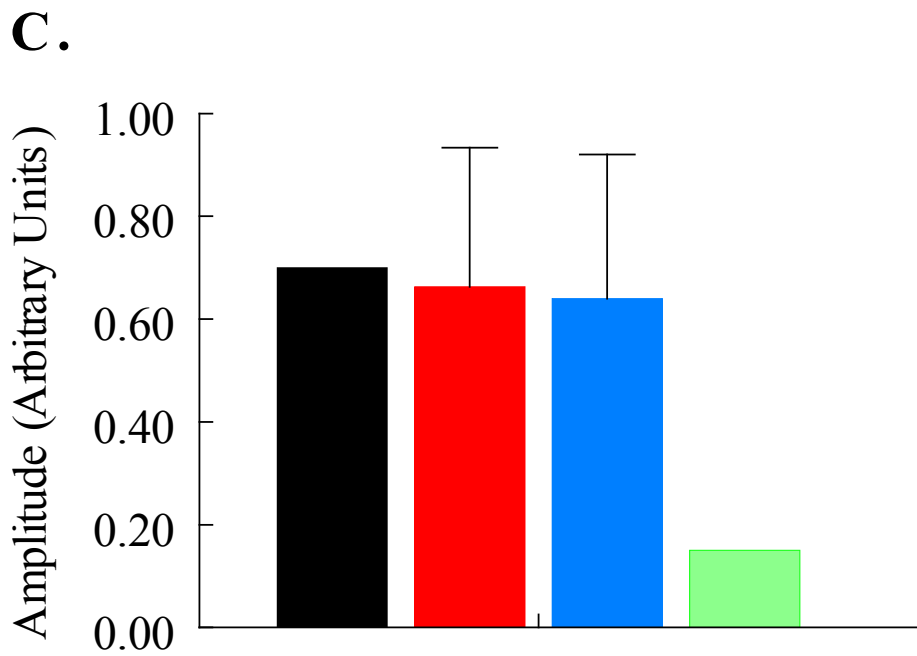
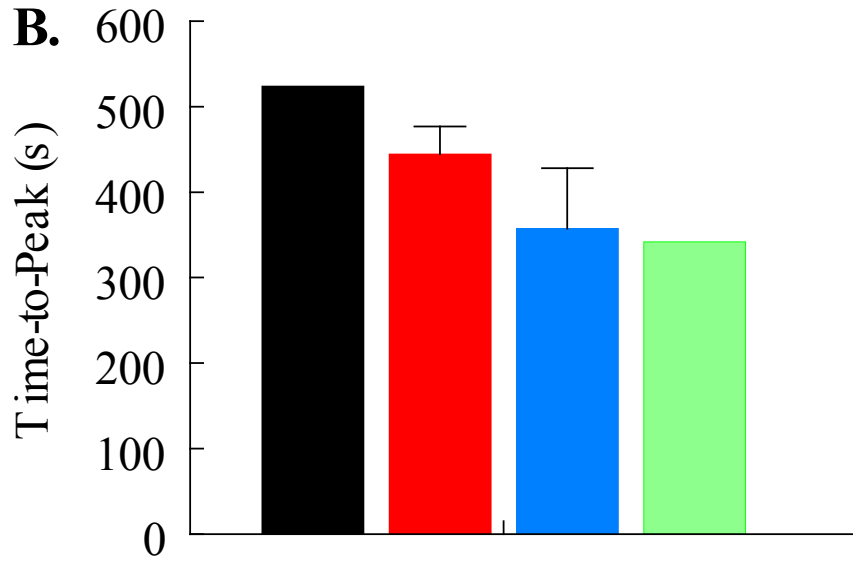


Figure 4.10. Twelve month MeHg or Isr/MeHg did not alter striatal response to NMDA-induced $[Ca^{2+}]_i$ increase. Striatal slices were loaded with fura-2AM and then exposed to 50 μ M NMDA and 10 μ M glycine for 2min followed by 8min of ACSF. Fura-2 fluorescence was continuously monitored. Data are presented as relative fura-2 fluorescence (Fluorescence at time 0/fluorescence at time x). An increase in fura-2 fluorescence corresponds to an increase in $[Ca^{2+}]_i$. Time-to-peak fluorescence was determined for each treatment group. **(A)** Striatal $[Ca^{2+}]_i$ response to 50 μ M NMDA. **(B)** Time-to-peak and **(C)** amplitude of response was quantified. Many slices did not respond to NMDA application resulting in an n value less than 3.

(Figure 4.10 cont'd)

■ Con/Con ■ Con/MeHg ■ Isr/Con ■ Isr/MeHg



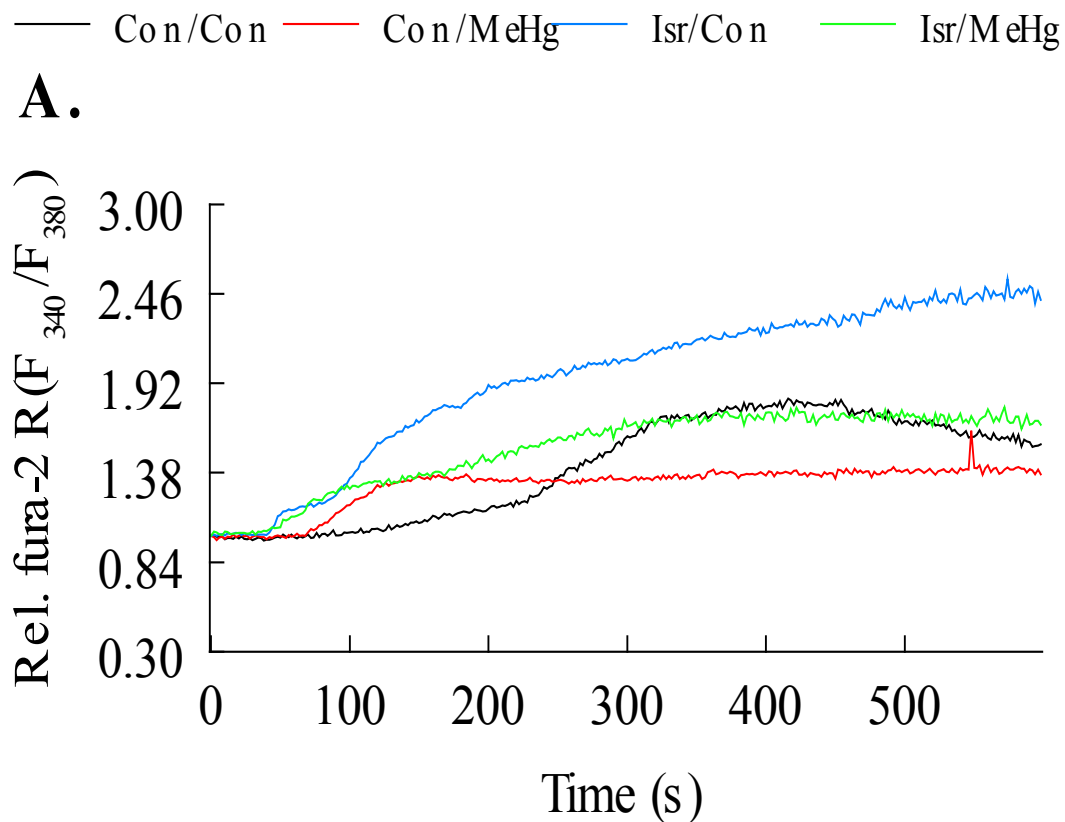
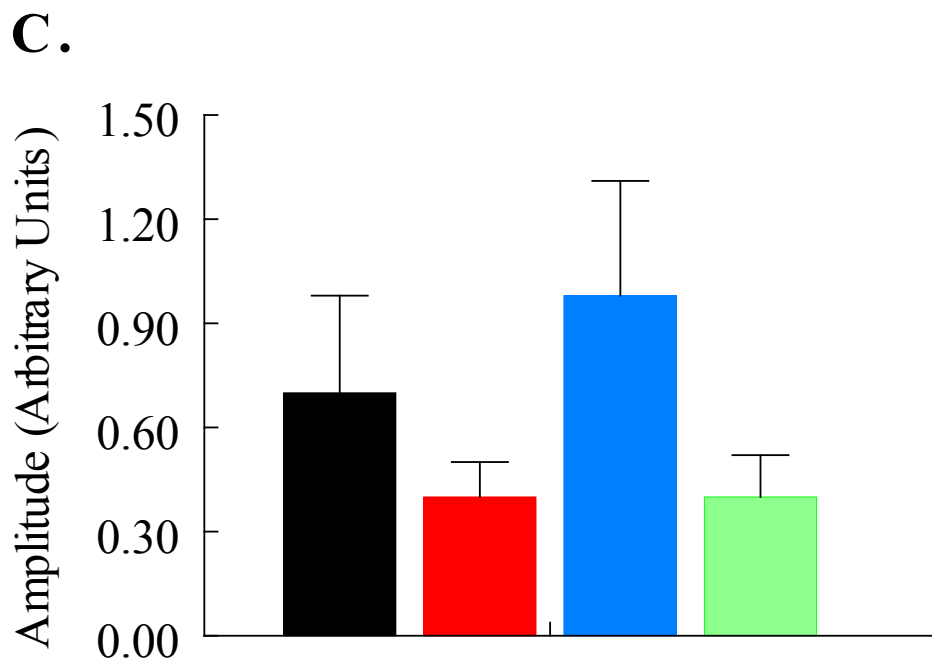
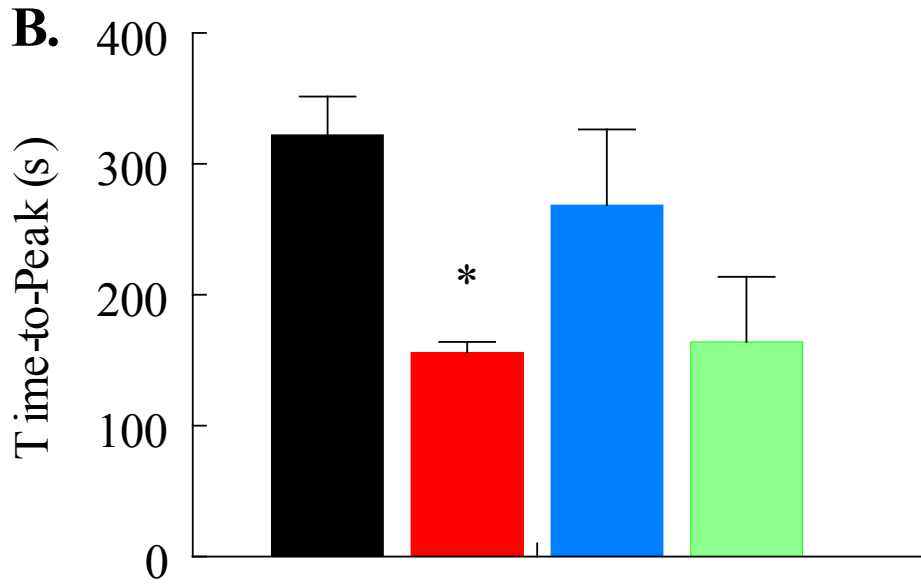


Figure 4.11. Twelve month MeHg treatment caused a significantly decreased time-to-peak fluorescence following application of AMPA. Striatal slices were loaded with fura-2AM and then exposed to 25 μ M AMPA for 2min followed by 8min of ACSF. Fura-2 fluorescence was continuously monitored. Data are presented as relative fura-2 fluorescence (Fluorescence at time 0/fluorescence at time x). An increase in fura-2 fluorescence corresponds to an increase in $[Ca^{2+}]_i$. Time-to-peak fluorescence was determined for each treatment group. (A) Striatal $[Ca^{2+}]_i$ response to AMPA (B) 12mo MeHg treatment caused a significantly faster time-to-peak fluorescence in response to AMPA ($p < 0.05$, unpaired student t-test, $n \geq 3$). (C) Amplitude of response was not affected by treatment. Data are means \pm SEM ($n \geq 3$).

(Figure 4.11 cont'd)

■ Con/Con ■ Con/MeHg ■ Isr/Con ■ Isr/MeHg



D) Discussion

The objective of this study was to determine whether chronic adult-onset exposure to low-dose MeHg would alter mitochondrial function or Ca^{2+} regulation and if co-treatment with a L-type VGCC antagonist would prevent or delay those effects. Studies focused on striatal synaptosome mitochondrial function and striatal MSN Ca^{2+} regulation. The NSDA cell bodies lie in the SNc and project to the striatum where they release DA. They are autonomously active and firing of action potentials is due to Ca^{2+} influx through $\text{Ca}_v1.3$ channels (Bonci et al, 1998; Ping and Shepard, 1996; Puopolo et al., 2007). Due to the continual fluctuations in $[\text{Ca}^{2+}]_i$ we hypothesized that chronic MeHg treatment would result in decreased mitochondrial function and Isr would prevent or delay those effects. In Chapter 3 we established that striatal MSNs are susceptible to MeHg-induced Ca^{2+} dysregulation. Therefore we hypothesized that chronic MeHg exposure would disrupt Ca^{2+} regulation and Isr co-treatment would prevent effects associated with VGCCs.

Results of this study are consistent with the following conclusions. First, chronic exposure to Isr/MeHg treatment causes increased ATP demand in both striatal and cortical synaptosomes, an effect consistent with MeHg-induced $[\text{Ca}^{2+}]_i$ increase. Second, chronic exposure to MeHg results in a faster time-to-peak of $[\text{Ca}^{2+}]_i$ in response to AMPA, indicative of sensitized or increased expression of AMPA receptors.

This was the first study of its kind to expose adult mice to an environmentally relevant dose of MeHg for 12mo and investigate the potential effects in a wide range of tissues and end points. This was a highly collaborative study with researchers investigating the effects of MeHg

in a variety of tissues on Ca^{2+} regulation, neurotransmission, and ion-channel expression. The work presented in this chapter was a small piece to a larger puzzle that will be assembled to provide a better understanding of a lifetime exposure to a low dose of MeHg on neuronal function. Previous studies have investigated the long-term effects of an environmentally relevant dose of MeHg on oxidative stress, mitochondrial function, and cell death (Huang et al., 2008; Bourdineaud et al., 2008; Cambier et al., 2009; Bourdineaud et al., 2011; Sokolowski et al., 2011), however these studies lack the integrative nature of ours and do not provide an overall understanding of what occurs following a long-term exposure to MeHg.

This study demonstrates that following a 6mo exposure MeHg in adult mice there were no significant differences in striatal synaptosome mitochondrial function. However, there was a slight change in ATP production that is worthy of discussion. ATP production of both Isr/Con and Isr/MeHg groups were slightly lower than the non-Isr treated groups. This is consistent with previous reports demonstrating that dihydropyridines slow the utilization of ATP (Sauter and Rudin, 1987; Rudin and Sauter, 1989). These studies demonstrated that dihydropyridines slow ATP consumption not by changing the rate of ATP production but by reducing its consumption in a rat model of global ischemia (Rudin and Sauter, 1989).

In contrast to the 6mo treatment, 12mo MeHg treatment caused a small reduction in ATP production in striatal synaptosomes that was not seen in cortical synaptosomes. Although the reduction in ATP was not significant if the power of study had been increased we may have found a significant difference. It is interesting that this decrease was seen solely in the striatal synaptosomes and not in the cortical synaptosomes. This supports our hypothesis that SNc neurons may be uniquely sensitive to MeHg-induced damage. Numerous studies have shown acute exposure to MeHg causes mitochondrial dysfunction resulting in increased ROS (Oyama et

al., 1994; Yee and Choi, 1996; Polunas et al., 2011), loss of mitochondrial membrane potential (Bondy and McKee, 1991; Hare and Atchison, 1992; Limke and Atchison, 2002) and a reduction of ATP production (Sone et al., 1977; Verity et al., 1975). Studies, which used a low-dose and long-term exposure, also found that MeHg caused a mitochondrial dependent increase in ROS (Sokolowski et al., 2011; Mori et al., 2011), reduction in mitochondrial respiration (Bourdineaud et al., 2008) and ATP production (Cambier et al., 2009). Our data demonstrate that an adult onset low-dose 12mo exposure results in decreased ATP production. This reduction may be due to a loss of the mitochondrial membrane potential, which drives ATP production (Hill et al., 2012) or MeHg-induced damage to the electron transport chain (Yee and Choi, 1996; Mori et al., 2011) causing a reduction in ATP production or a combination of the two. Experiments utilizing single synaptosome fluorescent imaging (Choi et al., 2009) to measure mitochondrial membrane potential could address these possibilities.

Twelve-month treatment with Isr/MeHg resulted in a significant increase in both striatal and cortical synaptosome ATP production. Isr is a vasodilator and is known to increase cerebral blood flow (Rudin and Sauter, 1989). The pharmacokinetics of Isr have also been shown to change with age in humans due to reduced liver function resulting in increased bioavailability, prolonged elimination half life, and increased peak plasma concentrations (Schachter, 1991). No adjustments were made in [MeHg] or [Isr] to accommodate potential changes in metabolism in the mice due to advanced age by the end of the study (15mo). Thus, Isr treatment may have increased cerebral blood flow throughout the duration of the study resulting in increased exposure of all brain regions to MeHg. This might lead to higher neuronal stress due to elevations in $[Ca^{2+}]_i$ increasing ATP demand. Therefore, the Isr/MeHg synaptosomal mitochondria increased ATP production to account for increased demand. This theory could be

tested by analyzing Hg content in frozen brain samples from a representative sample of mice from each treatment group.

In an attempt to investigate that effects of chronic MeHg treatment on the function of VGCCs and Ca^{2+} -permeable glutamate receptors, Ca^{2+} imaging experiments were performed in striatal slices. As discussed earlier, there are 2 major subsets of MSNs which cannot be differentiated based on morphology. The striatonigral MSNs predominantly express the D1 receptor, which is positively coupled to adenylyl cyclase, and activation causes an increase in $[\text{Ca}^{2+}]_i$ (Surmeier et al., 2007). The striatopallidal MSNs mainly express the D2 receptor and are coupled to $G_{i/o}$ which inhibits adenylyl cyclase and reduces the opening of VGCCs (Surmeier et al., 2007). We were unable to identify if we were collecting data from striatonigral or striatopallidal MSNs in these Ca^{2+} imaging experiments. Regardless, we found that 12mo exposure to MeHg resulted in a faster time-to-peak of $[\text{Ca}^{2+}]_i$ in response to AMPA. This could be due to sensitization of the AMPA receptor to agonists, or increased AMPA receptor expression. A similar response was seen in a study investigating the possible contribution of MeHg to the onset of an amyotrophic lateral sclerosis- (ALS) like phenotype in genetically-susceptible mice. Intracellular Ca^{2+} fluorescence recordings in brainstem slices from mice exposed to MeHg for 120 days had enhanced Ca^{2+} influx in response to AMPA application (Johnson et al., 2011). Therefore, chronic MeHg may sensitize the AMPA receptor by inducing a conformational change allowing more Ca^{2+} to enter the cell upon activation. However, the alternative possibility is that chronic MeHg caused increased receptor expression. Activation of the D1 receptor in striatonigral MSNs enhances the expression of both AMPA and NMDA

receptors (Surmeier et al., 2007). Exposure to MeHg induces DA release (Faro et al., 2007; Dreiem et al., 2009) at SNc nerve terminals. Therefore chronic MeHg treatment may cause persistent increases in DA release, which activate post-synaptic D1 receptors on MSNs and result in increased AMPA receptor expression. Isr treatment inhibits DA release (Nakane et al., 1995) and prevents the MeHg-induced change in AMPA receptor expression.

In conclusion, this study demonstrated that 12mo exposure to low-dose MeHg does not significantly alter striatal synaptosome mitochondrial function. However co-treatment with the VGCC antagonist Isr results in significantly increased ATP production consistent with MeHg-induced Ca^{2+} -dysregulation causing an increased ATP demand. We also demonstrated that 12mo exposure altered AMPA receptor response supporting a role for MeHg-induced alterations in glutamate signaling. These results support a role for the interaction of MeHg with the basal ganglia altering its function.

CHAPTER FIVE
SUMMARY AND CONCLUSIONS

SUMMARY AND CONCLUSIONS

This thesis presents the results of experiments designed to understand the effects of chronic exposure to low levels of MeHg on Ca^{2+} regulation and mitochondrial function. I knew from the literature that acute exposure to MeHg alters neuronal Ca^{2+}_i regulation (Komulainen and Bondy, 1987; Denny and Atchison, 1994; Marty and Atchison, 1997; Edwards et al., 2005), VGCC function (Shafer et al., 1990; Shafer and Atchison, 1991; Sirois and Atchison 2000; Peng et al., 2002; Yuan et al., 2005), mitochondrial function (Levesque and Atchison, 1991; Limke and Atchison, 2002), and induces cell death (Marty and Atchison, 1998; Edwards et al., 2005). The central hypothesis guiding these studies was that MeHg toxicity is due to its dysregulation of the Ca^{2+} homeostasis system, mainly by disrupting mitochondrial and Ca^{2+} -permeable ion channel function. Based on our *in vitro* experiments we found that prolonged exposure to low-nanomolar MeHg causes a time- and subtype-dependent block of VGCCs, as well as increased resting $[\text{Ca}^{2+}]_i$. This is shown in Figure 5.1. The *in vivo* experiments suggest that MeHg interacts with the post-synaptic response to glutamate at MSN AMPA receptors. Following Isr/MeHg treatment, mitochondrial ATP production was increased in striatal synaptosomes. This suggests that chronic exposure to MeHg alters neuronal glutamatergic neurotransmission and ATP demand. This is shown in Figure 5.2.

In the first set of experiments, Ca^{2+}_i regulation and L- and N-type VGCC function in differentiated SH-SY5Y cells were investigated following acute and prolonged MeHg exposure. Overall this study demonstrated that differentiated SH-SY5Y cells respond to acute MeHg exposure in the characteristic biphasic manner. This response has been demonstrated in

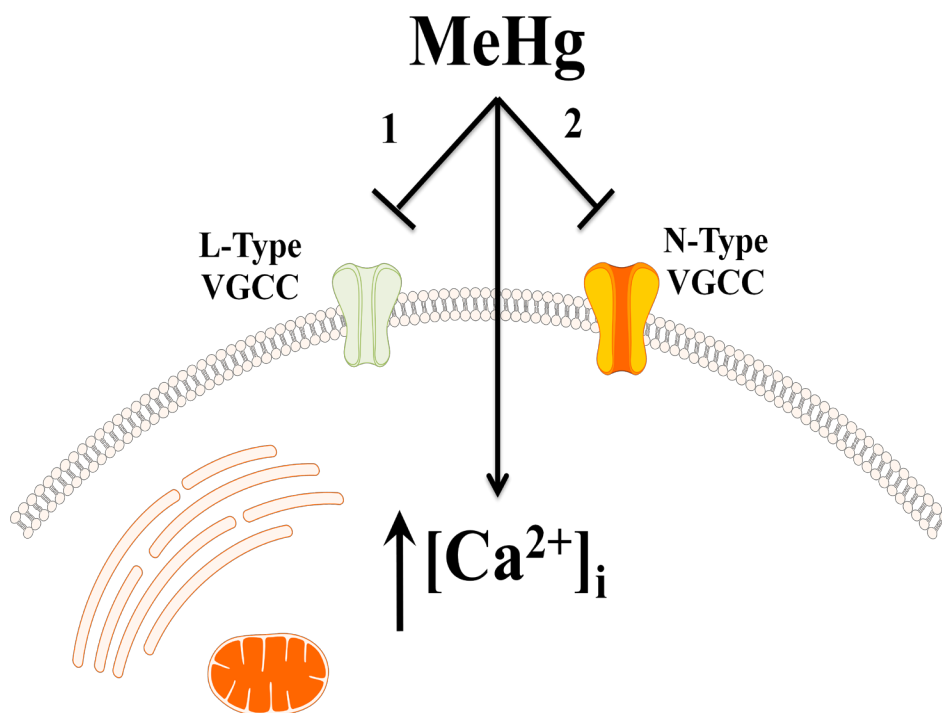


Figure 5.1. A schematic representation of the effects of prolonged exposure to MeHg in differentiated SH-SY5Y cells. Exposure of differentiated SH-SY5Y cells with 20nM MeHg resulted in a time- and VGCC subtype-dependent block of depolarization-dependent $[Ca^{2+}]_i$ increase. MeHg blocked KCl-induced Ca^{2+} increase through L-type VGCCs after a 48h exposure and through both L- and N-type VGCCs after 72h exposure. The resting $[Ca^{2+}]_i$ was also significantly increased following 72h MeHg exposure.

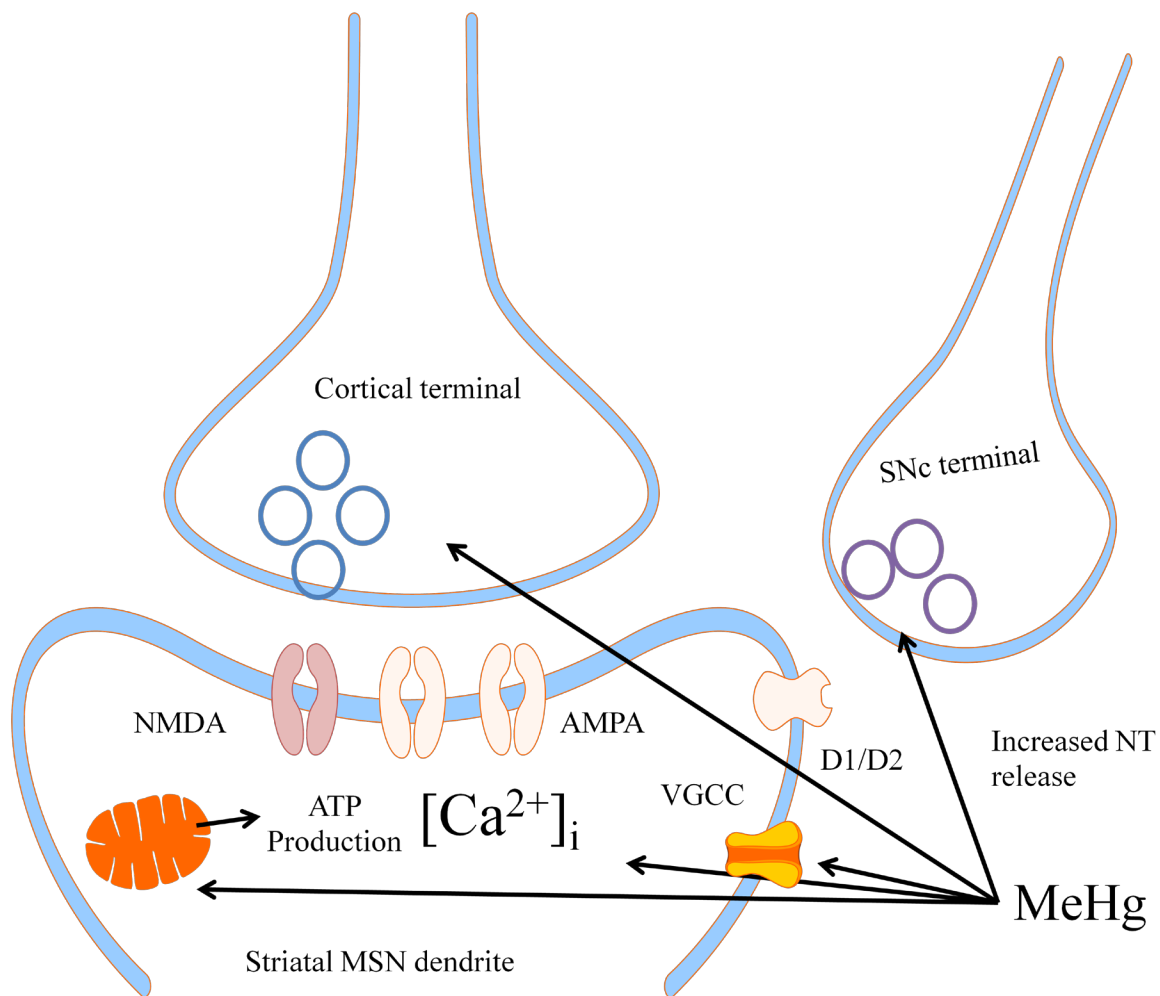


Figure 5.2. Schematic diagram of the effects of MeHg on the striatal circuit. MeHg acts at striatal MSNs to causes increases in $[Ca^{2+}]_i$ as well as alter mitochondrial ATP production. It has also been shown to cause increase in both DA and glutamate release. These actions along with potential direct interactions with AMPA receptors results in altered post-synaptic Ca^{2+} response to AMPA receptor activation.

cerebellar granule cells (Marty and Atchison, 1997), cerebellar purkinje cells (Edwards et al., 2005), spinal motor neurons (Ramanathan and Atchison, 2011), and NG108-15 cells (Hare and Atchison, 1995). Also, treatment with L- and N-type VGCC antagonists delayed the onset of phase 2 in differentiated SH-SY5Y cells. The ability to delay the onset of phase 1 or phase 2 with VGCC antagonists varies amongst cell types. The addition of GVIA or Nif delays the onset of both phase 1 and phase 2 in primary cerebellar granule cells and primary motor neurons (Marty and Atchison 1997; Ramanathan and Atchison, 2011) however they delay only phase 2 in NG108-15 (Hare and Atchison, 1995) and SH-SY5Y cells. The difference in response seen may be due to the fact that primary neurons are more sensitive to acute MeHg treatment than immortalized cells lines. They also differ in their ion channel expression, specifically in expression of the P/Q-type VGCC. Cerebellar granule cells and motor neurons express the P/Q-type channel (Westenbrook et al., 1998; Bawa and Abbott, 2008) while the NG108-15 and SH-SY5Y cells express negligible levels of P/Q VGCCs (Lukyanetz., 1998; Sousa et al., 2013). We hypothesize that MeHg uses VGCCs as a portal of entry into the cell and differences in VGCC expression may account for the differences in protection afforded by VGCC antagonists.

After characterizing the acute response of differentiated SH-SY5Y cells to MeHg we characterized the effects of prolonged exposure to MeHg on VGCC function. We demonstrated that prolonged exposure to low nanomolar MeHg causes a time- and subtype-dependent block of VGCCs. This is consistent with previous studies, which found that exposure to MeHg blocked depolarization-dependent Ca^{2+} entry into forebrain synaptosomes and differentiated PC12 cells (Atchison et al., 1986; Shafer et al., 1990; Shafer and Atchison., 1991; Shafer et al., 2002). The exact mechanism by which MeHg blocks Ca^{2+} entry via VGCCs is not currently understood. Shafer and Atchison (1991) suggested that due to its lipophilicity MeHg may diffuse across the

plasma membrane and then access the pore of the Ca^{2+} channel from the cytoplasmic side and block the entry of Ca^{2+} . Acute treatment studies found that the block was not dependent upon the configuration of the channel (Shafer et al., 1990) and could occur when the channel was in the resting, activated, or inactivated state. In our experiments we found that L-type VGCCs were more sensitive to block by MeHg than N-type channels. This suggests that L-type channels have a unique characteristic which make them more vulnerable to MeHg-induced block, such as the amount of time it spends open or amino acid composition. Our prolonged exposure experiments also demonstrated that when exposed to the nanomolar MeHg, the VGCC block does not occur immediately. This differs from the acute treatment studies, which used low micromolar MeHg and observed a block within seconds (Shafer et al., 1990; Shafer and Atchison, 1991). When at very low [MeHg], the kinetics of its actions are much slower demonstrating that 1) it takes longer to enter into the cell; 2) there are other cellular targets that MeHg interacts with prior to altering VGCC function; or 3) intracellular [MeHg] needs to reach a certain level before it interacts with VGCCs. Regardless of the exact mechanism by which MeHg blocks VGCCs these effects will impact neurotransmission, further altering neuronal function.

This study could be strengthened with the addition of a number of experiments. Decreased KCl-induced Ca^{2+} influx may have been due to an altered concentration gradient across the plasma membrane, altered VGCC expression, or block of the channel by MeHg. We found that prolonged exposure to nanomolar MeHg causes an increase in the resting $[\text{Ca}^{2+}]_i$. An increase in intracellular cations would depolarize the membrane altering the electrogenic gradient. Experiments utilizing fluorescent potentiometric probes or an electrophysiology current clamp could test for changes in membrane potential in treated and untreated cells. Prolonged

exposure to MeHg may also alter the expression of VGCCs. Gene expression of both N- and L-type VGCCs could be measured using real-time polymerase chain reaction (RT-PCR). The protein expression could be measured using western blot or immunocytochemistry. Although western blots are a more quantitative method, the use of immunocytochemistry may prove to be more useful in this situation. Only those channels located at the cell membrane are functional, so omission of the permeabilization agent when performing immunocytochemistry would allow for staining of channels located only at the cell membrane. However the availability of an antibody that recognizes an extracellular component of the $\alpha 1$ (pore-forming subunit of VGCCs) subunit may be the limiting factor in the utilization of this technique.

The next step for this project would be to perform the same MeHg treatments but add both earlier and later time points. By adding more time points we would gain a better understanding of the temporal action of MeHg. Is it blocking L-type channels immediately or does it occur after a set period of time? At later time points is the same profile of block seen or does the cell compensate by inserting more VGCCs into the plasma membrane? Investigation of mitochondrial function and the dynamics of DA release and at each time point would create a comprehensive overview of MeHg-induced neuronal changes following prolonged exposure. Acute MeHg exposure *in vitro* alters mitochondrial function (Limke and Atchison, 2002) and DA dynamics (Tiernan et al., 2013). We expect to find that mitochondrial function is decreased in a time-dependent manner resulting in the loss of ATP production. We expect to find that prolonged MeHg exposure would initially cause increased DA release followed by a reduction or complete block of DA release. The block of DA release would occur at the same time that the N-type channels were blocked, as they are known to be involved in neurotransmitter release (Catterall, 2011). Completion of these experiments would provide a comprehensive overview of

changes in Ca^{2+} homeostasis and neurotransmission following prolonged MeHg exposure. Once we have a better understanding of the temporal changes occurring following prolonged treatment *in vitro*, we can design *in vivo* experiments to test if these events occur in the whole animal.

Experiments described in Chapter 3 were aimed at investigating whether age alters the susceptibility of striatal MSNs to acute MeHg exposure. We found that aged MSNs are more susceptible than young MSNs to MeHg-induced Ca^{2+} dysregulation. This finding supports the hypothesis that aged neurons are unable to handle neuronal stressors predominantly, those which interact with the Ca^{2+} homeostasis system. Impairment of Ca^{2+} homeostasis, particularly alterations in mitochondrial function have been associated with neuronal aging (Troescu and Vreugdenhil, 2010). Aged neurons have depolarized mitochondria and reduced ATP production (Troescu, 2005). These factors would make them uniquely susceptible to MeHg-induced Ca^{2+} dysregulation. Aged neurons may not be able to buffer increases in $[\text{Ca}^{2+}]_i$ due to depolarized mitochondria, and they are unable to extrude Ca^{2+} via ATP-dependent pathways due to decreased availability to ATP. The experiments in Chapter 3 support these previous findings and suggest that a neuron's propensity to handle toxicants which interfere with Ca^{2+}_i decreases with age.

The work in Chapter 3 led us to a very interesting and unexpected finding. Following treatment with 20 μM or 100 μM MeHg, comparisons of time-to-peak Ca^{2+} response from 1, 9, and 21mo MSNs were no different than those of cerebellar granule cells. Cerebellar granule cells are extremely sensitive to MeHg toxicity (Hunter and Russell, 1954) and we expected that they would have a faster time-to-peak Ca^{2+}_i response than striatal MSNs. However, under the

conditions utilized in this study striatal MSNs and cerebellar granule cells are equally sensitive to MeHg-induced Ca^{2+} dysregulation. Cerebellar granule cells are more sensitive than cerebellar purkinje neurons (Edwards et al., 2005) to MeHg-induced changes in $[\text{Ca}^{2+}]_i$ and cytotoxicity. Because the granule cell is a sensitive target of MeHg-cytotoxicity they have been used as a model to understand changes in $[\text{Ca}^{2+}]_i$, mitochondrial function, and neurotransmission (for review see: Denny and Atchison 1996; Limke et al., 2004; Farina et al., 2011). The role of MeHg toxicity in striatal MSNs, specifically its effect on Ca^{2+}_i regulation has not been studied. Lesions occur in the striatum following administration of MeHg in rats (O'Kusky et al., 1988; O'Kusky and McGeer, 1989; Wakabayashi et al., 1995; Sakamoto et al., 1998). However, our understanding of the neurophysiological changes that occur in the striatum following MeHg exposure are limited. We know that MeHg alters DA neurotransmission (Tsuzuki, 1982; Kallisch and Racz, 1996; Faro et al., 1998, 2000, 2003, 2007), but very little is known about the direct effects of MeHg on MSNs. This study was the first to demonstrate that acute MeHg treatment causes increased $[\text{Ca}^{2+}]_i$ on a similar time scale to cerebellar granule cells. Taken together this study demonstrated that aged neurons are more susceptible to MeHg-induced damage than young neurons. This is of particular importance in populations of people that rely on fish or marine mammals as a main food source. Bjerregaard and Mulvad (2012) discussed the dietary habits of Greenlanders in a recent paper. They demonstrated that between the daily consumption of fish and marine mammals in a person 60yrs of age is double that of a 30yr old. Increased fish consumption and consequent exposure to MeHg may lead to more pronounced neuronal damage and accelerated neuronal aging. More studies need to be done to investigate the relationship

between aging and susceptibility to toxicants but a consideration must be made in reducing in the reference dose for senior citizens.

A number of improvements could have been made to the experiments described in Chapter 3. We utilized confocal microscopy and the Ca^{2+} sensitive fluorophore, Fluo-4 to monitor spatial changes in $[\text{Ca}^{2+}]_i$. Confocal microscopy allows for visualization through the entire thickness of the slice (200 μm) as opposed to only visualizing cells in one plane when using an inverted microscope. However, a drawback of using confocal microscopy is the length of time it takes to scan through the entirety of the slice. This limits the frequency at which you can scan without causing significant photobleaching. Therefore the data represent spatial changes in $[\text{Ca}^{2+}]_i$ at relatively static time points. While spatial changes are helpful in understanding what is occurring in a general region we cannot continuously monitor changes in $[\text{Ca}^{2+}]_i$ as we could in single cells. Utilization of high-speed imaging and fura-2 similar to that described in Chapter 4, would allow us to monitor continuously changes in fluorescence. The temporal data obtained from those experiments would provide more precise tracking of changes in $[\text{Ca}^{2+}]_i$. This may tease out differences in responses between striatal MSNs and cerebellar granule cells. Resting $[\text{Ca}^{2+}]_i$ could also be calculated with the use of fura-2 because of the ability to make ratiometric measurements. This would allow us to determine if one cell type starts at a significantly higher resting $[\text{Ca}^{2+}]_i$ causing it to be more susceptible to MeHg. The addition of these experiments would provide more insight into neuronal changes due to aging and a more in-depth view of the temporal events following acute MeHg exposure in each cell type.

The objective of experiments described in Chapter 4 was to investigate the effects of adult-onset chronic MeHg exposure on striatal synaptosome mitochondrial function and MSN Ca^{2+} regulation of exposure to MeHg. Contrary to our hypothesis we found that mitochondrial function was unchanged following 6mo of exposure to MeHg or Isr/MeHg. However, ATP production was slightly reduced in striatal synaptosomes but not in cortical synaptosomes following 12mo MeHg treatment. This indicates that SNc neurons may be more sensitive to MeHg-induced neuronal damage than other neuronal types. MeHg treatment disrupts mitochondrial function and decreases ATP production following acute (Verity et al., 1975; Sone et al., 1977; Kuznetsov et al., 1986; Levesque at Atchison, 1991) and long-term exposure (Bourdineaud et al., 2008; Cambier et al., 2009; Kong et al., 2013). Based on these studies we expected to find a significantly decreased ATP production following the 12mo MeHg treatment. Changes in ATP production may not have occurred in our study for a number of reasons. First, SNc synaptosomal mitochondria may not be a sensitive target for MeHg-induced damage. To understand if this is the case we could perform a comparative study between cerebellar and SNc mitochondria following chronic MeHg exposure. Another possibility is that SNc neurons are a sensitive target and we did not see a change in mitochondrial function because our synaptosome preparation contains a mixed population of nerve terminals. The striatum receives input from both the SNc and cortex so the synaptosome preparation would contain SNc, cortical, and MSN nerve terminals. It is possible that the SNc neurons were sensitive to MeHg-induced damage and began to degenerate. At the 12mo time point there were fewer SNc synaptosomes present and only the terminals of 'healthy' neurons present so no changes in ATP production were detected. We could have avoided this problem by isolating the SNc terminals using magnetic microbeads and performing mitochondrial function analysis on only those terminals. However, this technique

adds a significant cost to an already expensive study and experiment and was not pursued. We could also perform immunohistochemistry in fixed striatal slices probing for tyrosine hydroxylase to visualize if there was a loss of DA nerve terminals in the striatum. It could also be a possibility that the [MeHg] or length of exposure does not disrupt mitochondrial function. If we increased either of those variables we may find a disruption of mitochondrial function.

In Chapter 4 we also found that 12mo Isr/MeHg treatment caused a significant increase in mitochondrial ATP production in both striatal and cortical synaptosomes. An increase in ATP production could be thought of as being protective because the mitochondria are functional and able to respond to the ATP demand. Isr is protective in a number of models of neurodegenerative disease (Guzman et al., 2010; Ilijic et al., 2011), ischemia (Campbell et al., 1997), hypoxia (Barhwal et al., 2009), stroke (Berjukow and Hering, 2001) and senescence (Yu et al., 2013). The protective action may be due to a combination of the blockade of L-type Ca^{2+} channels (Schachter, 1991) and its antioxidant capacity (Takamura et al., 2000; Toniolo et al., 2002). Isr has also been shown to disrupt Ca^{2+}_m by blocking the main Ca^{2+}_m exit pathway, Na^+ -dependent release (Uceda et al., 1995). This may increase neuronal ATP demand because Ca^{2+} buffering would need to occur through ATP dependent pathways such as SERCA and the plasma membrane Ca^{2+} -ATPase. However, animals treated with Isr alone had no change in mitochondrial ATP production so any disruption in Ca^{2+} buffering due to Isr did not increase ATP demand. Only when animals were co-treated with MeHg was there a significant increase ATP production, suggesting that the increased demand is due to MeHg. Schafer et al (1990) found that MeHg disrupts VGCC antagonist binding in PC12 cells. Therefore, it is possible that instead of being protective co-treatment with Isr facilitated MeHg-induced damage. In the

presence of MeHg, Isr is unable to bind VGCCs offering no protection while increasing MeHg distribution by increasing cerebral blood flow. Consequently, there is an increased demand for ATP due to MeHg-induced Ca^{2+} -dysregulation. While we do not fully understand the interaction between Isr and MeHg and the change in ATP production it raises the possibility that drugs which increase cerebral blood flow cause increased neuronal exposure to toxicants. Drugs such as Isr, are typically prescribed in adults who may be more sensitive to damage by neurotoxicants, as seen in Chapter 3.

In Chapter 4 we also found that striatal MSNs from animals treated for 12mo with MeHg had a faster time-to-peak Ca^{2+} response following addition of AMPA than untreated animals. This may be due to increased AMPA receptor expression via the mechanism discussed in Chapter 4 or receptor sensitization, similar to what was seen by Johnson et al. (2011). The striatum receives glutamatergic input from the cortex and dopaminergic input from the midbrain (Surmeier et al., 2007). MeHg interacts with both dopaminergic (Faro et al., 2007; Dreiem et al., 2009) and glutamatergic (Juarez et al., 2002; Farina et al., 2003) nerve terminals to induce release. MeHg also inhibits glutamate uptake in cerebellar granule cells (Porciuncula et al., 2003) and astrocytes (Aschner et al., 2000). While these studies demonstrate that MeHg causes increase neurotransmitter release, electrophysiological studies have shown that acutely applied MeHg causes a increase and then cessation of spontaneous synaptic current (Yuan and Atchison, 2007). This suggests that while MeHg initially increases neurotransmitter release and subsequent post-synaptic current, the current is eventually blocked; possibly due to interactions of MeHg with the post-synaptic receptor. Glutamatergic post-synaptic receptors are also involved in MeHg-induced Ca^{2+} -dysregulation and cytotoxicity. Application of both NMDA and AMPA receptor

antagonists delays the onset of MeHg induced Ca^{2+} -dysregulation in spinal motor neurons (Ramanathan et al., 2011) but not cerebellar granule cells (Marty and Atchison, 1997). Also, application of MK-801, a NMDA receptor antagonist protects SH-SY5Y cells from MeHg cytotoxicity (Petroni et al., 2011). These data support a role for MeHg's interaction with post-synaptic glutamatergic receptors altering their function and possibly leading to altered expression. RT-PCR or immunohistochemistry could be completed on striatal tissue to determine if AMPA receptor expression was increased in MeHg-treated animals. Electrophysiological single channel recordings could be performed to measure channel conductance and rates of activation and inactivation to determine if MeHg altered the function of AMPA receptors.

We recognize that there are several limitations in these studies. Because animals had free access to MeHg in their drinking water and Isr in their feed there was no control over the amount or timing of their consumption. This may have introduced variability within and amongst treatment groups. A better method would have been to inject mice with MeHg at the same time on a daily basis as well as insert an osmotic pump, which would release Isr. An alternative to administering Isr would be to use $\text{Ca}_v1.3$ knockout mice. These mice are commercially available and do not have a lethal phenotype. These methods would greatly reduce the variability in the study. Another improvement would be to increase the number of time-points. It is not possible to understand the time course of changes in neuronal function by only sampling at 2 time-points, an improved approach may be to sample 5-6 mice every month. Having more time-points would allow for a better overall picture of alterations that occur in the neuron. However a deficiency of this approach is the lack of statistical power that would be necessary by lowering the sample size, or a major increase in cost if the number of animals was kept at the power level utilized in the present study.

There are a number of experiments that would complement the work already completed. In order to have a better understanding of the effects of chronic MeHg treatment on mitochondrial function electron microscopy experiments could be completed to examine the number and structure of synaptosomal mitochondria. Aging and exposure to toxicants has been shown to alter the number of mitochondria present at the nerve terminal as well as their structure (Pivovarova et al., 2013; Quiroz-Baez et al., 2013). Examination of the ultra-structural properties of synaptosomal mitochondria would offer insight into whether the mitochondria are healthy or if there are an increased number of mitochondria present to handle the increased demand to buffer Ca^{2+} and produce ATP. Simultaneous Ca^{2+} imaging and electrophysiological experiments similar to those done by Dryanovski et al. (2013) could be performed in both striatal MSNs and midbrain SNc neurons. This would greatly contribute to our understanding of both the Ca^{2+}_i as well as any alterations in neurotransmission that occur due to chronic MeHg treatment. Upon completion of electrophysiological recordings the intracellular contents of the cell could be collected and single-cell RT-PCR (Toledo-Rodriguez and Markram, 2007) performed to determine changes in gene expression. Another experiment that would contribute to the overall understanding of MeHg-induced alterations in neuronal function would be the continuous monitoring of DA and glutamate in the striatum by implementation of a microdialysis probe (Bazzu et al., 2013). Completion of these experiments would provide a comprehensive overview of MeHg-induced changes in neuronal function of the basal ganglia.

This work highlights the need to have a better understanding of the consequences of long-term exposure to environmental toxicants, especially in aged individuals. Due to the complexity and cost of performing chronic treatment studies, the scientific field has largely avoided such experiments. However, due to an aging population (Abbott et al., 2011) and an increased interest

in the possible role of environmental contaminants in the development of neurodegenerative diseases (Johnson and Atchison, 2009; Vance et al., 2010; Williams et al., 2010; Cannon and Greenamyre, 2011; Madison et al., 2012) scientists must begin to investigate the consequences of long-term exposure to low levels of environmental toxicants. These studies demonstrate that prolonged exposure to MeHg alters the function of VGCCs *in vitro* and AMPA receptors *in vivo*. Alteration in the function of both VGCC and AMPA receptors could have detrimental effects on neuronal function and ultimately the behavior or disease state of an individual. The role of MeHg in the development of neurodegenerative and neuropsychiatric disorders is controversial. However, it is clear that disruption of neuronal homeostatic synaptic plasticity leads to neurological diseases (for review see: Wondolowshi and Dickman, 2013), and these studies support a role for MeHg disrupting this process by altering the function of key components of neuronal synaptic plasticity.

In conclusion, this dissertation shows that prolonged exposure to MeHg *in vitro* causes a time- and subtype-dependent block of VGCCs. It also causes a significant increase in resting $[Ca^{2+}]_i$. We presented novel data demonstrated that striatal MSNs from aged animals are more susceptible to MeHg-induced Ca^{2+} dysregulation than young animals. The MeHg-induced Ca^{2+} increase occurs at a similar time as cerebellar granule cells. Chronic exposure to low levels of MeHg *in vivo* did not alter mitochondrial function. However, when animals were co-treated with Isr and MeHg there was a significant increase in striatal synaptosome mitochondrial function. Finally, chronic exposure to MeHg altered postsynaptic Ca^{2+} response to AMPA receptor activation.

REFERENCES

REFERENCES

- Abbott A, Dementia: a problem for our age. *Nature* **475**:S2-4.
- Agholme L, Nath S, Domert J, Marcusson J, Kagedal K, Hallbeck M (2013) Proteasome inhibition induces stress kinase dependent transport deficits – Implications for Alzheimer’s disease. *Mol Cell Neurosci* [Epub ahead of print].
- Andersen P, Sundberg SH, Sveen O, Wigstrom H (1977) Specific long-lasting potentiation of synaptic transmission in hippocampal slices. *Nature* **266**:737-39.
- Ashner M, Farina M, Rocha J (2013) Mercury Neurotoxicity. In *Encyclopedia of Metalloproteins*. (1362-66). New York, New York: Springer Science.
- Aschner M, Yao CP, Allen JW, Tan KH (2000) Methylmercury alters glutamate transport in astrocytes. *Neurochem Int* **37**:199-06.
- Atchison WD, Joshi U, Thornburg J (1986) Irreversible suppression of calcium entry into nerve terminals by methylmercury. *J Pharmacol Exp Ther* **238**:618-24.
- Atchison WD, Hare MF (1994) Mechanisms of methylmercury-induced neurotoxicity. *FASEB J* **8**: 622-29.
- Bailey J, Hutsell B, Newland C (2013) Dietary nimodipine delays the onset of methylmercury neurotoxicity in mice. *Neurotoxicology* **37**:108-17.
- Bakir S, Damluji S, Amin-Zaki L, Murtadha M, Khalidi A, al-Rawi N, Tikriti S, Dahahir H, Clarkson T, Smith J, Doherty R (1973) Methylmercury poisoning in Iraq. *Science* **181**:230-241.
- Barhwal K, Hota SK, Baitharu I, Prasad D, Singh SB, Ilavazhagan G (2009) Isradipine antagonizes hypobaric hypoxia induced CA1 damage and memory impairment: Complementary roles of L-type calcium channel and NMDA receptors. *Neurobiol Dis* **34**:230-44.
- Bartolome J, Trepanier P, Chait EA, Seidler FJ, Deskin R, Slotkin TA (1982) Neonatal methylmercury poisoning in rat: effects on development of central catecholamine neurotransmitter systems. *Toxicol Appl Pharmacol* **65**:92-99.
- Basu N, Scheuhammer AM, Rouvinen-Watt K, Grochowina N, Evans RD, O’Brien M, Chan HM (2007) Decreased N-methyl-D-aspartic acid (NMDA) receptor levels are associated with mercury exposure in wild and captive mink. *Neurotoxicology* **28**:587-93.

- Bawa B, Abbott LC (2008) Analysis of calcium ion homeostasis and mitochondrial function in cerebellar granule cells of adult Cav2.1 calcium ion channel mutant mice. *Neurotox Res* **13**:1-18.
- Bazzu G, Rocchitta G, Migheli R, Alvau MD, Zinellu M, Puggioni G, Calia G, Mercanti G, Giusti P, Desole MS, Serra PA (2013) Effects of the neurotoxin MPTP and pargyline protection on extracellular energy metabolites and dopamine levels in the striatum of freely moving rats. *Brain Res* **1538**:159-71.
- Bracken WM, Sharma RP, Kleinschuster SJ (1981) The effects of select neurotoxic chemicals on synaptosomal monoamine uptake and K⁺-dependent phosphatase. *Fundam Appl Toxicol* **1**:432-36.
- Bellum S, Thuett KA, Grajeda R, Abbott LC (2007) Coordination deficits induced in young adult mice treated with methylmercury. *Int J Toxicol* **26**:115-21.
- Bergman H, Feingold A, Nini A, Raz A, Slovin H, Abeles M, Vaadia E (1998) Physiological aspects of information processing in the basal ganglia of normal and parkinsonism primates. *TINS* **21**:32.
- Berjukow S, Hering S (2001) Voltage-dependent acceleration of Cav1.2 channel current decay by (+)- and (-)-isradipine. *Br J Pharmacol* **133**:959-66.
- Bernardi P, Scorrano L, Colonna R, Petronilli V, Di Lisa F (1999) Mitochondria and cell death. *Eur J Biochem* **264**:687-01.
- Biedler JL, Helson L, Spengler BA (1973) Morphology and growth, tumorigenicity, and cytogenetics of human neuroblastoma cells in continuous culture. *Cancer Res* **33**:3751-57.
- Biedler JL, Roffler-Tarlov S, Schachner M, Freedman L (1978) Multiple neurotransmitter synthesis by human neuroblastoma cell lines and clones. *Cancer Res* **38**:3751-57.
- Bjerregaard P, Mulvad Gert (2012) The best of two worlds: how the Greenland Board of Nutrition has handled conflicting evidence about diet and health. *Int J Circumpolar Health* **71**:18588-93.
- Bolam J, Hanley J, Booth P, Bevan M (2000) Synaptic organisation of the basal ganglia. *J Anat* **196**:527-42.
- Bondy SC, McKee M (1991) Disruption of the potential across the synaptosomal plasma membrane and mitochondria by neurotoxic agents. *Toxicol Lett* **58**:13-31.

- Bonci A, Grillner P, Mercuri N, Bernardi G (1998) L-type calcium channels mediate a slow excitatory synaptic transmission in rat midbrain dopaminergic neurons. *J. Neurosci* **18**:6693-03.
- Bourdineaud JP, Bellance N, Benard G, Brethes D, Fujimura M, Gonzalez P, Marighetto A, Maury-Brachet R, Mormede C, Pedron V, Philippin JN, Rossignol R, Rostene W, Sawada M, Laclau M (2008) Feeding mice with diets containing mercury-contaminated fish flesh from French Guiana: a model for the mercurial intoxication of the Wayana Amerindians. *Environ Health* **7**:1-13.
- Braak H, Braak E (2000) Pathoanatomy of Parkinson's disease. *J Neurol* **247**:113-20.
- Bracken WM, Sharma RP, Kleinschuster SJ (1989) The effects of select neurotoxic chemicals on synaptosomal monoamine uptake and K⁺-dependent phosphatase. *Fundam Appl Toxicol* **1**:432-36.
- Brand MD, Nicholls D (2011) Assessing mitochondrial dysfunction in cells. *Biochem J* **435**:297-312.
- Brunton L, Parker K, Blumenthal, Buxton I (2008) *Goodman and Gilman's Manual of Pharmacology and Therapeutics*. (1134-1137) New York, New York: McGraw Hill.
- Bygrave FL, Ramachandran C, Smith RL (1977) On the mechanism by which inorganic phosphate stimulates mitochondrial calcium transport. *FEBS Lett* **83**:155-58.
- Cambier S, Benard G, Mesmer-Dudons N, Gonzalez P, Rossignol R, Brethes D, Bourdineaud JP (2009) At environmental doses, dietary methylmercury inhibits mitochondrial energy metabolism in skeletal muscles of zebra fish (*Danio rerio*). *Int J Biochem Cell Biol* **41**:791-19.
- Campbell CA, Mackay KB, Patel S, King PD, Stretton JL, Hadingham SJ, Hamilton TC (1997) Effects of isradipine, an L-type calcium channel blocker on permanent and transient focal cerebral ischemia in spontaneously hypertensive rats. *Exp Neurol* **148**:45-50.
- Cannon JR, Greenamyre JT (2011) The role of environmental exposures in neurodegeneration and neurodegenerative diseases. *Toxicol Sci* **124**:225-50.
- Castoldi AF, Onishchenko N, Johansson C, Coccini T, Roda E, Vahter T, Ceccatelli S, Manzo L (2008) Neurodevelopmental toxicity of methylmercury: Laboratory animal data and their contribution to human risk assessment. *Regul Toxicol Pharmacol* **2**:215-29.
- Catterall WA (2011) Voltage-gated calcium channels. *Cold Spring Harb Perspect Biol* **3**:1-23.
- Catterall WA, Perez-Reyes E, Snutch TP, Streissnig J (2005) International union of pharmacology. XLVIII. Nomenclature and structure-function relationships of voltage-gated calcium channels. *Pharmacol Rev* **57**: 411-25.

- Chan CS, Gertler TS, Surmeier DJ (2009) Calcium homeostasis, selective vulnerability and Parkinson's disease. *TINS* **32**:249-56.
- Chan C, Gunzman J, Ilijic E, Mercer J, Rick C, Tkatch T, Meredith G, Surmeier D (2007) 'Rejuvenation' protects neurons in mouse models of Parkinson's disease. *Nature* **447**:1081-86.
- Chernyak BV, Bernardi P (1996) The mitochondrial permeability transition pore is modulated by oxidative agents through both pyridine nucleotides and glutathione at two separate sites. *Eur J Biochem* **238**:623-30.
- Choi SW, Gerencser AA, Nicholls DG (2009) Bioenergetic analysis of isolated cerebrocortical nerve terminals on a microgram scale: spare respiratory capacity and stochastic mitochondrial failure. *J Neurochem* **109**:1179-91.
- Chuhma N, Tanaka K, Hen R, Rayport S (2011) Functional connectome of the striatal medium spiny neuron. *J Neurosci* **26**:1183-92.
- Clarkson TW and Magos L (2006) The toxicology of mercury and its chemical compounds. *Crit Rev Toxicol* **8**:609-62.
- Crompton M, Capano M, Carafoli E (1976) Respiration-dependent efflux of magnesium ions from heart mitochondria. *Biochem J* **154**:735-42.
- Dauer W, Przedborski S (2003) Parkinson's disease: mechanisms and models. *Neuron* **39**:889-09.
- Davidson PW, Myers GJ, Cox C, Wilding GE, Shamlaye CF, Huang LS, Cernichiari E, Sloane-Reeves J, Palumbo D, Clarkson TW (2006) Methylmercury and neurodevelopment: longitudinal analysis of the Seychelles child development cohort. *Neurotoxicol Teratol* **28**:529-35.
- Daidson PW, Leste A, Benstron E, Burns CM, Valentin J, Sloane-Reeves J, Huang LS, Miller WA, Gunzler D, van Wijngaarden E, Watson GE, Zareba G, Shamlaye CF, Myers GJ (2010) Fish consumption, mercury exposure, and their associations with scholastic achievement in the Seychelles Child Development Study. *Neurotoxicology* **31**:439-47.
- Davidson T, Cory-Slechta D, Thurston S, Huang L, Shamlaye C, Gunzler D, Watson G, van Wijngaarden E, Zareba G, Klein J, Clarkson T, Strain J, Myers G (2011) Fish consumption and prenatal methylmercury exposure: cognitive and behavioral outcomes in the main cohort at 17 years from the Seychelles child development study. *Neurotoxicology* **32**:711-17.

- Debes F, Budtz-Jørgensen E, Weihe P, White RF, Grandjean P (2006) Impact of prenatal methylmercury exposure on neurobehavioral function at age 14 years. *Neurotoxicol Teratol* **28**:536-47.
- de Lau L, Giesbergen P, Rijk M, Hofman A, Koudstaal P, Breteler M (2004) Incidence of parkinsonism and Parkinson disease in general population: the Rotterdam Study. *Neurology* **63**:1240-44.
- Denny MF, Hare MF, Atchison WD (1993) Methylmercury alters intrasynaptosomal concentrations of endogenous polyvalent cations. *Toxicol Appl Pharmacol* **122**:222-32.
- Denny MF, Atchison WD (1994) Methylmercury alters intrasynaptosomal concentrations of endogenous polyvalent cations. *Toxicol Appl Pharmacol* **122**:222-32.
- Denny MF, Atchison WD (1996) Mercurial-induced alterations in neuronal divalent cation homeostasis. *Neurotoxicology* **17**:47-61.
- Denton RM, McCormack JG (1980) The role of calcium regulation of mitochondrial metabolism. *Biochem Soc Trans* **8**:266-68.
- Dexter DT, Carter CJ, Wells FR, Javoy-Agid F, Agid Y, Lees A, Jenner P, Marsden CD (1989) Basal lipid peroxidation in substantia nigra is increased in Parkinson's disease. *J Neurochem* **52**:381-89.
- Dorsey R, Songer T, Zgibor J, Kelsey S, Ibrahim S, Orchard T (2007) Projected number of people with Parkinson disease in the most populous nations, 2005 through 2030. *Neurology* **68**:383-86.
- Dreiem A, Seegal RF (2007) Methylmercury-induced changes in mitochondrial function in striatal synaptosomes are calcium-dependent and ROS-independent. *Neurotoxicology* **28**:720-26.
- Dreiem A, Shan M, Okoniewski R, Sanchez-Morrissey, Seegal RF (2009) Methylmercury inhibits dopaminergic function in rat pup synaptosomes in an age-dependent manner. *Neurotoxicol Teratol* **31**:312-17.
- Dryanovski DI, Guzman JN, Xie Z, Galteri DJ, Volpicelli-Daley LA, Lee VM, Miller RJ, Schumacker PT, Surmeier DJ (2013) Calcium entry and α -synuclein inclusions elevate dendritic mitochondrial oxidant stress in dopaminergic neurons. *J Neurosci* **33**:10154-64.
- Dunkley P, Jarvie P, Robinson P (2008) A rapid percoll gradient procedure for preparation of synaptosomes. *Nat Protoc* **3**:1718-28.
- Edwards JR, Marty MS, Atchison WD (2005) Comparative sensitivity of rat cerebellar neurons to dysregulation of divalent cations and cytotoxicity caused by methylmercury. *Toxicol Appl Pharmacol* **208**:222-32.

- Fahn S (2003) Description of Parkinson's disease as a clinical syndrome. *Ann NY Acad Sci* **991**:1-14.
- Fang KM, Chang WL, Wang SM, SU MJ, Wu ML (2008) Arachidonic acid induces both Na⁺ and Ca²⁺ entry resulting in apoptosis. *Neurochem* **104**:1177-89.
- Farina M, Dahm KC, Schwalm FD, Brusque AM, Frizzo ME, Zeni G, Souza DO, Rocha JB (2003) Methylmercury increases glutamate release from brain synaptosomes and glutamate uptake by cortical slices from suckling rat pups: modulatory effect of ebselen. *Toxicol Sci* **73**:135-40.
- Farina M, Rocha J, Aschner (2011) Mechanisms of methylmercury-induced neurotoxicity: evidence from experimental studies. *Life Sci* **89**:555-63.
- Faro LR, do Nascimento JL, San Jose J, Alfonso M, Duran R (2000) Intrastratial administration of methylmercury increases in vivo dopamine release. *Neurochem Res* **25**:225-29.
- Faro LR, do Nascimento JL, Alfonso M, Duran R (1998) Acute administration of methylmercury changes in vivo dopamine release from rat striatum. *Bull Environ Contam Toxicol* **60**:632-38.
- Faro LR, do Nascimento JL, Alfonso M, Duran R (2002) Protection of methylmercury effects on the in vivo dopamine release by NMDA receptor antagonists and nitric oxide synthase inhibitors. *Neuropharmacology* **42**:612-18.
- Faro LR, Duran R, do Nascimento JL, Perez-Vences D, Alfonso M (2003) Effects of successive intrastratial methylmercury administrations on dopaminergic system. *Ecotoxicol Environ Saf* **55**:173-77.
- Faro LR, Rodrigues K, Santana M, Vidal L, Alfonso M, Duran R (2007) Comparative effects of organic and inorganic mercury on in vivo dopamine release in freely moving rats. *Braz J Med Biol Res* **40**:1361-65.
- Fonfria E, Vilaro MT, Babot Z, Rodriguez-Farre E, Sunol C (2005) Mercury compounds disrupt neuronal glutamate transport in cultured mouse cerebellar granule cells. *J Neurosci Res* **79**:545-53.
- Franco JL, Posser R, Dunkley PR, Dickson PW, Mattos JJ, Martins R, Bains AC, Marques MR, Dafre AL, Farina M (2009) Methylmercury neurotoxicity is associated with inhibition of the antioxidant enzyme glutathione peroxidase. *Free Radic Biol Med* **47**:449-57.
- Gandhi S, Wood-Kaczmar A, Yao Z, Plun-Favreau H, Deas E, Klupsch K, Downward J, Latchman DS, Tabrizi SJ, Wood NW, Duchon MR, Abramov AY (2009) PINK1-associated Parkinson's disease is caused by neuronal vulnerability to calcium induced cell death. *Mol Cell* **33**:627-38.

- Girault JA (2012) Integrating neurotransmission in striatal medium spiny neurons. *Adv Exp Med Biol* **970**:407-29.
- Gorell JM, Rybicki BA, Cole Johnson C, Peterson EL (1999) Occupational metal exposures and the risk of Parkinson's disease. *Neuroepidemiology* **18**:303-08.
- Gotz M, Koutsilieri E, Riederer P, Ceccatelli S, Dare E (2002) Methylmercury induces neurite degeneration in primary cultures of mouse dopaminergic mesencephalic cells. *J Neural Transm* **109**:597-05.
- Grace AA and Bunney BS (1984) Intracellular and extracellular electrophysiology of nigral dopaminergic neurons: action potential generating mechanisms and morphological correlates. *Neuroscience* **10**:317-31.
- Grandjean P, Weihe P, Nielsen F, Heinzow B, Debes F, Budta-Jorgenson E (2012) Neurobehavioral deficits at age 7 years associated with prenatal exposure to toxicants from maternal seafood diet. *Neurotoxicol Teratol* **34**:446-72.
- Gray EG (1963) Electron microscopy of presynaptic organelles of the spinal cord. *J Anat* **97**:101-06.
- Grynkiewicz G, Poenie M, Tsien Y (1985) A new generation of Ca^{2+} indicators with greatly improved fluorescence properties. *J Biol Chem* **260**:3440-50.
- Gunter KK, Gunter TE (1994) Transport of calcium by mitochondria. *Journal of Bioenergetics and Biomembranes* **26**:471-85.
- Gunzman JN, Sanchez-Padilla J, Chan CS, Surmeier DJ (2009) Robust pacemaking in substantia nigra dopaminergic neurons. *J. Neurosci* **29**:11011-19.
- Hajela RK, Peng SQ, Atchison WD (2003) Comparative effects of methylmercury and Hg^{2+} on human neuronal N- and R-type high-voltage activated calcium channels transiently expressed in human embryonic kidney 293 cells. *J Pharmacol Exp Ther* **306**:1129-36.
- Hansford RG (1985) Relation between mitochondrial calcium transport and control of energy metabolism. *Rev Physiol Biochem Pharmacol* **102**:1-72.
- Hansford RG, Castro F (1981) Effects of micromolar concentrations of free calcium ions on the reduction of heart mitochondrial NAD(P) by 2-oxoglutarate. *Biochem J* **198**:525-33.
- Harada Y, Miyamoto Y, Nonaka I, Ohta S, Ninomiya T (1968) Electroencephalographic studies of Minamata disease in children. *Dev Med Child Neurol.* **10**:257-8.
- Harada M (1995) Minamata disease: methylmercury poisoning in Japan caused by environmental pollution. *Crit Rev Toxicol* **1**:1-24.

- Hare MF, Atchison WD (1992) Comparative action of methylmercury and divalent inorganic mercury on nerve terminal and intraterminal mitochondrial membrane potentials. *J Pharmacol Exp Ther* **261**:166-72.
- Hare MF, Atchison WD (1995) Methylmercury mobilizes Ca^{++} from intracellular stores sensitive to inositol 1,4,5-triphosphate in NG108-15 cells. *J Pharmacol Exp Ther* **272**:1016-23.
- Hare MF, McGinnis KM, Atchison WD (1993) Methylmercury increases intracellular concentrations of Ca^{++} and heavy metals in NG108-15 cells. *J Pharmacol Exp Ther* **266**:1626-35.
- He L, Poblentz AT, Medrano CJ, Fox DA (2000) Lead and calcium produce rod photoreceptor cell apoptosis by opening the mitochondrial permeability transition pore. *J Biol Chem* **275**:12175-84.
- Hebb CO, Whittaker VP (1958) Intracellular distributions of acetylcholine and choline acetylase. *J Physiol* **142**:187-96.
- Hill BG, Benavides GA, Lancaster JR, Ballinger S, Dell'Italia L, Zhang J, Darley-Usmar VM (2012) Integration of cellular bioenergetics with mitochondrial quality control and autophagy. *Biol Chem* **393**:1485-12.
- Huang CF, Hsu CJ, Lui SH, Lin-Shiau SY (2008) Neurotoxicological mechanism of methylmercury induced by low-dose and long-term exposure in mice: oxidative stress and down-regulated $\text{Na}^{+}/\text{K}^{+}$ -ATPase involved. *Toxicol Lett* **176**:188-97.
- Hunter D, Russell DS (1954) Focal cerebral and cerebellar atrophy in a human subject due to organic mercury compounds. *J Neurol Neurosurg Psychiatry* **17**:69-235.
- Ilijic E, Guzman JN, Surmeier DJ (2011) The L-type antagonist isradipine is neuroprotective in a mouse model of Parkinson's disease. *Neurobiol Dis* **43**:364-71.
- Johnson FO, Atchison WD (2009) The role of environmental mercury, lead and pesticide exposure in development of amyotrophic lateral sclerosis. *Neurotoxicology* **30**:761-65.
- Johnson F, Yuan Y, Hajela R, Chitrakar A, Parsell D, Atchison WD (2011) Exposure to an environmental neurotoxicant hastens the onset of amyotrophic lateral sclerosis-like phenotype in human $\text{Cu}^{2+}/\text{Zn}^{2+}$ superoxide dismutase-1 G93A mice: glutamate-mediated excitotoxicity. *J Pharmacol Exp Ther* **38**:518-27.
- Juarez BI, Martinez ML, Montante M, Dufour L, Garcia E, Jimenez-Capdeville ME (2002) Methylmercury increases glutamate extracellular levels in frontal cortex of awake rats. *Neurotoxicol Teratol* **24**:767-71.

- Kalisch BE, Racz WJ (1996) The effects of methylmercury on endogenous dopamine efflux from mouse striatal slices. *Toxicol Lett* **89**:43-9.
- Karagas MR, Choi AL, Oken E, Horvat M, Schoeny R, Kamai E, Cowell W, Grandjean P, Korrick S (2012) Evidence on the human health effects of low-level methylmercury exposure. *Environ Health Perspect* **120**:799-06.
- Kerr LM, Yoshikami D (1984) A venom peptide with a novel presynaptic blocking action. *Nature* **308**:282-84.
- Khachaturian Z (1987) Hypothesis on the regulation of cytosol calcium concentration and the aging brain. *Neurobiol Aging* **8**:345-46.
- Kim YI, Kim YS, Kim MS, Ryu JC (2007) The inhibitory mechanism of methylmercury on differentiation of human neuroblastoma cells. *Toxicol* **234**:1-9.
- Kobayashi H, Yuyama A, Matsusaka N, Takeno K, Yanagiya I (1981) Neuropharmacological effect of methylmercury in mice with special reference to the central cholinergic system. *Jpn J Pharmacol* **31**:711-18.
- Kochevarov AA (2003) Pharmacological modulators of voltage-gated calcium channels and their therapeutical application. *Cell Calcium* **33**:145-62.
- Komulainen H, Bondy SC (1987) Increased free intrasynaptosomal Ca^{2+} by neurotoxic organometals: distinctive mechanisms. *Toxicol Appl Pharmacol* **88**:77-86.
- Komulainen H, Tuomisto J (1982) Effects of heave metals on monoamine uptake and release in brain synaptosomes and blood platelets. *Neurobehav Toxicol Teratol* **4**:647-49.
- Komulainen H, Tuomisto J (1985) 3H-dopamine uptake and 3H-haloperidol binding in striatum after administration of methyl mercury to rats. *Arch Toxicol* **57**:268-71.
- Kong HK, Wong MH, Chan HM, Lo SC (2013) Chronic exposure of adult rats to low doses of methylmercury induced a state of metabolic deficit in the somatosensory cortex. *J Proteome Res* **12**:5233-45.
- Kreitzer AC, Malenka RC (2008) Striatal plasticity and basal ganglia circuit function. *Neuron* **60**:543-54.
- Kuznetsov DA, Zaviialov NV, Govorkov AV, Ivanov-Snaryad AA (1986) Methyl mercury-induced conbined inhibition of ATP regeneration and protein synthesis in reticulocyte lysate cell-free translation system. *Toxicol Lett* **30**:267-71.

- Landrigan PJ, Sonawane B, Butler RN, Trasande L, Callan R, Droller D (2005) Early environmental origins of neurodegenerative disease in later life. *Environ Health Perspect* **113**:1230-33.
- LeBel C, Ali S, McKee M, Bondy S (1990) Organometal-induced increases in oxygen reactive species: The potential for 2'7'-dichlorofluorescein diacetate as an index of neurotoxic damage. *Toxicol Appl Pharmacol* **104**:17-24.
- Levesque PC, Atchison WD (1991) Disruption of brain mitochondrial calcium sequestration by methylmercury. *J. Pharmacol Exp Ther* **256**:236-42.
- Levesque PC, Hare MF, Atchison WD (1992) Inhibition of mitochondrial Ca²⁺ release diminishes the effectiveness of methylmercury to release acetylcholine from synaptosomes. *Toxicol Appl Pharmacol* **115**:11-20.
- Limke TL, Atchison WD (2001) Acute exposure to methylmercury opens the mitochondrial permeability transition pore in rat cerebellar granule cells. *Toxicol Appl Pharmacol* **178**:52-61.
- Limke TL and Atchison WD (2002) Evidence for interactions between intracellular calcium during methylmercury-induced intracellular calcium dysregulation in rat cerebellar granule neurons. *J. Pharmacol Exp Ther* **304**:949-57.
- Limke TL, Heidemann SR, Atchison WD (2004) Disruption of intraneuronal divalent cation regulation by methylmercury: are specific targets involved in altered neuronal development and cytotoxicity in methylmercury poisoning? *Neurotoxicology* **25**:741-60.
- Liu W, Xu Z, Deng Y, Xu B, Yang H, Wei Y, Feng S (2012) Excitotoxicity and oxidative damages induced by methylmercury in rat cerebral cortex and the protective effects of tea polyphenols. *Environ Toxicol* [Epub ahead of print].
- Lopes F, Schroder R, Junior M, Zanotto-Filho A, Muller C, Pires A, Meurer R, Colpo G, Gelain D, Kapczinski F, Moreira J, Fernandes M, Klamt F (2010) Comparison between proliferative and neuron-like SH-SY5Y cells as *in vitro* model for Parkinson disease studies. *Brain Research* **1337**:85-94.
- Lubick N, Malakoff D (2013) With pact's completion, the real work begins. *Science* **341**:1443-45.
- Lukyanetz EA (1998) Diversity and properties of calcium channel types in NG108-15 hybrid cells. *Neuroscience* **87**:265-74.
- Madison JL, Wegrzynowicz M, Aschner M, Bowman AB (2012) Disease-toxicant interactions in manganese exposed Huntington disease mice: early changes in striatal neuron morphology and dopamine metabolism. *PLoS One* **7**:e31024.

- Marrero-Rosado B, Fox SM, Hannon HE, Atchison WD (2013) Mercury and lead, effects on voltage-gated calcium channel function. In *Encyclopedia of Metalloproteins* (1336-46). New York, New York: Springer Science.
- Marty MS, Atchison WD (1997) Pathways mediating Ca^{2+} entry in rat cerebellar granule cells following *in vitro* exposure to methylmercury. *Toxicol Appl Pharmacol* **147**:319-30.
- Marty MS, Atchison WD (1998) Elevations of intracellular Ca^{2+} as a probably contributor to decreased viability in cerebellar granule cells following acute exposure to methylmercury. *Toxicol Appl Pharmacol* **150**:98-05.
- McKay SJ, Reynolds JN, Racz WJ (1986) Effects of mercury compounds on the spontaneous and potassium-evoked release of [^3H]dopamine from mouse striatal slices. *Can J Physiol Pharmacol* **64**:1507-14.
- Minnema DJ, Cooper GP, Greenland RD (1989) Effects of methylmercury on neurotransmitter release from rat brain synaptosomes. *Toxicol Appl Pharmacol* **99**:510-21.
- Møller-Madsen B, Danscher G (1991) Localization of mercury in CNS of the rat. *Toxicol and Appl Pharmacol* **108**:457-58.
- Mori N, Yasutake A, Marumoto M, Hirayama K (2011) Methylmercury inhibits electron transport chain activity and induces cytochrome c release in cerebellum mitochondria. *J Toxicol Sci* **36**:253-59.
- Morton A, Hammond C, Mason W, Henderson G (1992) Characterisation of the L- and N-type calcium channels in differentiated SH-SY5Y neuroblastoma cells: calcium imaging and single channel recording. *Brain Res Mol Brain Res* **13**:53-61.
- Nakane H, Ibayashi S, Fujii K, Irie K, Sadoshima S, Fujishima M (1995) Cerebral blood flow and metabolism in hypertensive patients with cerebral infarction. *Angiology* **46**:801-10.
- Nelson D, Cox M (2005) *Lehninger Principles of Biochemistry*. (690-722) New York, New York: W.H Freeman and Company.
- Ngim C, Devathasan G (1989) Epidemiologic study on the association between body burden mercury level and idiopathic Parkinson's disease. *Neuroepidemiology* **8**:128-41.
- Nicholls DG (2002) Mitochondrial function and dysfunction in the cell: its relevance to aging and aging-related disease. *The International Journal of Biochemistry and Cell Biology* **34**:1372-81.
- Nicholls DG (2005) Mitochondria and calcium signaling. *Cell Calcium* **38**:311-17.

- Noelker C, Schwake M, Balzer-Geldsetzer M, Bacher M, Popp J, Schlegel J, Eggert K, Oertel W, Klockgether T, Dodel R (2012) Differentially expressed gene profile in the 6-hydroxy-dopamine-induced cell culture model of Parkinson's disease. *Neurosci Lett* **507**:10-15.
- Nordin-Andersson M, Forsby A, Heldring N, Dejongh J, Kjellstrand P, Walum E (1998) Neurite degeneration in differentiated human neuroblastoma cells. *Toxicol In Vitro* **12**:557-60.
- Obeso JA, Marin C, Rodriguez-Oroz C, Blesa J, Benitez-Temifio B, Mena-Segovia J, Rodriguez M, Olanow CW (2008) The basal ganglia in Parkinson's disease: current concepts and unexplained observations. *Ann Neurol* **64**:S30-46.
- Ohlson CG, Hogstedt C (1981) Parkinson's disease and occupational exposure to organic solvents, agricultural chemicals and mercury—a case-referent study. *Scand J Work Environ Health* **7**:252-56.
- O'Kusky JR, McGeer EG (1989) Methylmercury-induced movement and postural disorders in developing rat: high-affinity uptake of choline, glutamate, and gamma-aminobutyric acid in the cerebral cortex and caudate-putamen. *J Neurochem* **53**:999-06.
- O'Kusky JR, Radke JM, Vincent SR (1988) Methylmercury-induced movement and postural disorders in developing rat: loss of somatostatin-immunoreactive interneurons in the striatum. *Brain Res* **468**:11-23.
- Olivera BM, McIntosh JM, Cruz LJ, Luque FA, Gray WR (1984) Purification of sequence of a presynaptic peptide toxin from *Conus geographus* venom. *Biochemistry* **23**:5087-90.
- Oyama Y, Tomiyoshi F, Uneo S, Furukawa K, Chikahisa L (1994) Methylmercury-induced augmentation of oxidative metabolism in cerebellar neurons dissociated from rats: its dependence on intracellular Ca^{2+} . *Brain Res* **660**:154-57.
- Paredes RM, Etzler JC, Watts LT, Zheng W, Lechleiter JD (2008) Chemical calcium indicators. *Methods* **46**:143-51.
- Parkinson Study Group (2013) Phase II safety, tolerability, and dose selection study of isradipine as a potential disease-modifying intervention in early Parkinson's disease. *Mov Disord* **28**:1823-31.
- Pastorino JG, Tafani M, Rothman RJ, Marcinkeviciute A, Hoek JB, Farber JL, Marcineviciute A (1999) Functional consequences of the sustained or transient activation by Bax of the mitochondrial permeability transition pore. *J Biol Chem* **274**:31734-39.
- Pahlman S, Mamaeva S, Meyerson G, Mattson M, Bjelfman C, Ortoft E, Hammerling U (1990) Human neuroblastoma cells in culture: a model for neuronal cell differentiation and function. *Acta Physiol Scand* **592**:25-37.

- Peng S, Hajela RK, Atchison WD (2002) Characteristics of block by Pb^{2+} of function of human neuronal L-, N-, and R-type Ca^{2+} channels transiently expressed in human embryonic kidney 293 cells. *Mol Pharmacol* **62**:1418-30.
- Petersen MS, Halling J, Bech S, Wermuth L, Weihe P, Nielsen F, Jørgensen PJ, Budtz-Jørgensen E, Grandjean P (2008) Impact of dietary exposure to food contaminants on the risk of Parkinson's disease. *Neurotoxicology* **29**: 584-90.
- Petersen MS, Weihe P, Choi A, Grandjean P (2008) Increased prenatal exposure to methylmercury does not affect the rise in Parkinson's disease. *Neurotoxicol* **29**:591-15.
- Petroni D, Tsai J, Agrawal K, Mondal D, George W (2013) Attenuation of low dose methylmercury and glutamate induced-cytotoxicity and tau phosphorylation by an N-methyl-D-aspartate antagonist in human neuroblastoma (SH-SY5Y) cells. *Environ Toxicol* **28**:700-06.
- Petroni D, Tsai J, Agrawal K, Mondal D, George W (2012) Low-dose methylmercury-induced oxidative stress, cytotoxicity, and tau-hyperphosphorylation in human neuroblastoma (SH-SY5Y) cells. *Environ Toxicol* **27**:549-55.
- Petronilli V, Penzo D, Scorrano L, Bernardi P, Di Lisa F (2001) The mitochondrial permeability transition, release of cytochrome c and cell death. Correlation with the duration of pore openings in situ. *J Biol Chem* **276**:12030-34.
- Ping HX and Shepard PD (1996) Apamin-sensitive Ca^{2+} -activated K^{+} channels regulate pacemaker activity in nigral dopamine neurons. *Neuroreport* **7**:809-14.
- Pivovarova NB, Stanika RI, Kazanina G, Villaneueva I, Andrews SB (2013) The interactive roles of zinc and calcium in mitochondrial dysfunction and neurodegeneration. *J Neurochem* [Epub ahead of print].
- Polunas M, Halladay A, Tialkens RB, Philbert MA, Lowndes H, Reuhl K (2011) Role of oxidative stress and the mitochondrial permeability transition in methylmercury cytotoxicity. *Neurotoxicology* **32**:526-34.
- Porciuncula LO, Rocha JB, Tavares RG, Ghisleni G, Reis M, Souza DO (2003) Methylmercury inhibits glutamate uptake by synaptic vesicles from rat brain. *Neuroreport* **14**: 577-80.
- Puopolo M, Raviola E, Bean BP (2007) Roles of subthreshold calcium current and sodium current in spontaneous firing of mouse midbrain dopamine neurons. *J. Neurosci* **27**:645-46.

- Qu M, Nan X, Gao Z, Guo B, Liu B, Chen Z (2013) Protective effects of lycopene against methylmercury-induced neurotoxicity in cultured rat cerebellar granule neurons. *Brain Res* **1540**:92-102.
- Qualls Z, Brown D, Ramlochansingh C, Hurley LL, Tizabi Y (2013) Protective effects of curcumin against rotenone and salsolinol-induced toxicity: implications for Parkinson's disease. *Neurotox Res* [Epub ahead of print].
- Quiroz-Baez R, Flores-Dominguez D, Arias C (2013) Synaptic aging is associated with mitochondrial dysfunction, reduced antioxidant contents and increased vulnerability to amyloid- β toxicity. *Curr Alzheimer Res* **10**:324-31.
- Rajanna B, Hobson M (1985) Influence of mercury on uptake of [3H]dopamine and [3H]norepinephrine by rat brain synaptosomes. *Toxicol Lett* **27**:7-14.
- Rajanna B, Hobson M, Harris L, Ware L, Chetty CS (1990) Effects of cadmium and mercury on $\text{Na}^+ - \text{K}^+$ ATPase and uptake of 3H-dopamine in rat brain synaptosomes. *Arch Int Physiol Biochem* **98**:291-96.
- Ramanathan G, Atchison WD (2011) Ca^{2+} entry pathways in mouse spinal motor neurons in culture following in vitro exposure to methylmercury. *Neurotoxicology* **32**:742:50.
- Reid RA, Moyle J, Mitchell P (1966) Synthesis of adenosine triphosphate by a protonmotive force in rat liver mitochondria. *Nature* **212**:257-58.
- Reuveny E, Narahashi T (1993) Two types of high voltage-activated calcium channels in SH-SY5Y human neuroblastoma cells. *Brain Res* **603**:64-73.
- Ritz B, Rhodes SL, Qian L, Schernhammer E, Olsen J, Friis S (2010) L-type calcium channel blockers and Parkinson disease in Denmark. *Ann Neurol* **67**:600-07.
- Ross RA, Spengler BA, Bielder JL (1983) Coordinate morphological and biochemical interconversion of human neuroblastoma cells. *J Natl Cancer Inst* **71**:741-47.
- Rudin M and Sauter A (1989) Dihydropyridine calcium antagonists reduce the consumption of high-energy phosphates in the rat brain. A study using combined $^{31}\text{P}/^1\text{H}$ magnetic resonance spectroscopy and ^{31}P saturation transfer. *JPET* **251**:700-06.
- Sakamoto M, Ikegami N, Nakano A (1996) Protective effects of Ca^{2+} channel blockers against methyl mercury toxicity. *Pharmacol Toxicol* **78**:193-99.
- Sakamoto M, Wakabayashi K, Kakita A, Hitoshi T, Adachi T, Nakano A (1998) Widespread neuronal degeneration in rats following oral administration of methylmercury during postnatal developing phase: a model of fetal-type minamata disease. *Brain Res* **784**:351-54.

- Sanfeliu C, Sebastia J, Ki SU (2001) Methylmercury neurotoxicity in cultures of human neurons, astrocytes, neuroblastoma cells. *Neurotoxicology* **22**:317-27.
- Sarafian T, Hagler J, Vartavarian L, Verity MA (1989) Rapid cell death induced by methyl mercury in suspension of cerebellar granule neurons. *Neuropathol Exp Neurol* **48**:1-10.
- Sarafian T, Verity MA (1991) Oxidative mechanisms underlying methyl mercury neurotoxicity. *Int J Dev Neurosci* **9**:147-53.
- Sauter A, Rudin M (1987) Effects of calcium antagonists on high-energy phosphates in ischemic rat brain measured by ³¹P NMR spectroscopy. *Magn Reson Med* **4**:1-8.
- Schapira AH (2008) Mitochondrial dysfunction in neurodegenerative diseases. *Neurochem Res* **12**:2502-09.
- Schachter M (1991) Isradipine. *J Clin Pharm Ther* **16**:79-91.
- Schwartzkroin PA, Andersen P (1975) Glutamic acid sensitivity of dendrites in hippocampal slices in vitro. *Adv Neurol* **12**:45-51.
- Semchuk KM, Love EJ, Lee RG (1993) Parkinson's disease: a test of the multifactorial etiologic hypothesis. *Neurology* **43**:1173-80.
- Senior DJ, Tsai CS (1988) Purification and characterization of aldehyde dehydrogenase from rat liver mitochondria. *Arch Biochem Biophys* **262**:211-20.
- Shafer TJ, Atchison WD (1989) Block of ⁴⁵Ca uptake into synaptosomes by methylmercury: Ca⁺⁺- and Na⁺-dependence. *J Pharmacol Exp Ther* **248**:696-02.
- Shafer TJ, Atchison WD (1991) Methylmercury blocks N- and L-type Ca⁺⁺ channels in nerve growth factor-differentiated pheochromocytoma (PC12) cells. *J Pharmacol Exp Ther* **258**:159-63.
- Shafer TJ, Contreras ML, Atchison WD (1990) Characterization of interactions of methylmercury with Ca²⁺ channels in synaptosomes and pheochromocytoma cells: radiotracer flux and binding studies. *Mol Pharmacol*. **1**:102-13.
- Shafer TJ, Meacham CA, Barone S (2002) Effects of prolonged exposure to nanomolar concentrations of methylmercury on voltage-sensitive sodium and calcium currents in PC12 cells. *Devel Brain Research* **136**:151-64.
- Simmons-Willis TA, Koh AS, Clarkson TW, Ballatori N (2002) Transport of a neurotoxicant by molecular mimicry: the methylmercury-L-cysteine complex is a substrate for human L-type large neutral amino acid transporter (LAT) 1 and LAT2. *Biochem J* **367**:239-46.

- Sirois JE, Atchison WD (1996) Effects of mercurial on ligand- and voltage-gated ion channels: a review. *Neurotoxicology* **17**:63-84.
- Sirois J, Atchison WD (2000) Methylmercury affects multiple subtypes of calcium channels in rat cerebellar granule cells. *Toxicol Appl Pharmacol* **167**:1-11.
- Skrede KK, Westgaard RH (1971) The transverse hippocampal slice: a well-defined cortical structure maintained in vitro. *Brain Res* **35**:589-93.
- Smith AD, Bolam JP (1990) The neural network of the basal ganglia as revealed by the study of synaptic connections of identified neurons. *Trends Neurosci* **13**:259-65.
- Sokolowski K, Falluel-Morel A, Zhou X, DiCicco-Bloom E (2011) Methylmercury (MeHg) elicits mitochondrial-dependent apoptosis in developing hippocampus and acts at low exposures. *Neurotoxicology* **32**:535-44.
- Somlyo AP, Urbanics R, Vadasz G, Kovach AG, Somlyo AV (1985) Mitochondrial calcium and cellular electrolytes in brain cortex frozen in situ: electron probe analysis. *Biochem Biophys Res Commun* **132**:1071-78.
- Sone N, Larsstuvold MK, Kagawa Y (1977) Effect of methylmercury on phosphorylation, transport, and oxidation in mammalian mitochondria. *J Biochem* **82**:859-68.
- Sousa SR, Vetter I, Ragnarsson L, Lewis RJ (2013) Expression and pharmacology of endogenous Cav channels in SH-SY5Y human neuroblastoma cells. *PLoS One* **8**: e59293. doi:10.1371/journal.pone.0059293
- Sparagna GC, Gunter KK, Sheu SS, Gunter TE (1995) Mitochondrial calcium uptake from physiological-type pulses of calcium. A description of the rapid uptake mode. *J Biol Chem* **270**:27510-15.
- Strain JJ, Davidson PW, Thurston SW, Harrington D, Mulhern MS, McAfee AJ, van Wijngaarden E, Shamlaye CF, Henderson J, Watson GE, Zareba G, Cory-Slechta DA, Lynch M, Wallace JM, McSorley EM, Bonham MP, Stokes-Riner A, Sloane-Reeves J, Janciuras J, Wong R, Clarkson TW, Myers GJ (2012) Maternal PUFA status but not prenatal methylmercury exposure is associated with children's language functions at age five years in the Seychelles. *J Nutr* **142**:1943-49.
- Stokes-Riner A, Thurston SW, Myers GJ, Duffy EM, Wallace J, Bonham M, Robson P, Shamlaye CF, Strain JJ, Watson G, Davidson PW (2011) A longitudinal analysis of prenatal exposure to methylmercury and fatty acids in the Seychelles. *Neurotoxicol Teratol* **33**:325-28.
- Surmeier DJ, Ding J, Day M, Wang Z, Shen W (2007) D1 and D2 dopamine-receptor modulation of striatal glutamatergic signaling in striatal medium spiny neurons. *Trends Neurosci* **30**:228-35.

- Swanson GT, Kamboi SK, Cull-Candy SG (1997) Single-Channel properties of recombinant AMPA receptors depend on RNA editing, splice variation, and subunit composition. *J Neurosci* **17**:58-69.
- Szabo I, Zoratti M (1992) The mitochondrial megachannel is the permeability transition pore. *J Bioenerg Biomembr* **24**:111-17.
- Szalai G, Krishnamurthy R, Hajnoczky G (1999) Apoptosis driven by IP₃-linked mitochondrial calcium signals. *EMBO J* **18**:6349-61.
- Takamura k, Kusu F Abdel-Wadood H, El-Rabbat N, Saleh G, Refaat I (2000) Redox properties of isradipine and its electrochemical detection in the HPLC determination of the compound in human serum. *Biomed Chromatogr* **14**:453-58.
- Tarasov AI, Semplici F, Li D, Rizzuto R, Ravier MA, Gilon P, Rutter GA (2013) Frequency-dependent mitochondrial Ca²⁺ accumulation regulates ATP synthesis in pancreatic β cells. *Pflungers Arch* **465**:543-54.
- Tiernan C, Edwin E, Goudreau J, Atchison WD, Lookingland K (2013) The role of de novo catecholamine synthesis in mediating methylmercury-induced vesicular dopamine release from rat pheochromocytoma (PC12) cells. *Toxicol Sci* **133**:125-32.
- Toescu E (2005) Normal brain aging: models and mechanisms. *Phil Trans R Soc B* **360**:2347-54.
- Toescu E (2007) Altered calcium homeostasis in old neurons. *Brain Aging: Models, Methods, and Mechanisms*. CRC Press.
- Toescu E, Vreugdenhil M (2010) Calcium and normal brain ageing. *Cell Calcium* **47**:158-64.
- Toimela T, Tahiti H (2004) Mitochondrial viability and apoptosis induced by aluminum, mercuric mercury and methylmercury in cell lines of neural origin. *Arch Toxicol* **78**:565-74.
- Toledo-Rodriguez M, Markram H (2007) Single-cell RT-PCR, a technique to decipher the electrical, anatomical, and genetic determinants of neuronal diversity. *Methods Mol Biol* **403**:123-39.
- Toyama T, Sumi D, Shinkai Y, Yasutake A, Taguchi K, Tong KI, Yamamoto M, Kumagai Y (2007) Cytoprotective role of Nrf2/Keap1 system in methylmercury toxicity. *Biochem Biophys Res Commun* **363**:645-50.
- Troulinaki K, Bano D (2012) Mitochondrial deficiency: a double-edged sword for aging and neurodegeneration. *Front Genet* **26**:244.

- Tse FL, Jaffe JM, Hassell AE, Schran HF (1989) Bioavailability of isradipine in young and old rats: effect of mode of administration. *J Pharm Pharmacol* **41**:657-60.
- Tseng KY, Snyder-Keller A, O'Donnell P (2007) Dopaminergic modulation of striatal plateau depolarizations in corticostriatal organotypic cocultures. *Psychopharmacol (Berl)* **191**:627-40.
- Tsuzuki Y (1982) Effect of methylmercury exposure on different neurotransmitter systems in rat brain. *Toxicol Lett* **13**:159-62.
- Uceda G, Garcia AG, Guantes JM, Michelena P, Montiel C (1995) Effects of Ca²⁺ channel antagonist subtypes on mitochondrial Ca²⁺ transport. *Eur J Pharmacol* **289**:73-80.
- Vance JM, Ali S, Bradley WG, Singer C, Di Monte DA (2010) Gene-environment interactions in Parkinson's disease and other forms of parkinsonism. *Neurotoxicology* **31**:598-02.
- Vanduy N, Nass R (2013) The putative multidrug resistance protein MRP-7 inhibits methylmercury-associated animal toxicity and dopaminergic neurodegeneration in *Caenorhabditis elegans*. *J Neurochem* [Epub ahead of print].
- Vanduy N, Settivari R, Wong G, Nass R (2010) SKN-1/Nrf2 inhibits dopamine neuron degeneration in a *Caenorhabditis elegans* model of methylmercury toxicity. *Toxicol Sci* **118**:613-24.
- Verity MA, Brown WJ, Cheung M (1975) Organic mercurial encephalopathy: in vivo and in vitro effects of methyl mercury on synaptosomal respiration. *J Neurochem* **25**:759-66.
- Wade L (2013) Gold's dark side. *Science* **341**:1448-49.
- Wakabayashi K, Kakita A, Sakamoto M, Su M, Iwanaga K, Ikuta F (1995) Variability of brain lesions in rats administered methylmercury at various postnatal development phases. *Brain Res* **705**:267-72.
- Wang N, Wang U, Guohua Y, Yuan C, Ma J (2011) Quinoprotein adducts accumulate in the substantia nigra of aged rats and correlate with dopamine-induced toxicity in SH-SY5Y cells. *Neurochem Res* **36**:2169-75.
- Weihe P, Grandjean P, Debes F, White R (1996) Health implications for Faroe islanders of heavy metals and PCBs from pilot whales. *Sci Total Environ* **186**:141-18.
- Wermuth L, Joesen P, Bungler N, Jeune B (1997) High prevalence of Parkinson's disease in the Faroe Islands. *Neurology* **49**:426-32.
- Wermuth L, von Weitzel-Mudersbach P, Jeune B (2000) A two-fold difference in the age-adjusted prevalences of Parkinson's disease between the island of Als and the Faroe Islands. *Eur J Neural* **7**:655-60.

- Wermuth L, Pakkenberg H, Jeune B (2002) High age-adjusted prevalence of Parkinson's disease among Inuits in Greenland. *Neurology* **58**:1422-25.
- Wermuth L, Bech S, Petersen MS, Joesen P, Weihe P, Grandjean P (2007) Prevalence and incidence of Parkinson's disease in the Faroe Islands. *Acta Neurol Scand* **11**:126-31.
- Whittaker VP (1993) Thirty years of synaptosome research. *J Neurocytol* **22**:735-42.
- Whittaker VP, Michaelson I, Jeanette R, Kirkland A (1964) The separation of synaptic vesicles from nerve-ending particles ('synaptosomes'). *Biochem J* **90**:293-03.
- Williams BB, Li D, Wegrynowicz M, Vadodaria BK, Anderson JG, Kwakye GF, Aschner M, Erikson KM, Bowman AB (2010) Disease-toxicant screen reveals a neuroprotective interaction between Huntington's disease and manganese exposure. *J Neurochem* **112**:227-37.
- Wilson CJ, Callaway JC (2000) Coupled oscillator model of the dopaminergic neuron of the substantia nigra. *J. Neurophysiol* **83**:3084-00.
- Wingrove DE, Gunter TE (1986) Kinetics of mitochondrial calcium transport. II. A kinetic description of the sodium-dependent calcium efflux mechanism of liver mitochondria and inhibition by ruthenium red and by tetraphenylphosphonium. *J Biol Chem* **261**:15166-71.
- Wondolowski J, Dickman D (2013) Emerging links between homeostatic synaptic plasticity and neurological disease. *Front Cell Neurosci* **7**:1-9.
- Xu B, Xu Z, Deng Y, Liu W, Yang H, Wei YG (2013) MK-801 protects against intracellular Ca^{2+} overloading and improves N-methyl-D-aspartate receptor expression in cerebral cortex of methylmercury-poisoned rats. *J Mol Neurosci* **49**:162-71.
- Xu B, Xu Z, Deng Y, Liu W, Yang HB, Wei YG (2012) Protective effects of MK-801 on methylmercury-induced neuronal injury in rat cerebral cortex: involvement of oxidative stress and glutamate metabolism dysfunction. *Toxicol* **300**:112-20.
- Yamamoto C, McIlwain H (1966) Potentials evoked in vitro preparations from the mammalian brain. *Nature* **210**:1055-56.
- Yee S, Choi BH (1996) Oxidative stress in neurotoxic effects of methylmercury poisoning. *Neurotoxicology* **17**:17-26.
- Yin A, Jiang H, Syversen T, Rocha JB, Farina M, Aschner M (2008) The methylmercury-L-cysteine conjugate is a substrate for the L-type large neutral amino acid transporter. *J Neurochem* **107**:1083-90.

- Yorifuji T, Debes F, Weihe P, Grandjean P (2011) Prenatal exposure to lead and cognitive deficit in 7- and 14-year-old children in the presence of concomitant exposure to similar molar concentration of methylmercury. *Neurotoxicol Teratol* **33**:205-11.
- Yu X, Li X, Jiang G, Wang X, Chang HC, Hsu WH, Li Q (2013) Isradipine prevents rotenone-induced intracellular calcium rise that accelerates senescence in human neuroblastoma SH-SY5Y cells. *Neuroscience* [Epub ahead of print].
- Yuan Y, Atchison WD (1993) Disruption by methylmercury of membrane excitability and synaptic transmission of CA1 neurons in hippocampal slices of the rat. *Toxicol Appl Pharmacol* **120**:203-15.
- Yuan Y, Atchison WD (1994) Comparative effects of inorganic divalent mercury, methylmercury and phenylmercury on membrane excitability and synaptic transmission of CA1 neurons in hippocampal slices of the rat. *Neurotoxicology* **15**:403-11.
- Yuan Y, Atchison WD (1995) Methylmercury acts at multiple sites to block hippocampal synaptic transmission. *J Pharmacol Exp Ther* **275**:1308-16.
- Yuan Y, Atchison WD (1997) Action of methylmercury on GABA(A) receptor-mediated inhibitory synaptic transmission is primarily responsible for its early stimulatory effects on hippocampal CA1 excitatory synaptic transmission. *J Pharmacol Exp Ther* **282**:64-73.
- Yuan Y, Atchison WD (1999) Comparative effects of methylmercury on parallel-fiber and climbing-fiber responses of rat cerebellar slices. *J Pharmacol Exp Ther* **288**:1015-25.
- Yuan Y, Atchison WD (2003) Methylmercury differentially affects GABA(A) receptor-mediated spontaneous IPSCs in Purkinje and granule cells of rat cerebellar slices. *J Physiol* **550**:191-04.
- Yuan Y, Otero-Montañez J, Yao A, Herden C, Sirois J, Atchison WD (2005) Inwardly rectifying and voltage-gated outward potassium channels exhibit low sensitivity to methylmercury. *Neurotoxicology* **26**:439-54.
- Yuan Y, Atchison WD (2007) Methylmercury-induced increase of intracellular Ca^{2+} increases spontaneous synaptic current frequency in rat cerebellar slices. *Mol Pharm* **71**:1109-21.